

A SWITCHED SYSTEMS APPROACH TO HUMAN-MACHINE INTERACTION

By

COURTNEY ANN ROUSE

A DISSERTATION PRESENTED TO THE GRADUATE SCHOOL
OF THE UNIVERSITY OF FLORIDA IN PARTIAL FULFILLMENT
OF THE REQUIREMENTS FOR THE DEGREE OF
DOCTOR OF PHILOSOPHY

UNIVERSITY OF FLORIDA

2019

© 2019 Courtney Ann Rouse

To my Mom and Dad for fostering my creative spirit and supporting me unconditionally

ACKNOWLEDGMENTS

I would like to acknowledge my advisor, Dr. Warren E. Dixon, for the past four years of fruitful guidance, without which this dissertation would not exist. Dr. Dixon, along with past and present members of the Nonlinear Controls and Robotics lab, have cummulatively produced a healthy and productive work environment that has allowed me to become the engineer and scientist that I am today. I would like to thank all of my family and friends for their constant love and support from both near and far, and to those in Gainesville, FL for turning what was once just a college town in a swamp, into a place I can call home. Lastly, I am grateful for the financial support provided by the University of Florida Department of Mechanical and Aerospace Engineering. While it would be impossible to repay all of these contributions, I promise to use what has been given to me to continue to challenge myself and improve the world around me the best I can. Thank you all.

TABLE OF CONTENTS

	<u>page</u>
ACKNOWLEDGMENTS	4
LIST OF TABLES	7
LIST OF FIGURES	8
ABSTRACT	10
CHAPTER	
1 INTRODUCTION	12
1.1 Motivation	12
1.2 Literature Review	14
1.3 Outline of the Dissertation	17
2 SYSTEM MODEL	19
2.1 Switched Muscle Subsystem	20
2.2 Combined Muscle-Motor System	21
3 VARYING THE POINT OF STIMULATION WITHIN A SINGLE MUSCLE GROUP: A SWITCHED SYSTEMS APPROACH	24
3.1 Switching Methods	24
3.1.1 Single Electrode Switching	26
3.1.2 Multi-Electrode Switching	26
3.2 Control Development	27
3.3 Stability Analysis	29
3.4 Experiments	31
3.4.1 Experimental Testbed	32
3.4.2 Single Electrode Switching Protocol	34
3.4.3 Single Electrode Switching Results	35
3.4.4 Multi-Electrode Switching Protocol	41
3.4.5 Multi-Electrode Switching Results	41
3.4.6 Discussion	43
3.5 Concluding Remarks	45
4 SWITCHED MOTORIZED ASSISTANCE DURING SWITCHED FUNCTIONAL ELECTRICAL STIMULATION FOR BICEPS CURLS	47
4.1 Control Development	47
4.2 Stability Analysis	50
4.3 Experiments	54
4.3.1 Arm Testbed	55
4.3.2 Protocol	55

4.3.3	Results	56
4.4	Discussion	56
4.5	Concluding Remarks	59
5	CADENCE TRACKING FOR SWITCHED FES CYCLING COMBINED WITH VOLUNTARY PEDALING AND MOTOR RESISTANCE	60
5.1	Control Development	61
5.2	Stability Analysis	63
5.3	Experiments	70
5.3.1	Motorized FES-Cycling Testbed	70
5.3.2	Experimental Setup	72
5.3.3	Results	73
5.3.4	Discussion	85
5.4	Concluding Remarks	89
6	SPLIT-CRANK CYCLING	91
6.1	Split-Crank Model	92
6.2	Control Development	95
6.2.1	Non-dominant Side	95
6.2.2	Dominant Side	96
6.3	Stability Analysis	98
6.3.1	Stability of the Non-Dominant Subsystem	98
6.3.2	Stability of the Dominant Side	102
6.4	Experiments	105
6.4.1	Split-Crank Motorized FES-Cycling Testbed	106
6.4.2	Protocol	106
6.4.3	Results	108
6.4.4	Discussion	108
6.5	Concluding Remarks	122
7	CONCLUSION	124
	REFERENCES	126
	BIOGRAPHICAL SKETCH	134

LIST OF TABLES

<u>Table</u>	<u>page</u>
3-1 Mean and standard deviation for position and velocity tracking error for all participants	38
3-2 Difference in post-trial torque-time integral during comparison of single electrode switching vs single electrode non-switching, for five participants.	40
3-3 Comparison of average RMS errors for position and velocity tracking during single electrode switching vs. single electrode stimulation.	40
4-1 Average position and velocity errors, FES control input, and motor control input for both arms (one impaired, one unimpaired) for both Participants. P1 and P2 denote Participants 1 and 2; R and L denote the right and left arms. . .	57
5-1 Participant description	75
5-2 Cycling metrics from nine stroke participants.	76
5-3 R correlation coefficients for various data amongst all nine participants.	77
6-1 Participant Demographics	105
6-2 Performance metrics from the volitional and controlled trials	118

LIST OF FIGURES

<u>Figure</u>	<u>page</u>
3-1 Isometric torques produced by stimulating 6 electrodes (channels) across the biceps brachii were measured at every 10 degrees of elbow flexion from 0 to 100 degrees in a healthy normal volunteer for five trials.	25
3-2 The proportion of total stimulation input sent to each electrode for all elbow angles for the same healthy normal volunteer in Figure 3-1.	28
3-3 Setup for protocol	33
3-4 Desired and actual trajectory for Participant 1, right arm, for five biceps curls is depicted on top with the stimulation intensity below.	36
3-5 Position Error for the right arm of Participant 1 for the performance of 5 biceps curls by switching stimulation amongst 3 electrodes.	37
3-6 The spread of mean position error over the stimulation region of each of the five biceps curls in the first set of single electrode switching experiments, for all participants.	37
3-7 The spread of mean velocity error over the stimulation region of each of the five biceps curls in the first set of single electrode switching experiments, for all participants.	39
3-8 Actual and desired forearm position during a multi-electrode switching experiment of the left arm of Participant 1.	42
3-9 Comparison of single-electrode switching (left) to multi-electrode switching (right) for the left arm of Participant 1.	45
4-1 Position error and stimulation pulsewidth (i.e., FES input) for the right arm of Participant 2 during trials where the lower stimulation threshold iteratively decreased according to the constant $\rho = 0.8$	57
5-1 The motorized FES-cycling test bed used for experiments	71
5-2 Cycle Cadence (top plot), stimulation pulse width (middle plot), and motor current (bottom plot) for 180 seconds of cycling.	74
5-3 Cycling cadence in comparison to the desired cadence range during volitional pedaling of target 5 minutes.	79
5-4 Cycling cadence (top), stimulation pulsewidth (middle) sent to the right (blue) and left (red) quadriceps, and motor current (bottom) across nine participants.	81
5-5 Cadence error from each participant and average cadence error, for both the volitional (top) and 3 mode (bottom) trials.	83

5-6	Cadence averaged over the nine subjects +/- the standard deviation over time for both the volitional (top) and 3 mode (bottom) trials.	83
5-7	RMS cadence errors of each of the nine participants for the volitional (top) and 3 mode (bottom) trials.	84
5-8	Average percentage of time in each of the three modes during the entire trial, first 240s, and final portion of both the volitional (top) and 3 mode (bottom) trials.	84
6-1	FES cycling data for Participant N1.	109
6-2	FES cycling data for Participant N2.	110
6-3	FES cycling data for Participant N3.	111
6-4	FES cycling data for Participant C4/V4 during both the controlled and uncontrolled trials.	112
6-5	FES cycling data for Participant C5/V5 during both the controlled and uncontrolled trials.	113
6-6	FES cycling data for Participant C6.	114
6-7	FES and motor control inputs for seconds 14-20 of Experiment N1.	115
6-8	FES and motor control inputs for seconds 74-80 of Experiment N2.	115
6-9	FES and motor control inputs for seconds 74-80 of Experiment N3.	116
6-10	FES and motor control inputs for seconds 64-70 of Experiment C4.	116
6-11	FES and motor control inputs for seconds 76-82 of Experiment C5.	117
6-12	FES and motor control inputs for seconds 53-59 of Experiment C6.	117

Abstract of Dissertation Presented to the Graduate School
of the University of Florida in Partial Fulfillment of the
Requirements for the Degree of Doctor of Philosophy

A SWITCHED SYSTEMS APPROACH TO HUMAN-MACHINE INTERACTION

By

Courtney Ann Rouse

May 2019

Chair: Warren E. Dixon

Major: Mechanical Engineering

Functional Electrical Stimulation (FES) is an established method for enhancing rehabilitation exercises for people with neurological conditions. This dissertation explores the use of switched systems theories to improve robotic FES rehabilitation. Switched systems theory provides a framework to examine the intermittent use of various actuators such as different muscles and motors. Switching between muscle and motor subsystems can improve range of motion, improve patient comfort, and mitigate muscle fatigue, which is a common obstacle when using FES. Theoretical advancements in this dissertation are tested on a biceps curl machine, a traditional recumbent tricycle, and a recumbent tricycle with decoupled crank arms (i.e., split-crank), each of which present unique challenges associated with multi-level switched systems control (i.e., multiple logic-based switching laws).

Chapter 1 provides an overview and motivation for the dissertation including a review of relevant literature. Chapter 2 provides a generic model for upper or lower body human-robot systems. Chapter 3 explores how the muscle belly and motor point shift in the biceps brachii as the forearm rotates about the elbow, and how switching stimulation along the biceps muscle belly as a function of position may result in maximum torque production throughout the range of motion. Chapter 4 presents a switched system where the muscle, motor, or both, are activated depending on the direction of forearm movement and a saturation limit on stimulation intensity. Within the muscle subsystem,

the position-based switched system developed in Chapter 3 is used. Chapter 5 involves a two-sided control problem for cadence tracking on a recumbent tricycle. Desired upper and lower cadence bounds form a desired volitional pedaling region. A high-level switched system based on velocity error is used to assist, resist, or provide no input to the volitionally pedaling rider. A low-level position-based switched system alternates the control input between muscle groups and the motor when pedaling in the assistive mode. In Chapter 6, the two sides of the cycle-rider system are decoupled and treated as separate subsystems, only linked by their desired trajectories. A third level of switching is added to ensure full control authority when the FES control input is saturated at a comfort threshold, by activating the corresponding motor. In all chapters, a Lyapunov function common to all subsystems is used to prove stability of the robust sliding mode controllers. Experiments on a biceps curl testbed or recumbent cycle demonstrate the stability and practicality of each novel control technique.

CHAPTER 1 INTRODUCTION

1.1 Motivation

Functional electrical stimulation (FES) is an established method for rehabilitation of people with neurological conditions. Benefits of FES include increased muscular strength [1, 2], range of motion [3], and improved bone mineral density [4]. Repetitive movements are known to improve muscle strength and movement coordination for people with neurological conditions [5, 6]. Results from [7] show that manipulating the forearm position and orientation while performing FES further increased strength benefits; however, passive motion (i.e., the only active actuator is the electric motor) is not as effective as FES exercises for increasing muscle mass and strength [8–10]. Thus, there is motivation to implement FES on repetitive exercises that cover a wide range of motion, such as biceps curls and cycling.

Closed-loop FES has significant potential for rehabilitative therapy; however, several challenges persist. For instance, due to the nonselective recruitment of motor neurons during FES [11, 12], the onset of fatigue occurs sooner than in volitional exercise, so it is important to stimulate the muscle as effectively as possible. It is well known that electrode placement affects motor unit recruitment and that the generated force varies with changing muscle geometry (i.e., muscle lengthening or shortening). In particular, [13] and [14] indicate that electrode proximity to the motor point (where the motor branch of a nerve enters the muscle belly) is critical for optimal force production. Altering muscle length by changing the joint angle varies the position of muscle fibers with respect to the electrodes, influencing the contribution of cutaneous input (sensory receptors) to the elicited contraction [15]. Manipulating the joint angle to cause a change in muscle geometry could maximize NMES benefits in a more practical way than high stimulation input or manually moving electrodes [7]. Thus, the motor point, or optimal

stimulation site, changes with limb motion, which motivates the use of state-dependent closed-loop switching control for varying the stimulation site within a single muscle during FES exercises. With limb movement, the biceps brachii undergoes significant change in geometry, so varying the stimulation site has particular application to the biceps brachii.

Even with various stimulation techniques to delay fatigue, fatigue onset is still unavoidable. The more fatigued the muscle, the more stimulation necessary to achieve the same torque production; however, each person has an intensity threshold up to which they are comfortable being stimulated (or the safety limit on the stimulator is reached). Moreover, increasing the stimulation intensity in a fatigued muscle will not necessarily result in more torque. Motivated to continue tracking the desired trajectory and to prolong exercise, an electric motor can be added to assist in tracking when necessary.

Another obstacle for FES exercises is that people, in particular people with neurological impairments, have a wide range of strength, mobility, and sensitivity to stimulation, motivating the design of an FES exercise method that automatically adjusts according to the user's performance. Efficiently sending stimulation amongst multiple muscle groups (as in cycling [16]), using an electric motor for either assistance or resistance, and allowing volitional contribution could allow the FES control system to be applicable to a broader range of users. Moreover, some users have asymmetries due to hemiplegia, and the work in [17] makes claims on the importance of promoting equal contribution from both the dominant (i.e., stronger) and non-dominant (i.e., weaker) legs. Unlike a traditional cycle, a split-crank cycle has uncoupled pedals so that a person's dominant leg cannot do more work to compensate for their non-dominant leg [18–21]. While [21] explores closed-loop control methods for a split-crank cycle, none of the aforementioned studies on a split-crank cycle use FES to control the muscles, which is

the goal of this dissertation. By pedaling on an uncoupled crank, each leg can be sufficiently exercised and the stimulation and motor assistance levels can be individualized for each side.

Switched systems control methods can be used to implement a system that discontinuously switches amongst multiple actuators (i.e., muscles and a motor). With multiple needs for switching, it is often necessary to use multiple switching signals that redirect control input to different actuators based on states, state errors, calculated input values, etc. Moreover, FES-motor control systems can be composed of multiple levels of switched systems to support multiple overlapping switched control objectives. Lyapunov methods that utilize a common Lyapunov function candidate can be used to prove stability of a switched system [22].

1.2 Literature Review

Switched control has been implemented in many upper and lower body FES applications, using some combination of multiple muscle groups, portions of a single muscle group, and/or a motor. Examples of switching the area of stimulation within a single muscle group include methods for fatigue reduction [23–25] and for performing tasks that involve multiple smaller muscle groups, such as pinching or grasping [26, 27]. Asynchronous stimulation [25, 27, 28] and spatially distributed sequential stimulation [24] utilize time-based switching to switch the location of stimulation within a single muscle group to delay fatigue effects that are often exacerbated during FES exercises. Varying stimulation within a single muscle group is often accomplished via an electrode array [26, 29–37]; however, proof of stability of a closed-loop controller that switches within a single muscle group has only been done in [38, 39], which are the basis for Chapter 3 of this dissertation.

Switching amongst multiple muscle groups and/or a motor is often used in open-loop [40–44] and closed-loop [45, 46] FES cycling. In FES cycling, position-based switching is used to switch amongst muscle groups according to crank angles for

which each muscle can contribute positive torque. Often a motor subsystem is also included to control in regions of the crank cycle where no muscle can significantly contribute positive torque (i.e., kinematically inefficient regions [47]), meaning that position-based switching occurs between stable muscle-controlled subsystems and stable motor-controlled subsystems. When a motor is not used to control motion in these kinematically inefficient regions of the crank cycle, switching occurs between stable and unstable subsystems (i.e., muscles and uncontrolled regions, [16]). However, uncontrolled regions, and thus unstable subsystems, may be desirable when a person can contribute volitional effort and produce torque with no FES or motor assistance. While the level of volitional input is not determined by a controller, a person's volitional contribution can be thought of as an additional actuator. Moreover, bounding an uncontrolled region by two stable controlled regions ensures overall system stability.

Although passive motion via a motor is not as affective for rehabilitation as using the muscle [8–10], rehabilitation robots that assist and/or resist the user, either with [48–51] or without FES [52], could improve the rehabilitation outcome. Combining FES and voluntary efforts with motor assistance and resistance as needed is promising for the development of upper or lower body FES rehabilitation methods that fit the needs and abilities of a broader range of people. It was shown in [53] that a combination of electrical stimulation and voluntary contribution may allow stroke patients to achieve and maintain functional improvements. Chapter 4 seeks to switch between FES and motor control depending on the calculated FES control input and desired direction of movement (denoted as upper level switching), in addition to switching the stimulation location within a single muscle group (denoted as lower level switching). While FES-induced exercises have been a topic of research for decades, most research has ignored the loss of control authority associated with saturating the stimulation control input, which is common practice for participant comfort. The level of stimulation needed to invoke the desired movement often rises above the comfort threshold (i.e., the

saturation point), especially as the person fatigues over time. Moreover, some people have low comfort thresholds due to hyper-sensitivity associated with their movement disorder. In FES-induced exercises, an electric motor is often used to control the system regions of motion where muscles do not efficiently produce torque [47]; however, in this dissertation (Chapters 4 and 6) and in [54, 55], the motor is introduced to assist in FES regions as well, but only as needed when the FES control input saturates at the comfort threshold.

Patients with a higher level of muscle control benefit less from following a precise trajectory [51, 56]. Assist-as-needed controllers are implemented on some rehabilitation robots so that the motor assists in movement only when the person is not meeting a range of desired performance specifications, rather than a precise performance metric [51, 57–61]. In Chapter 5, as in [62], a cycle-rider system can discontinuously switch between assistive (FES and motor control), uncontrolled (only volitional input from the subject), and resistive (motor control) modes, based on cadence, in addition to position-based switching to determine which muscle group or motor to stimulate when in the assistive mode. Chapter 6 implements a similar 3-mode control scheme; however, the crank of the cycle is decoupled so the non-dominant leg (in the case of hemiparesis) tracks cadence while the dominant side tracks position to stay around 180 degrees out of phase from the non-dominant leg. All previous works referenced focus on one switching signal and are either time- or position-based, whereas this dissertation will highlight FES exercises with multiple switching objectives that are based on a threshold for the control input and cadence. In contrast to state-based switching, in [63], FES is discontinuously switched on and off based on electroencephalogram (EEG) signals; however, this is also a single switching signal and a stability analysis for the controller is not included. An FES system that switches between FES, volition, and a motor, with multiple switching signals for objectives within each mode, has yet to be established.

Oftentimes one side of the body is affected more than the other, a condition known as hemiparesis. When a person with hemiparesis pedals a traditional single-crank cycle, their dominant side can mask the weakness in their impaired side due to the pedal coupling of traditional crank mechanisms. While the person may meet their tracking goals (e.g., pedaling at a desired cadence), challenging the impaired side may improve hemiparesis. Moreover, primarily using the stronger side may create a larger gap in their existing bilateral asymmetry. Thus, cycling for rehabilitation of disorders involving hemiparesis should promote equal contribution from the dominant and impaired limbs [17]. Controllers with a goal of balancing torques on either side of a single-crank FES-cycle have been used to reduce muscular imbalances associated with hemiparesis [64–66]. Other FES-cycling studies have used split-crank cycles to address muscular asymmetries [18–21, 67, 68], as in Chapter 6 of this dissertation. However, only [21, 67, 68] have focused on closed-loop control of the cycle-rider system, and aside from the prolegomenous work in [67, 68], which are the basis of Chapter 6 in this dissertation, no previous split-crank cycling studies have used FES to control the rider’s muscles.

1.3 Outline of the Dissertation

In Chapter 2, a generic dynamic model for a combined human and motorized testbed system is presented to be used in the subsequent chapters, and can be applied to either the upper or lower body. Relevant system properties and assumptions are given.

In Chapter 3, a novel position-based switching strategy is presented for stimulation of the biceps brachii. Preliminary experiments measured isometric torque data produced by the stimulation of six electrodes placed across the biceps brachii at eleven different elbow angles. Results from the preliminary experiments were then used to determine the most efficient elbow angles for which to stimulate each electrode during a biceps curl. Two switching strategies are presented, one of which may discontinuously switch

stimulation input to the single most effective electrode every ten degrees, and the other which continuously varies stimulation intensity sent to any number of the six electrodes that can produce a torque above a specified threshold but may discontinuously switch the set of electrodes used every ten degrees. For both methods, a robust sliding mode controller determines the stimulation intensity, Lyapunov methods prove stability, and experimental results demonstrate feasibility and robustness.

Chapter 4 presents the addition of a motor subsystem to both yield tracking control when the FES sliding mode controller saturates at a comfort threshold and enable control when the stimulated muscle cannot contribute positive torque. For the biceps curl experimental setup, full motor control occurs during negative desired velocities (i.e., forearm lowering). A common Lyapunov function is again used to prove exponential convergence of the tracking error.

Rather than switching stimulation within a single muscle group, Chapter 5 presents a strategy to switch amongst multiple muscle groups, which applies directly to cycling. In this chapter, switching also occurs between an assistance mode that consists of both FES and motor input, a passive mode where the subject pedals freely with no FES or motor contribution, and a resistance mode that consists of only motor control. Unlike Chapters 3 and 4, volitional forward torque contribution is permitted throughout the exercise and the control objective is two-sided due to the upper and lower thresholds defining the passive mode and the two error systems. A common Lyapunov function proves exponential convergence to the desired passive region from both of the controlled modes (i.e., assistive and resistive).

Chapter 6 combines switching concepts from Chapters 4 and 5, and implements them on a split-crank cycle, where the two sides of the cycle-rider system are decoupled and have different control objectives.

CHAPTER 2 SYSTEM MODEL

This section is focused on the development of the dynamics of a generic control system consisting of FES of a limb to assist in the operation of a motorized testbed, and will be used for the subsequent results in Chapters 3, 4, 5, and 6. The dynamics of a motorized FES system are modeled as in [69] as

$$\tau_{testbed}(\dot{q}(t), \ddot{q}(t), t) + \tau_{human}(q(t), \dot{q}(t), \ddot{q}(t), t) = \tau_e(t) \quad (2-1)$$

where $q : \mathbb{R}_{\geq 0} \rightarrow \mathcal{Q}$ denotes the measurable testbed joint angle and $\mathcal{Q} \subseteq \mathbb{R}$ denotes the set of all joint angles. The measurable angular velocity is denoted by $\dot{q} : \mathbb{R}_{\geq 0} \rightarrow \mathbb{R}$, and the unmeasured angular acceleration is denoted by $\ddot{q} : \mathbb{R}_{\geq 0} \rightarrow \mathbb{R}$. Effects of inertia, friction, and disturbances in the motorized testbed are denoted by $\tau_{testbed} : \mathbb{R} \times \mathbb{R} \times \mathbb{R}_{\geq 0} \rightarrow \mathbb{R}$; $\tau_{human} : \mathcal{Q} \times \mathbb{R} \times \mathbb{R} \times \mathbb{R}_{\geq 0} \rightarrow \mathbb{R}$ denotes the effects of the person's passive limb dynamics, active muscle contractions, and disturbances from the human, and $\tau_e : \mathbb{R}_{\geq 0} \rightarrow \mathbb{R}$ denotes the torque applied by the electric motor about the crank or joint axis of the testbed. The total torque from the testbed $\tau_{testbed}(\dot{q}(t), \ddot{q}(t), t)$ can be modeled as

$$\tau_{testbed}(\dot{q}(t), \ddot{q}(t), t) \triangleq J_{testbed}\ddot{q}(t) + \tau_b(\dot{q}(t)) + d_{testbed}(t), \quad (2-2)$$

where $J_{testbed} \in \mathbb{R}_{>0}$ is the unknown inertia of the rotating testbed arm, $\tau_b : \mathbb{R}_{>0} \rightarrow \mathbb{R}$ denotes the torque due to viscous damping in the testbed, and $d_{testbed} : \mathbb{R}_{\geq 0} \rightarrow \mathbb{R}$ denotes unknown disturbances such as changes in the load. The net torque by the human $\tau_{human}(q(t), \dot{q}(t), \ddot{q}(t), t)$ can be modeled as

$$\tau_{human}(q(t), \dot{q}(t), \ddot{q}(t), t) = \tau_p(q(t), \dot{q}(t), \ddot{q}(t)) - \tau_{vol}(t) - \tau_m(q(t), \dot{q}(t), t) + d_{human}(t), \quad (2-3)$$

where $\tau_p : \mathcal{Q} \times \mathbb{R} \times \mathbb{R} \rightarrow \mathbb{R}$ denotes the passive torques by the human, $\tau_{vol} : \mathbb{R}_{\geq 0} \rightarrow \mathbb{R}$ and $\tau_m : \mathcal{Q} \times \mathbb{R} \times \mathbb{R}_{\geq 0} \rightarrow \mathbb{R}$ denote the torques produced by volitional and FES induced muscle contractions, respectively, and $d_{human} : \mathbb{R}_{\geq 0} \rightarrow \mathbb{R}$ denotes the disturbances from the human (e.g., spasticity or changes in load). The passive torques $\tau_p(q(t), \dot{q}(t), \ddot{q}(t))$ applied by the human are

$$\tau_p(q(t), \dot{q}(t), \ddot{q}(t)) = M_p(q(t)) \ddot{q}(t) + V(q(t), \dot{q}(t)) \dot{q}(t) + G(q(t)) + P(q(t), \dot{q}(t)), \quad (2-4)$$

where $M_p : \mathcal{Q} \rightarrow \mathbb{R}_{>0}$, $V : \mathcal{Q} \times \mathbb{R} \rightarrow \mathbb{R}$, $G : \mathcal{Q} \rightarrow \mathbb{R}$, and $P : \mathcal{Q} \times \mathbb{R} \rightarrow \mathbb{R}$, denote the inertial, centripetal-Coriolis, gravitational, and passive viscoelastic tissue forces, respectively. The motor torque $\tau_e : \mathbb{R}_{\geq 0} \rightarrow \mathbb{R}$ is defined as

$$\tau_e(t) = B_e u_e(t), \quad (2-5)$$

where $B_e \in \mathbb{R}_{>0}$ is the electric motor control constant relating input current to output torque and the subsequently designed current input applied to the motor is denoted as $u_e : \mathbb{R}_{\geq 0} \rightarrow \mathbb{R}$.

2.1 Switched Muscle Subsystem

Consider $w \in \mathbb{N}$ distinct electrode channels that are placed either within a single muscle group or on multiple muscle groups. Stimulation is applied to each electrode in predefined regions of \mathcal{Q} , where each combination of channels is characterized by an Euler-Lagrange subsystem. The portion of the desired trajectory over which a particular electrode channel is stimulated is denoted by $Q_m \subset \mathcal{Q}$, where $m \in \mathcal{M}$ denotes the m^{th} channel, $\mathcal{M} \triangleq \{1, 2, \dots, w\}$ denotes a finite indexed set of all channels, and

$Q_M \triangleq \bigcup_{m \in \mathcal{M}} Q_m$ denotes the range of angles corresponding to any stimulation channel's contribution to torque production. The torque due to muscle contractions is generated by the summation of the subject's volitional effort and the application of a potential field across a muscle, and is defined as

$$\tau_m(q(t), \dot{q}(t), t) = \sum_{m \in \mathcal{M}} B_m(q(t), \dot{q}(t), t) u_m(t), \forall m \in \mathcal{M}, \quad (2-6)$$

where the subsequently designed FES control input to the muscle is denoted by $u_m(t)$. where the uncertain muscle control effectiveness, denoted by $B_m : \mathcal{Q} \times \mathbb{R} \rightarrow \mathbb{R}_{>0}$, $\forall m \in \mathcal{S}$, relates the stimulation intensity applied to the m^{th} stimulation channel to the torque produced by the activated sensory-motor structures (cf. [25, 70]), and can be expanded as

$$B_m(q(t), \dot{q}(t), t) = \lambda_m(q(t)) \psi_m(q(t), \dot{q}(t)) \cos(\beta_m(q(t))) T_m(q(t)), \forall m \in \mathcal{M}, \quad (2-7)$$

where $\lambda_m : \mathcal{Q} \rightarrow \mathbb{R}_{>0}$ denotes the uncertain moment arm of each muscle group's force about its respective joint, $\psi_m : \mathcal{Q} \times \mathbb{R} \rightarrow \mathbb{R}_{>0}$ denotes the uncertain nonlinear function relating stimulation intensity to the force output by the muscle, and $\beta_m : \mathcal{Q} \rightarrow \mathbb{R}$ denotes the uncertain muscle fiber pennation angle. The function $T_m : \mathcal{Q} \rightarrow \mathbb{R}$ denotes the torque transfer ratio between the i^{th} stimulation channel and the axis of rotation [47, 71], calculated in subsequent chapters based on the application, using a known function of the limb position.

2.2 Combined Muscle-Motor System

Substituting (2-2)-(2-6) into (2-1) yields

$$M(q(t))\ddot{q} + V(q(t), \dot{q}(t))\dot{q}(t) + G(q(t)) \quad (2-8)$$

$$+P(q(t), \dot{q}(t)) + \tau_b(\dot{q}(t)) + \tau_d(t) = \sum_{m \in \mathcal{M}} B_m(q(t), \dot{q}(t), t)u_m(t) + B_e u_e(t) + \tau_{vol}(t),$$

where $M : \mathcal{Q} \rightarrow \mathbb{R}$ is defined as the summation $M(q(t)) \triangleq J_{testbed}(q(t)) + M_p(q(t))$, $\tau_d : \mathbb{R}_{\geq 0} \rightarrow \mathbb{R}$ is defined as the summation $\tau_d(t) \triangleq d_{testbed}(t) + d_{human}(t)$. A combination of w channels allows for 2^w possible FES-only subsystems, including the empty set for uncontrolled activity. Since motor control could be added during stimulation or as the only actuator and preserving one subsystem as uncontrolled, there are a total of 2^{w+1} possible subsystems, consisting of FES, motor, both, or neither. The parameters in (2-8) capture the torques that affect the dynamics of the combined muscle-motor system, but the exact value of these parameters are unknown for each human and testbed. However, the designed FES and motor controllers in the subsequent chapters only require known bounds on the aforementioned parameters. Thus, the system model in (2-8) has the following properties [47]:

Property 1. $c_{M1} \leq M(q(t)) \leq c_{M2}$, where $c_{M1}, c_{M2} \in \mathbb{R}_{>0}$ are known constants.

Property 2. $|V(q(t), \dot{q}(t))| \leq c_V |\dot{q}|$, where $c_V \in \mathbb{R}_{>0}$ is a known constant.

Property 3. $|G(q(t))| \leq c_G$, where $c_G \in \mathbb{R}_{>0}$ is a known constant.

Property 4. $|P(q(t), \dot{q}(t))| \leq c_{P1} + c_{P2} |\dot{q}|$, where $c_{P1}, c_{P2} \in \mathbb{R}_{>0}$ are known constants.

Property 5. $|\tau_b(\dot{q}(t))| \leq c_b |\dot{q}|$, where $c_b \in \mathbb{R}_{>0}$ is a known constant.

Property 6. $|\tau_d(t)| \leq c_d$, where $c_d \in \mathbb{R}_{>0}$ is a known constant.

Property 7. The time derivative of the inertia matrix and the centripetal-Coriolis matrix are skew symmetric, $\frac{1}{2}\dot{M}(q(t)) = V(q(t), \dot{q}(t))$.

Property 8. The unknown moment arm of each muscle group about their respective joint is non-zero, (i.e., $\lambda \neq 0$) [72].

Property 9. The auxiliary term ψ in (2-7) depends on the force-length and force-velocity relationships of the muscle being stimulated and is upper and lower bounded

by known positive constants, $c_\psi, c_\Psi \in \mathbb{R}_{>0}$, respectively, provided the muscle is not fully extended [73] or contracting concentrically at its maximum shortening velocity [45].

Property 10. The function relating the unknown muscle fiber pennation angle to output torque is never zero, (i.e., $\cos(\beta_m(q(t))) \neq 0$) [74].

Property 11. By Properties 8-10, B_m has a lower bound for all m , and thus, $c_m \leq B_m(q(t), \dot{q}(t), t) \leq c_M$, where $c_m, c_M \in \mathbb{R}_{>0}$.

Property 12. $c_e \leq B_e \leq c_E$, where $c_e, c_E \in \mathbb{R}_{>0}$.

Assumption 1. The subject only contributes positive volitional torque and the volitional torque output is bounded due to physical limitations, such that $0 \leq \tau_{vol}(t) \leq c_{vol}$, where $c_{vol} \in \mathbb{R}_{>0}$.

CHAPTER 3 VARYING THE POINT OF STIMULATION WITHIN A SINGLE MUSCLE GROUP: A SWITCHED SYSTEMS APPROACH

In this chapter, the biceps brachii is used as an example muscle group where the muscle geometry significantly changes with limb motion. FES contracts the biceps brachii and controls the movement of the forearm in performing a set of biceps curls. The location of stimulation is switched along the biceps brachii based on forearm angle, which is motivated by the fact that the force induced by a static electrode may change as the muscle geometry changes (i.e., muscle lengthening or shortening). Experimental results, depicted in Figure 3-1, suggest that switching stimulation across multiple electrodes along the biceps brachii based on the resulting torque effectiveness results in more efficient movements than using the same electrode throughout. Two methods for switching amongst w stimulation channels are presented. The first method switches to the channel which can produce the most torque at a set number of positions along the desired trajectory, such that only one electrode channel is activated at a time. In the second switching method, all electrodes which are capable of producing torque above a certain threshold at each measured angle are activated. As in [38] and [39], a switched robust sliding mode controller is designed for the FES muscle input. The controller is used to track a desired angular position trajectory of the forearm about the elbow. Global exponential tracking is proven using a common Lyapunov function.

3.1 Switching Methods

The subset of all angular positions to stimulate each electrode is defined as $Q_m \triangleq \{q(t) \in Q \mid q_{i,low} \leq q(t) \leq q_{i,high}\}$, where $m \in \mathcal{M}$ denotes the m^{th} channel and $\mathcal{M} \triangleq \{1, 2, \dots, w\}$ denotes a finite indexed set of all channels. In this development, the motor is not considered so $\bigcup_{m \in \mathcal{M}} Q_m = Q_M = Q$. Let $Q_\tau \subset Q$ denote the subset of all angles for which isometric torque measurements were taken. The bounds on q which define Q_m are denoted by $q_{m,low}$ and $q_{m,high}$ and are subsequently designed based on the switching protocol.

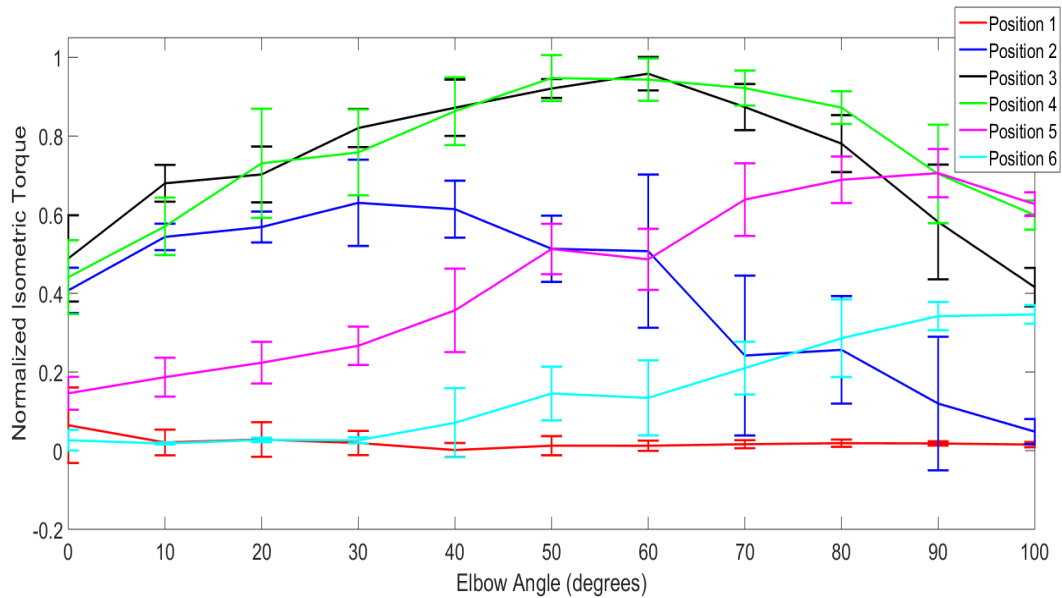


Figure 3-1. Isometric torques produced by stimulating 6 electrodes (channels) across the biceps brachii were measured at every 10 degrees of elbow flexion from 0 to 100 degrees in a healthy normal volunteer for five trials. Channel 1 refers to the most distal electrode and Channel 6 to the most proximal. Each data point depicts the mean isometric torque produced by the stimulated channel over five trials, normalized by the maximum torque generated during the protocol, with error bars showing the range of measurements over the five trials. The graph depicts that torque production depends on both electrode location and elbow angle. Channel 1 never reached a normalized isometric torque greater than $\varepsilon = 0.25$ and is excluded from experiments for this particular participant (see Figure 3-2).

3.1.1 Single Electrode Switching

During single electrode switching, $q_{m,low}$ and $q_{m,high}$ are defined as

$$q_{m,low} = q_{\tau,m} - \theta,$$

$$q_{m,high} = q_{\tau,m} + \theta,$$

where $\theta \in \mathbb{R}_{>0}$ is half of the selected interval between angles for which isometric torque was measured, and $q_{\tau,m} \in Q_{\tau}$ are any angles for which the m^{th} channel on average produced more isometric torque than any other channel, i.e.,

$$q_{\tau,m} \triangleq q(t) \in Q_{\tau} \mid \tau_m(q(t)) = \max_{m \in \mathcal{M}} (\tau_m(q(t))),$$

where τ_m is the normalized isometric torque produced by the m^{th} channel, averaged over all trials in preliminary experiments, which was measured a priori every 2θ degrees throughout a defined biceps curl. Trials depicted in Figure 3-1 used $\theta = 5^\circ$.

3.1.2 Multi-Electrode Switching

During the developed method for multi-electrode switching, the upper and lower limits, $q_{m,low}$ and $q_{m,high}$, are defined as

$$q_{m,low} = q(t) \in Q_{\tau} \mid \tau_m(q(t)) < \varepsilon, \tau_m(q(t) + 2\theta) > \varepsilon,$$

$$q_{m,high} = q(t) \in Q_{\tau} \mid \tau_m(q(t)) < \varepsilon, \tau_m(q(t) - 2\theta) > \varepsilon.$$

where the threshold, $\varepsilon \in (0, 1)$, is a design constant. The torque transfer ratio from each stimulation channel to the axis of rotation, T_m , is defined as

$$T_m(q(t)) \triangleq p_{1,m} + p_{2,m}q(t) + p_{3,m}q^2(t) + p_{4,m}q^3(t) + p_{5,m}q^4(t), \quad q(t) \in Q_m, \quad (3-1)$$

where $p_{1,m}, p_{2,m}, p_{3,m}, p_{4,m}, p_{5,m} \in \mathbb{R}_{\geq 0}$, $m \in \mathcal{M}$ are known constants selected to best approximate (in a least-squares sense) a continuous curve to a finite number of pre-measured torque effectiveness ratios, $r_m, \forall m \in \mathcal{M}$, defined as

$$r_m(q(t)) \triangleq \begin{cases} \frac{\tau_m}{\tau_\Sigma} & \tau_m > \varepsilon \\ 0 & \tau_m \leq \varepsilon \end{cases}, \quad q(t) \in Q_\tau,$$

where τ_Σ is the sum of measured isometric torques produced at the given angle only by channels with a normalized isometric torque above the constant threshold, ε (i.e., $\tau_\Sigma = \sum \tau_m, \tau_m \geq \varepsilon$). Since the fifth order polynomial, $T_m(q(t))$, is only valid during elbow angles that correspond to stimulation, it is only calculated based on r_m values for which $q \in Q_m$. An example plot summarizing five trials of normalized torque data, τ_m , for one participant is shown in Figure 3-1, and r_m (points) and T_m (curves) are depicted in Figure 3-2. The torque effectiveness polynomials, $T_m(q(t))$, in Figure 3-2, represent the portion of total stimulation control input sent to each individual channel and the subset of activated channels at any given time designates the corresponding subsystem. Note that isometric torque can only be measured at a finite number of pre-determined angles, n , every 2θ degrees; hence, a least-squares fit is used to determine the torque production effectiveness (T_m) for all joint angles.

In this chapter, the electrical stimulation intensity applied to each electrode channel, $u_m(q(t), t)$, is defined as

$$u_m(q(t), t) \triangleq \sigma_m(q(t)) T_m(q(t)) k_m u_M(t), \quad m \in \mathcal{M}, \quad (3-2)$$

where $k_m \in \mathbb{R}_{\geq 0}$ is a gain constant and $\sigma_m(q(t)) \in \{0, 1\}$ is a piecewise left-continuous switching signal for each channel such that $\sigma_m(q(t)) = 1$ when $q(t) \in Q_m$ and $\sigma_m(q(t)) = 0$ when $q(t) \notin Q_m, m \in \mathcal{M}$. The subsequently designed FES control input is denoted by $u_M(t)$.

3.2 Control Development

The control objective is to track a desired forearm trajectory, quantified by the position tracking error, defined as

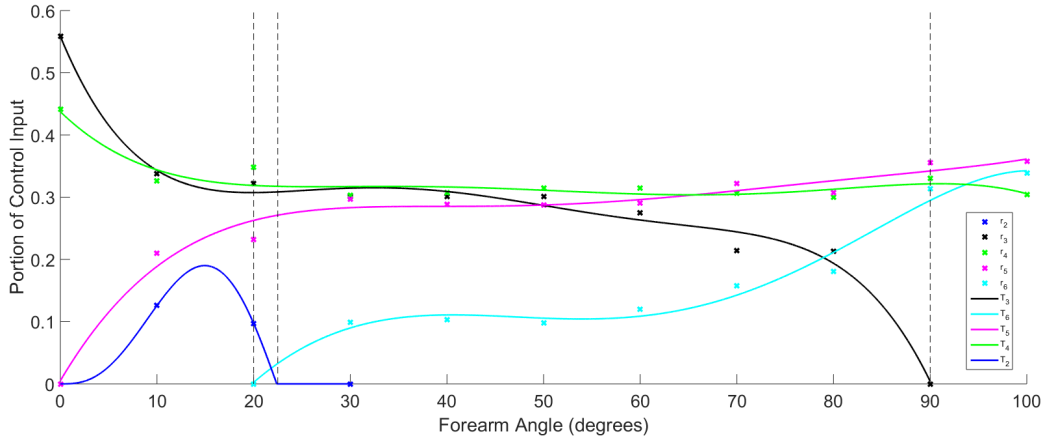


Figure 3-2. The proportion of total stimulation input sent to each electrode for all elbow angles (curves) for the same healthy normal volunteer in Fig. 3-1. The ratio of control input for each channel during multi-electrode stimulation is represented by the polynomials, $\{T_m\}$, which are fit to the data points, $\{r_m\}$, depicted in Figure 3-1. Each function, T_m , was also limited to positive values. The stimulated set of electrodes defines a subsystem, hence the vertical dotted lines indicate switching to a new subsystem.

$$e_1(t) \triangleq q_d(t) - q(t) \quad (3-3)$$

where $q_d : \mathbb{R}_{>0} \rightarrow \mathbb{R}$ is the desired forearm position, designed so its first and second derivatives exist, and are bounded. Without loss of generality, q_d is designed to monotonically increase, i.e., stopping or changing directions is not desired for the current study, which only focuses on motion that can be induced by stimulation of the biceps. To facilitate the subsequent development, an auxiliary tracking error $e_2 : \mathbb{R}_{>0} \rightarrow \mathbb{R}$ is defined as

$$e_2(t) \triangleq \dot{e}_1(t) + \alpha e_1(t), \quad (3-4)$$

where $\alpha \in \mathbb{R}_{>0}$ is a selectable constant gain. Taking the time derivative of (3-4), multiplying by M , adding and subtracting e_1 , using (2-8) and (3-3), and noting that the electric motor and voluntary contribution are not considered in this development yields

$$M\dot{e}_2(t) = \chi - e_1 - Ve_2 - B_M u_M(t), \quad (3-5)$$

where $B_M : Q \times \mathbb{R} \rightarrow \mathbb{R}$ is the combined switched control effectiveness, defined as

$$B_M(q(t), \dot{q}(t), t) = \sum_{m \in \mathcal{M}} B_m(q(t), \dot{q}(t), t) \sigma_m(q(t)) T_m(q(t)) k_m. \quad (3-6)$$

Also in (3-5), the auxiliary term $\chi : \mathbb{R}_{>0} \rightarrow \mathbb{R}$ is defined as

$$\chi \triangleq M(\ddot{q}_d + \alpha \dot{e}_1) + V(\dot{q}_d + \alpha e_1) + G - \tau_b - \tau_d + e_1. \quad (3-7)$$

From Properties 1-6, χ can be bounded as

$$|\chi| \leq c_1 + c_2 \|z(t)\| + c_3 \|z(t)\|^2, \quad (3-8)$$

where $c_1, c_2, c_3 \in \mathbb{R}_{>0}$ are known constants, $\|\cdot\|$ denotes the Euclidean norm, and the error vector $z \in \mathbb{R}^2$ is defined as $z(t) \triangleq \begin{bmatrix} e_1(t) & e_2(t) \end{bmatrix}^T$. Based on (3-5)-(3-8) and the subsequent stability analysis, the control input is designed as

$$u_M(t) \triangleq k_1 e_2 + k_2 (c_1 + c_2 \|z\| + c_3 \|z\|^2) \text{sgn}(e_2), \quad (3-9)$$

where $\text{sgn}(\cdot)$ denotes the signum function, and $k_1, k_2 \in \mathbb{R}_{>0}$ are constant control gains and c_1, c_2, c_3 were defined in (3-8). Substituting (3-9) into (3-5) yields

$$M\dot{e}_2 = \chi - e_1 - B_M [k_1 e_2 + k_2 (c_1 + c_2 \|z\| + c_3 \|z\|^2) \text{sgn}(e_2)]. \quad (3-10)$$

3.3 Stability Analysis

Theorem 3.1. *The controller in (3-9) yields global exponential tracking in the sense that*

$$\|z(t)\| \leq \sqrt{\frac{\lambda_2}{\lambda_1}} \|z(t_0)\| \exp\left[-\frac{1}{2}\lambda_s(t-t_0)\right], \quad (3-11)$$

$\forall t \in [t_0, \infty)$, where $t_0 \in \mathbb{R}_{>0}$ is the initial time, and $\lambda_s \in \mathbb{R}_{>0}$ is defined as

$$\lambda_s \triangleq \frac{1}{\lambda_2} \min(\alpha, c_m k_1), \quad (3-12)$$

where c_m is defined in Property 11, α in (3-4), and k_1 in (3-9), provided $k_2 \geq \frac{1}{c_m}$.

Proof. Let $V : \mathbb{R}^2 \rightarrow \mathbb{R}$ be a continuously differentiable, positive definite, common Lyapunov function candidate defined as

$$V(t) \triangleq \frac{1}{2} e_1^2(t) + \frac{1}{2} M e_2^2(t), \quad (3-13)$$

which satisfies the following inequalities:

$$\lambda_1 \|z(t)\|^2 \leq V(t) \leq \lambda_2 \|z(t)\|^2, \quad (3-14)$$

where $\lambda_1, \lambda_2 \in \mathbb{R}_{>0}$ are known positive constants defined as $\lambda_1 \triangleq \min\left(\frac{1}{2}, \frac{c_{M1}}{2}\right)$, $\lambda_2 \triangleq \max\left(\frac{1}{2}, \frac{c_{M2}}{2}\right)$. Because of the signum function in the closed-loop error system in (3-10) and the fact that B_M discontinuously varies over time as the forearm changes position, the time derivative of (3-13) exists almost everywhere (a.e.) and $\dot{V} \stackrel{a.e.}{\in} \tilde{V}$ [75] such that

$$\begin{aligned} \dot{V}(t) = & e_1(t) (e_2(t) - \alpha e_1(t)) + \frac{1}{2} \dot{M} e_2^2 - V e_2^2 + e_2(t) \chi(t) - e_2(t) e_1(t) \\ & - K [k_1 B_M e_2^2(t) + k_2 B_M (c_1 + c_2 \|z(t)\| + c_3 \|z(t)\|^2) e_2(t) \operatorname{sgn}(e_2(t))], \end{aligned} \quad (3-15)$$

where $K[\cdot]$ is defined in [76].

After some mathematical development, cancelling common terms, and using Properties 7 and 11, (3-15) can be upper bounded as¹

$$\dot{V}(t) \leq -\alpha e_1^2(t) + \chi(t) |e_2(t)| - c_m k_1 e_2^2(t) - c_m k_2 (c_1 + c_2 \|z(t)\| + c_3 \|z(t)\|^2) |e_2(t)|. \quad (3-16)$$

¹ There is an abuse of notation since \dot{V} is a set and the right hand side of the equation is a singleton. By this, it is meant that every member of \dot{V} is bounded by the right hand side.

Using (3–8), $\dot{\tilde{V}}$ is further upper bounded as

$$\dot{\tilde{V}}(t) \leq -\alpha e_1^2(t) - c_m k_1 e_2^2(t) - (c_m k_2 - 1) (c_1 + c_2 \|z(t)\| + c_3 \|z(t)\|^2) |e_2(t)|. \quad (3-17)$$

Provided the gain condition, $k_2 \geq \frac{1}{c_m}$, is satisfied,

$$\dot{\tilde{V}}(t) \leq -\alpha e_1^2(t) - c_m k_1 e_2^2(t). \quad (3-18)$$

Based on (3–12) and (3–18),

$$\dot{V}(t) \stackrel{a.e.}{\leq} -\lambda_s V(t), \quad (3-19)$$

where λ_s denotes a known positive bounding constant. Although the inequality does not exist at a discrete countable number of points, due to monotonicity of Lebesgue integration, (3–13) can be bounded as

$$V(t) \leq V(t_0) \exp[-\lambda_s(t - t_0)]. \quad (3-20)$$

Based on (3–13) and (3–14), the exponentially decaying envelope in (3–11) can now be developed for $\|z(t)\|$. □

Remark 3.1. The exponential decay rate λ_s represents the most conservative (i.e., smallest) decay rate for the closed-loop, switched error system. In practice, each subsystem has its own decay rate dependent on the lower bound of the corresponding B_m , but in the preceding stability analysis, c_m was used as the lower bound on B_m $\forall m \in \mathcal{M}$.

3.4 Experiments

Three sets of experiments were completed; two for single electrode switching protocol and one for the multi-electrode switching protocol. One female and nine male able-bodied participants, 20-45 years old, participated in the initial single electrode switching experiments, five of which participated in a follow up study that compared single electrode switching to a protocol that did not switch amongst electrodes. Lastly,

Participant 1 also participated in the experiments for multi-electrode switching. All participants gave written informed consent approved by the University of Florida Institutional Review Board. During the experiments, participants were instructed to relax and make no volitional effort to assist or inhibit the FES input.

3.4.1 Experimental Testbed

A customized testbed, depicted in Figure 3-3, was constructed using two aluminum plates for the forearm and upper arm, respectively, meeting and hinging at the elbow. The upper arm of the participant rested on a foam pad on one plate while the forearm was strapped to the second plate so that it rotated about the elbow hinge. An optical digital encoder was coupled at the elbow to continuously measure the angular position and velocity of the forearm. A 27 Watt, brushed, parallel-shaft gearmotor at the hinge was supplied current by a general purpose linear amplifier interfacing with the QUANSAR data acquisition hardware, which also measured the encoder signal.

Since a biceps curl only covers a limited range of elbow angles, the motor was used to bring the arm from the largest angle of testing (i.e., top of the biceps curl) back to the smallest angle of testing. A constant input to the motor was also used in the stimulation region to combat friction in the testbed, but was not a subsystem of nor had any effect on the analysis of the subsystems in the switched system. The contribution of the motor in the stimulation region is not sufficient to move the arm without FES. Stimulation region refers to the region when the biceps are contracting due to FES and the motor is also providing a small open-loop current to offset friction in the motor gear box. The controller was implemented on a personal computer running real-time control software.

A current-controlled stimulator (Hasomed RehaStim) delivered biphasic, symmetric, rectangular pulses to the participant's muscle via self-adhesive, PALS® electrodes.

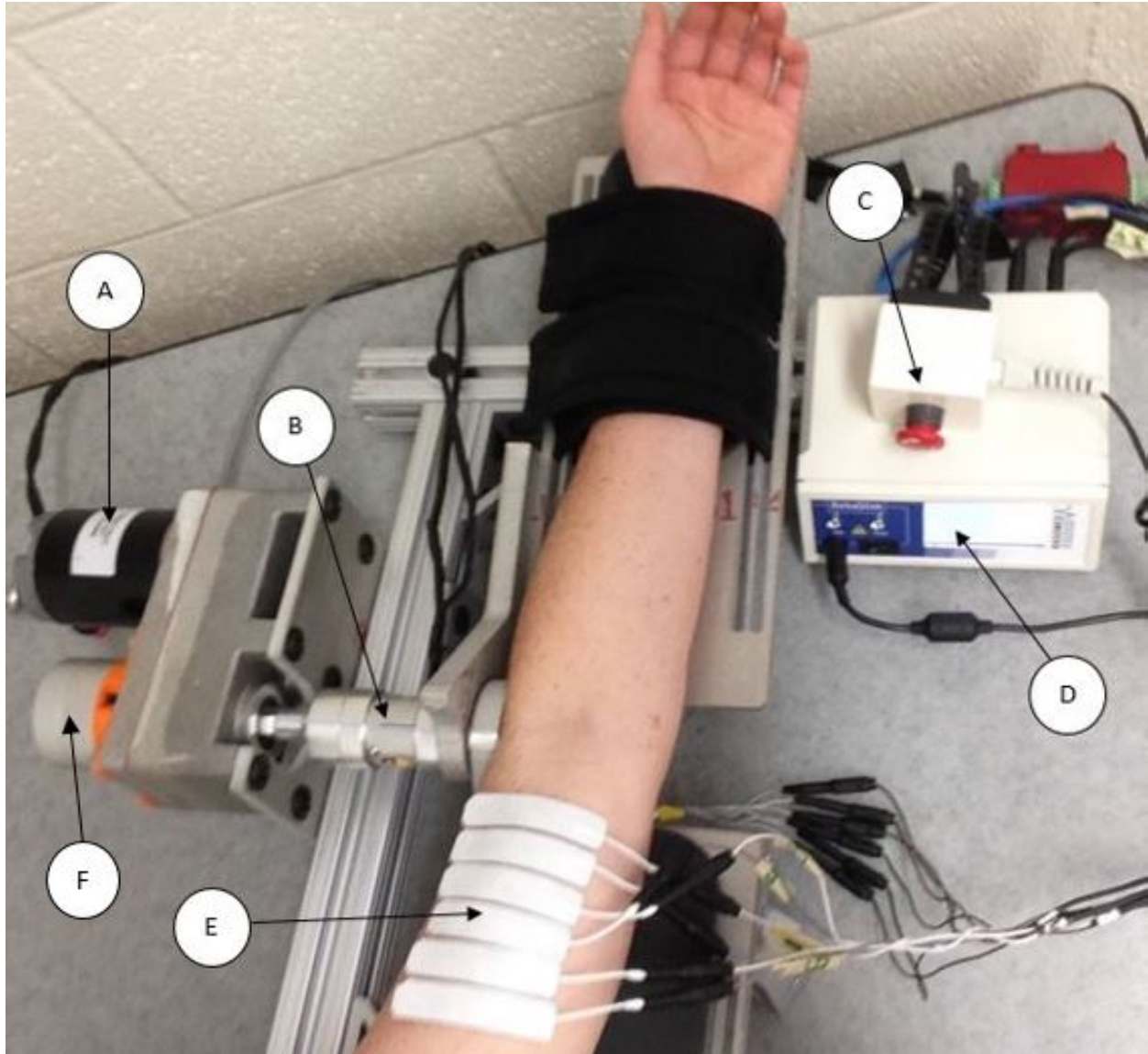


Figure 3-3. Setup for protocol, including (A) a brushed 12VDC motor, (B) torque sensor, (C) emergency stop button, (D) Hasomed neuromuscular electrical stimulator, (E) Axelgaard electrodes across the participant's biceps, and (F) optical encoder. Photo courtesy of the author. Gainesville, FL.

² Six 0.6" x 2.75" electrodes that are the six stimulation channels in this chapter's analysis were placed over the biceps between the elbow crease and acromion with the shared reference electrode on the shoulder. For consistent electrode placement despite varying arm lengths among participants, the first electrode was placed at 21% of the distance from the elbow crease to the acromion and the sixth electrode was placed at 50% of this distance for each of the participants. The other four electrodes were spaced evenly between the first and last, with small spaces between to avoid stimulation leak through the electrodes' gel. Based on comfort and torque levels, the pulse width was fixed at 90 μ s with a frequency of 35 Hz for each stimulation channel and the amplitude was determined by the developed feedback controller in (3-9), saturated at 55 mA for comfort, and commanded to the stimulator by the control software.

3.4.2 Single Electrode Switching Protocol

Prior to each experiment, a switching map similar to Figure 3-1 was developed. This data was then used to create a switching law for dynamic experiments so that the most effective electrode was stimulated throughout the arm's range of motion.

After the electrodes were placed on the participant's upper arm, the participant was comfortably seated with their arm properly resting in the testbed. The single electrode switching protocol was conducted on each arm with the arm order selected at random. The desired angular position, q_d , selected as

$$q_d(t) = \begin{cases} \frac{\pi t}{90} & t \leq 10 \\ \frac{\pi}{90} + \frac{7\pi}{36} [1 - \cos(\pi \frac{t-10}{10})] & t > 10 \end{cases},$$

and depicted in Figure 3-4, consists of a period where the motor brings the arm to 20 degrees, which was found to be the point where stimulation begins to produce a

² Surface electrodes for this study were provided compliments of Axelgaard Manufacturing Co., Ltd.

reasonable amount of torque by any electrode. The developed FES switching control was used to control the arm motion from 20 to 90 degrees. Motor control was used to bring the forearm from 90 degrees back to 20 degrees, where the trajectory was repeated four more times. The control gains introduced in (3-9), and the constant α introduced in (3-4), were adjusted to yield acceptable tracking performance with a range of values as follows: $\alpha \in [5, 10]$, $k_1 \in [12, 30]$, $k_2 = 1$. Note that while k_1 is much larger than k_2 , the portion of the control input due to k_2 also depends on the bounding terms of the dynamics (i.e., c_1, c_2, c_3).

3.4.3 Single Electrode Switching Results

All results represent data taken from the stimulation periods only (i.e., when $\dot{q} \geq 0$) since the performance of the motor-only section of the trajectory is not a product of the switching control design. Table 3-1 summarizes the overall position and velocity tracking performance of each participant during single electrode switching. Figure 3-4 depicts an example desired and actual trajectory and corresponding stimulation input for the right arm of Participant 1. Fig. 3-6 depicts the spread of mean position errors for all participants' arms, while Fig. 3-7 depicts the spread of mean velocity errors for all participants' arms during each of the five biceps curls of the first experiment.

The tracking results in Table 3-1 indicate the performance of the controller. A comparative study was also conducted to examine the effects of the developed electrode switching strategy compared to the typical single electrode strategy, where the channel that was most efficient for the majority of the biceps curl (as per pre-trial experiments depicted in Figure 3-1) was used throughout. The experiments were completed on a subset of the available participants from the original experiments. The left arm of Participant 1 was broken due to an unrelated event, and experiments on that arm were excluded from further experiments. The order of the two protocols was selected at random. During a pretrial test with the forearm angle at 30 degrees, the participant's

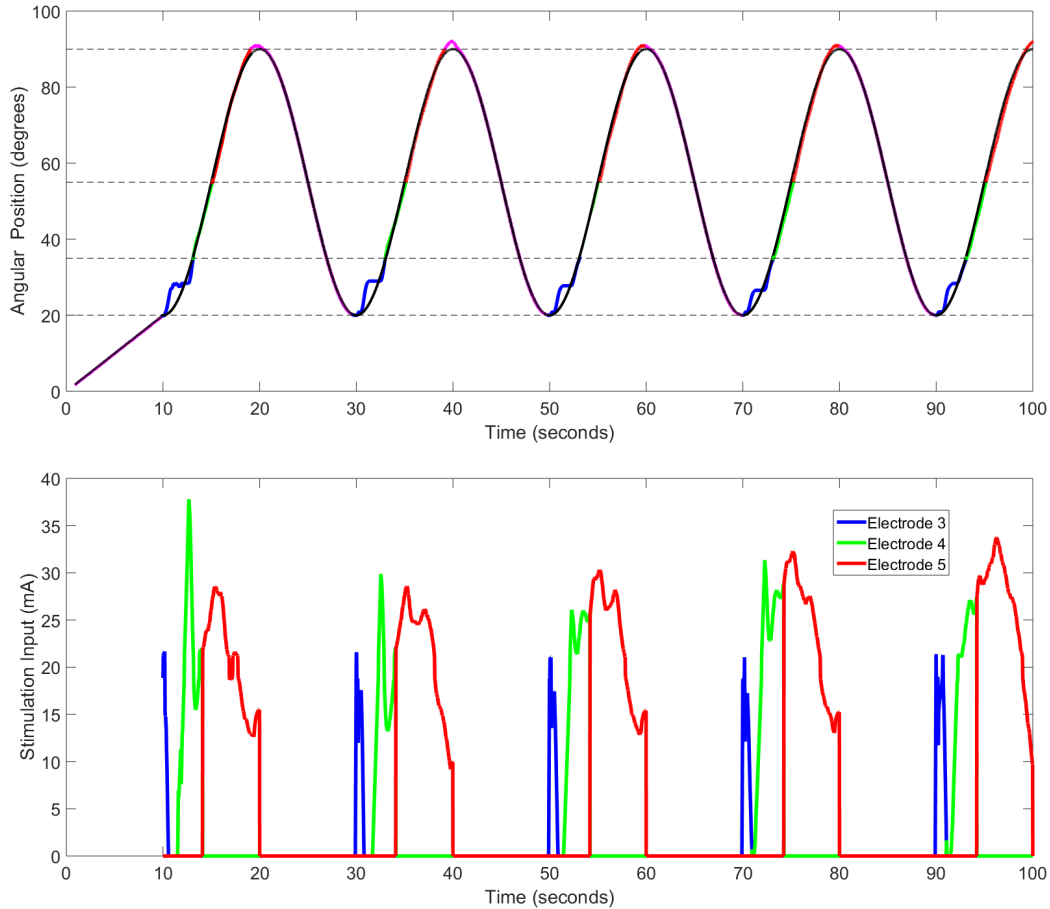


Figure 3-4. Desired and actual trajectory for Participant 1, right arm, for five biceps curls is depicted on top with the stimulation intensity below. The solid black line depicts the desired trajectory. The magenta line represents motor-only control regions. The blue, red, and green lines represent actual arm position for each stimulation channel in the FES control region. In general, switching could have occurred every 10 degrees with the option of six different channels. However, for this trial, switching only occurred at 35 degrees and 55 degrees between three channels, as determined by the pretrial isometric torque experiments. The dotted lines represent the two switching points as well as the angles for which the system changes from using the motor to stimulation, and vice versa. The position-based switching law is identical for all biceps curls in a trial.

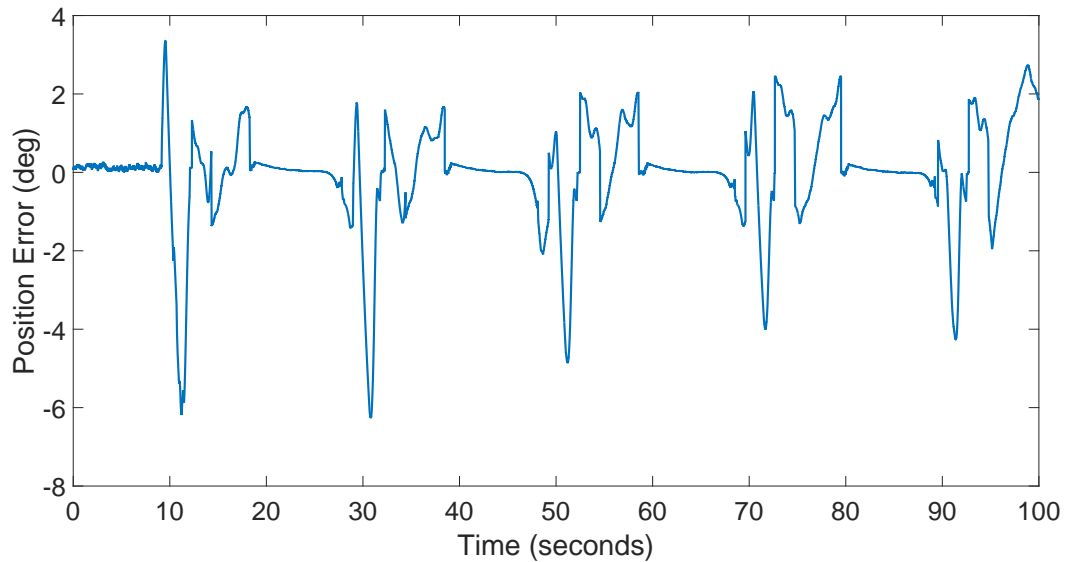


Figure 3-5. Position Error for the right arm of Participant 1 for the performance of 5 biceps curls by switching stimulation amongst 3 electrodes.

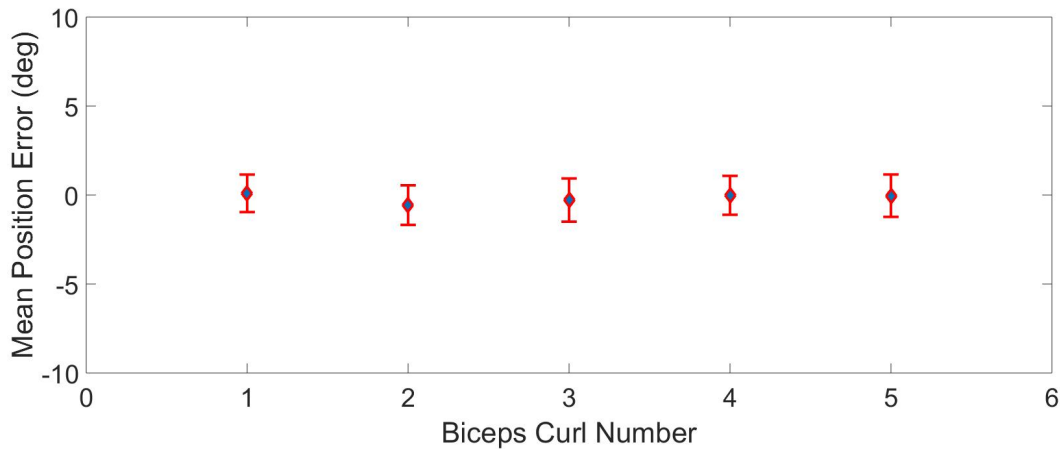


Figure 3-6. The spread of mean position error over the stimulation region of each of the five biceps curls in the first set of single electrode switching experiments, for all participants. The points represent the mean of all trials' mean position error. The error bars indicate the combined standard deviation for position error of all trials.

Table 3-1. Mean and standard deviation for position and velocity tracking error for all participants

Participant/arm	Mean position error, μ_{e_1} (deg)	St. dev. position error, σ_{e_1} (deg)	Mean velocity error, $\mu_{\dot{e}_1}$ (deg/s)	St. dev. velocity error, $\sigma_{\dot{e}_1}$ (deg/s)
1 Right	-1.61	1.53	-0.25	4.33
1 Left	-0.71	1.20	-0.34	4.70
2 Right	1.23	1.52	-0.32	5.03
2 Left	0.18	1.33	-0.39	5.42
3 Right	-0.51	0.91	-0.28	4.15
3 Left	-0.71	1.21	-0.62	5.90
4 Right	0.73	0.98	-0.26	4.88
4 Left	0.11	0.70	-0.40	4.86
5 Right	-0.54	0.76	-0.38	4.93
5 Left	-0.91	0.90	-0.50	5.67
6 Right	-0.32	0.76	-0.37	5.63
6 Left	-0.33	1.07	-0.42	7.19
7 Right	1.16	1.15	-0.28	7.37
7 Left	1.26	1.49	-0.32	7.42
8 Right	-0.37	1.37	-0.64	7.76
8 Left	-1.07	1.14	-0.61	4.58
9 Right	-0.89	1.58	-0.78	4.85
9 Left	-0.41	1.30	-0.60	4.90
Average	-0.21	1.17	-0.43	5.38

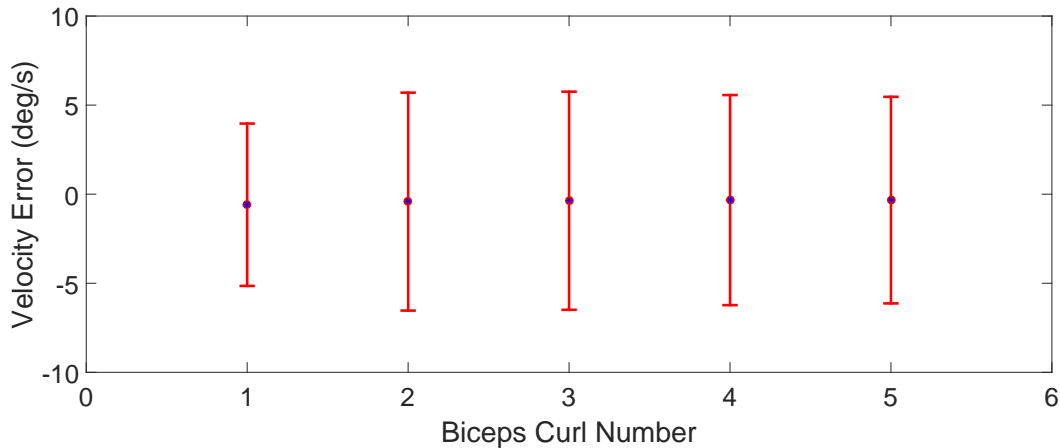


Figure 3-7. The spread of mean velocity error over the stimulation region of each of the five biceps curls in the first set of single electrode switching experiments, for all participants. The points represent the mean of all trials' mean velocity error. The error bars indicate the combined standard deviation for velocity error of all trials.

maximum voluntary torque was measured and the current amplitude which produced 30-40% of maximum voluntary torque was recorded, along with the isometric torque produced at that stimulation intensity. Next, the respective protocol (i.e., switching or single electrode) was performed for 10 biceps curls. A post-trial test included 20 seconds of constant stimulation at the same intensity and elbow angle as the pretrial. The torque-time integral (TTI), which measures sustained torque production was calculated and normalized by the pretrial maximum torque for both protocols as a commonly used method to quantify fatigue after exercise protocols [24]. The TTI was greater when stimulation was switched along the biceps than when a single electrode was stimulated, for all participants tested, with the exception of the right arm of Participant 2, as shown in Table 3-2. Position and velocity error, in Table 3-3, was also recorded during the second set of experiments to show that tracking performance was not compromised during switched stimulation.

Table 3-2. Difference in post-trial torque-time integral during comparison of single electrode switching vs single electrode non-switching, for five participants.

Participant/arm	TTI percent decrease	Overall average muscle current percent decrease	Average muscle current percent decrease per electrode
1 Right	12.7%	-1.22%	24.85%
2 Right	-33.5%	4.11%	6.68%
2 Left	14.0%	0.49%	6.92%
4 Right	25.4%	1.66%	24.74%
4 Left	38.4%	27.81%	48.97%
8 Right	28.8%	-13.39%	34.41%
8 Left	5.8%	-6.88%	21.80%
9 Right	0.0%	1.12%	1.65%
9 Left	31.0%	2.39%	15.51%
Average	13.6%	1.79%	20.61%

Table 3-3. Comparison of average RMS errors for position and velocity tracking during single electrode switching vs. single electrode stimulation.

	Mean	Std. deviation
Single electrode position RMS error (deg)	4.40	1.60
Switching position RMS error (deg)	4.12	1.76
Single electrode velocity RMS error (deg/s)	7.63	2.05
Switching velocity RMS error (deg/s)	7.54	1.69

3.4.4 Multi-Electrode Switching Protocol

Again, six electrodes were placed on the participant's upper arm and the participant was seated and the chair height was adjusted so that the table was chest height and the participant was comfortable with their arm resting in the testbed. The same protocol was conducted on each arm with desired angular position q_d selected as

$$q_d(t) = \begin{cases} \frac{4\pi}{9} \left(1 - \cos\left(\frac{\pi}{2} \frac{t-5}{T}\right)\right) + \frac{\pi}{9}, & t \geq 5 \\ 4t, & t < 5 \end{cases}$$

where the period, T , or amount of time for the forearm to move from 20 to 100 degrees, was 5 seconds. As done in the first set of experiments, the motor first brought the arm to 20 degrees.

The control gains introduced in (3-9), and the constant α introduced in (3-4) were adjusted to yield acceptable tracking performance with acceptable values for both the right and left arms as follows: $\alpha = 20$, $k_1 = 22$, $k_2 = 3$. Electrical stimulation was used to control the forearm from 20 to 100 degrees and the DC motor brought the forearm to the starting position (20 degrees). The channel to stimulate is based on angular position and was determined from previous results, as shown in Fig. 3-2, where $\varepsilon = 0.25$ was selected as the normalized torque threshold.

3.4.5 Multi-Electrode Switching Results

Fig. 3-8 depicts the participant's tracking performance during the protocol, showing that the actual trajectory closely followed the desired trajectory. The position tracking error of the participant's right arm had a mean of -1.05 deg with a standard deviation (SD) of 2.32 deg and the position tracking error of the participant's left arm had a mean of -0.29 deg with SD of 1.22 deg. The average velocity tracking error of the participant's right arm was 0.00 ± 3.19 deg/s and the average velocity tracking error of the participant's left arm was -0.03 ± 2.96 deg/s.

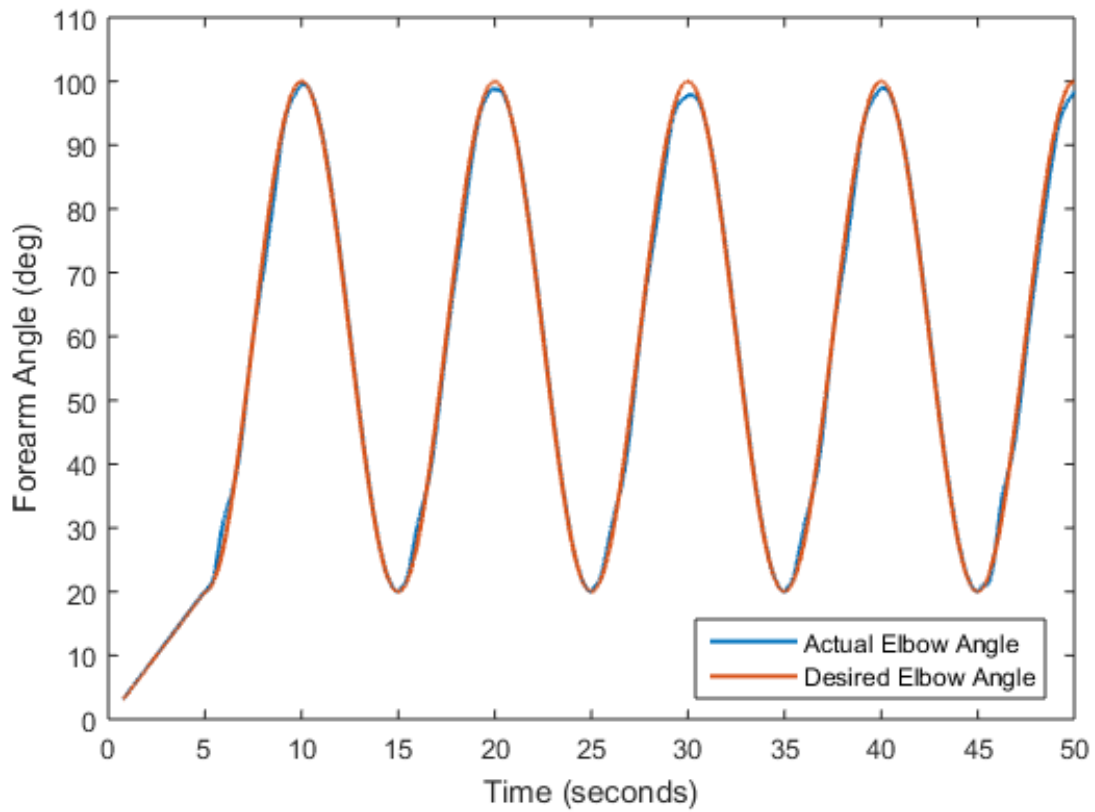


Figure 3-8. Actual and desired forearm position during a multi-electrode switching experiment of the left arm of Participant 1.

3.4.6 Discussion

Experimental results demonstrate the exponential tracking performance of the discontinuous switching controller designed in (3–9), for both switching protocols, despite parametric uncertainties (e.g., M , ς_i , φ_i , η_i , τ_b) and unknown disturbances (e.g., τ_d , $\dot{\tau}_d$). Errors are likely due to unmodeled effects such as electromechanical delay from activation time to time of muscle force production [77, 78]. The testbed joint also allowed small movements without opposing motor friction, which resulted in practically no additional position error but may have contributed to the larger velocity error. The range of position and velocity errors are similar to other published FES experiments [25]; however, the wider range of velocity errors are likely attributed to a bias in the tuning of control gains towards improving position error, as overshooting the arm’s comfortable range of motion presented a potential safety concern.

As shown in Table 3-2, switching amongst electrodes placed across the biceps brachii, according to the forearm angle and torque efficiency, resulted in less fatigue than stimulating one electrode throughout the biceps curls for all but one arm of one Participant. To quantify fatigue, the post-trial TTI was compared between single electrode switching and non-switching protocols, showing the potential impact of position-based switching of electrodes on fatigue. As shown in Table 3-3, the mean and standard deviation of RMS errors for position and velocity were very similar between switching and single-electrode protocols, showing that the novel switching approach tracks a desired trajectory just as well as single-electrode biceps curls, while reducing fatigue. The last two columns of Table 3-2 show the percent decrease in stimulation input overall, and the weighted average percent decrease per electrode. Although the overall percent decrease in stimulation intensity between single electrode and switching protocols does not correlate with the reduction in fatigue, column four shows that no single electrode receives as high of stimulation intensity for as long a duration as in single electrode

stimulation. Thus, no one part of the biceps is being fatigued as much as during single electrode stimulation.

Multi-electrode switching results show a much smaller range of velocity error than results from the single-electrode switching strategy, as shown in (3-9), which had a range of velocity standard deviation of 4.15 deg/s to 7.76 deg/s, compared to the 3.18 deg/s and 2.96 deg/s in the right and left arms of the participant for the multi-electrode switching strategy. While position errors are comparable, the velocity errors for Participant 1 were 0.00 ± 3.19 deg/s for the right arm and -0.03 ± 2.96 deg/s for the left arm during multi-electrode switching; whereas -0.25 ± 4.33 deg/s for the right arm and -0.34 ± 4.73 deg/s for the left arm were the velocity errors during single electrode switching for Participant 1. A comparison of velocity error for single- and multi-electrode switching for Participant 1's left arm is also shown in Figure 3-9. Moreover, the participant reported more comfort and more consistent motion during multi-electrode vs. single electrode switching. Note that control gains were similar to the experiments for the single-electrode switching controller but the desired velocity was twice as fast. Further experiments for the multi-electrode switching protocol would demonstrate reproducibility; however, results seem to favor multi-electrode switching, likely in part because the stimulation is further distributed across the biceps rather than fatiguing a small section at once.

Experiments on able-bodied participants validate the stability of the FES controller; however, the ultimate application for the developed controller is for people with neurological disorders, which may present additional challenges, such as variation in patient sensitivity to FES. Although unintentional contribution to muscle force production during able-bodied experiments is often a concern in the validity of FES research, the participants in this study were not shown the desired or actual trajectory so any unintentional contribution did not necessarily improve tracking and, thus, can be treated as a disturbance.

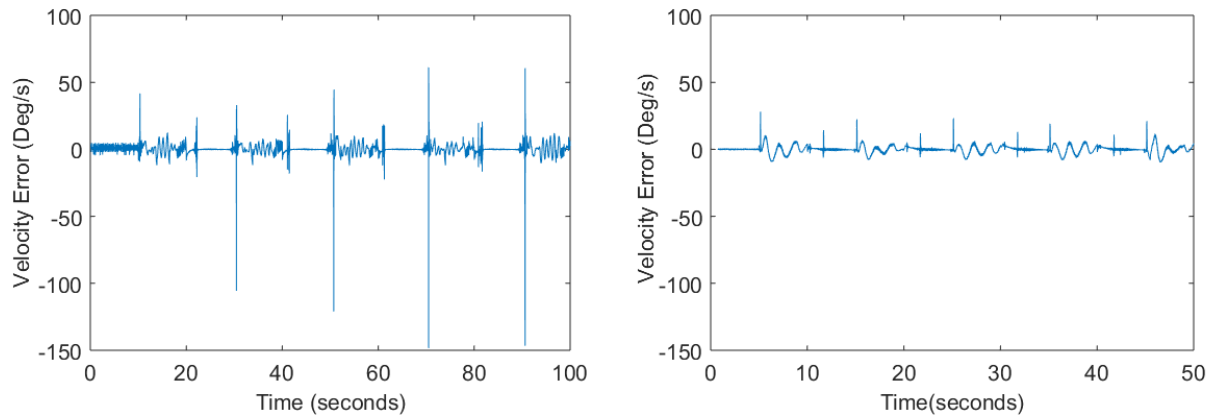


Figure 3-9. Comparison of single-electrode switching (left) to multi-electrode switching (right) for the left arm of Participant 1. For the multi-electrode switching, the initial velocity spike at the beginning of each biceps curl decreased and there is less fluctuation in comparison to single electrode switching. Note that the range of elbow angles for the five biceps curls are equal between the two protocols, although the target velocity was doubled in the multi-electrode switching (hence, half the experimental time).

3.5 Concluding Remarks

An uncertain, nonlinear model for FES forearm movement about the elbow was presented which includes the effects of a switched control input with unknown disturbances. Because the muscle geometry of the biceps changes as the forearm moves, switching strategies were developed that apply FES along the biceps brachii, based on the angular position of the forearm and torque production efficiency. In both cases, the switched sliding mode controller yields global exponential tracking of a desired forearm trajectory, provided sufficient gain conditions are satisfied. The control design of the single electrode switching method was validated in experiments with ten able-bodied participants, where average position and velocity tracking errors of -0.21 ± 1.17 deg and -0.43 ± 5.38 deg/s, respectively, were demonstrated. Switching also resulted in less fatigue, evaluated using a post-trial TTI. The results indicate that switching the stimulation channel with elbow position based on isometric torque data can reduce fatigue and yield similar tracking compared to traditional single channel stimulation methods. During experiments for the multi-electrode switching strategy, although the subsystems switched

discontinuously, the level of stimulation sent to each individual electrode was continuous for a larger portion of the biceps curl, resulting in a much smoother change in stimulation intensity for each individual channel than when switching between single electrodes. For one participant, the average position and velocity tracking errors were -1.05 ± 2.32 deg and 0.00 ± 3.19 deg/s for the right arm and -0.29 ± 1.22 deg and -0.03 ± 2.96 deg/s for the left arm, respectively. Of importance, significantly smoother forearm rotations were evident when compared to previous single electrode switching methods. Additional effects to be explored, such as arm orientation (vertical versus horizontal position) or muscle velocity conditions, may factor into the optimal stimulation pattern. While the protocol for multi-electrode switching resulted in less fluctuation in velocity errors and smoother movements than single electrode switching for Participant 1, it is necessary to complete experiments on more participants before declaring one method more effective than the other. Regardless, the development in this chapter shows that any chosen switching strategy that switches between multiple electrodes within a muscle will result in an overall stable system.

The results of this chapter establish a means for switching FES within a single muscle group. While the biceps brachii is used as an example muscle due to the nature of the muscle geometry changing with forearm orientation, the novel switching technique could be extended to any muscle group(s) that actuate a single joint to either maximize torque and/or reduce fatigue while producing consistent torque. Causing biceps contractions in both arms separately yields the opportunity for individuals with significant asymmetry in the upper limbs (e.g., hemiparetic stroke) to improve their strength balance. However, implementing this controller on people with neurological conditions may present additional challenges not considered here. Future efforts could also investigate more complex models that capture fatigue effects which could lead to altered switching conditions.

CHAPTER 4 SWITCHED MOTORIZED ASSISTANCE DURING SWITCHED FUNCTIONAL ELECTRICAL STIMULATION FOR BICEPS CURLS

In this chapter and in [54] and [55], FES of the biceps brachii, along with motor assistance when needed, is used to control the movement of the forearm in performing a set of biceps curls. The location of stimulation is switched among subsets of forearm angles along the biceps brachii based on forearm angle, as was done in Chapter 3 for multi-electrode switching. This is motivated by the fact that the force induced by a static electrode may change as the muscle geometry changes (i.e., muscle lengthening or shortening). The preliminary and comparative experiments from Chapter 3 suggest that switching stimulation across multiple electrodes along the biceps brachii based on the resulting torque effectiveness results in more efficient movements.

Often a threshold for stimulation intensity is selected for user comfort. As the user fatigues over time, the stimulation intensity necessary to induce movement increases and eventually reaches the threshold. Thus, an additional actuator is necessary to continue successful tracking and prolong the exercise. Rehabilitation robotics utilize motors to either assist or resist the user. In this chapter, a robotic system is used for two objectives: to track the desired trajectory during biceps brachii extension and to provide assistance during flexion when the muscle fatigues. Two switched robust sliding mode controllers are designed for the FES muscle input and for the motor input. Both controllers are used to track a desired angular position trajectory of the forearm about the elbow. Global exponential tracking is proven using a common Lyapunov function.

4.1 Control Development

The control objective is to track a desired forearm trajectory, quantified by the position tracking error, defined as

$$e_1(t) \triangleq q_d(t) - q(t), \quad (4-1)$$

where $q_d : \mathbb{R}_{>0} \rightarrow \mathbb{R}$ is the desired forearm position, designed so its first and second derivatives exist and are bounded. To facilitate the subsequent development, an auxiliary tracking error $e_2 : \mathbb{R}_{\geq 0} \rightarrow \mathbb{R}$ is defined as

$$e_2(t) \triangleq \dot{e}_1(t) + \alpha e_1(t), \quad (4-2)$$

where $\alpha \in \mathbb{R}_{>0}$ is a selectable constant gain. Taking the time derivative of (4-2), multiplying by M , adding and subtracting e_1 , and using (2-8) and (4-1) yields

$$M\dot{e}_2 = \chi - Ve_2 - B_M u_M - B_e u_e - e_1, \quad (4-3)$$

where B_M was defined in (3-6), u_M was introduced in (3-2), and the auxiliary term $\chi : Q \times \mathbb{R} \times \mathbb{R}_{\geq 0} \rightarrow 0$ is defined as

$$\chi \triangleq M(\ddot{q}_d + \alpha \dot{e}_1) + V(\dot{q}_d + \alpha e_1) + G - \tau_p - \tau_b - \tau_d + e_1.$$

Note that volitional torque is not encouraged (i.e., $\tau_{vol} = 0$) and any unintentional volitional torque is characterized as a disturbance. From Properties 1-6, χ can be bounded as

$$|\chi| \leq c_1 + c_2 \|z\| + c_3 \|z\|^2, \quad (4-4)$$

where $c_1, c_2, c_3 \in \mathbb{R}_{>0}$ are known constants, $\|\cdot\|$ denotes the Euclidean norm, and the error vector $z \in \mathbb{R}^2$ is defined as $z \triangleq \begin{bmatrix} e_1 & e_2 \end{bmatrix}^T$. Based on (4-3), (4-4), and the subsequent stability analysis, the control input to the muscle is designed as

$$u_M(t) \triangleq \Gamma \text{sat}_\beta(k_1 e_2 + (k_2 + k_3 \|z\| + k_4 \|z\|^2) \text{sgn}(e_2)), \quad (4-5)$$

where $\text{sat}_\beta(\cdot)$ is defined as $\text{sat}_\beta(\kappa) \triangleq \kappa$ for $|\kappa| \leq \beta$ and $\text{sat}_\beta(\kappa) \triangleq \text{sgn}(\kappa)\beta$ for $|\kappa| > \beta$, where $\beta \in \mathbb{R}_{>0}$ is a design constant, and $\text{sgn}(\cdot) : \mathbb{R} \rightarrow [-1, 1]$ is the signum function,

$\{k_i\}_{i=1}^4 \in \mathbb{R}_{>0}$ are constant control gains, and $\Gamma : \mathbb{R}_{\geq 0} \rightarrow \{0, 1\}$ is a piecewise constant time-based switching signal, designed as

$$\Gamma(\dot{q}_d(t)) = \begin{cases} 1, & \dot{q}_d > 0 \\ 0, & \dot{q}_d \leq 0 \end{cases}, \quad (4-6)$$

specifying that stimulation is only sent to the muscle during positive motion, i.e., flexion, of the desired biceps curl trajectory. Note that desired velocity, rather than the actual velocity, was used to define Γ because it is desired that FES contributes (i.e., $\Gamma = 1$) throughout flexion. Once the motor begins assisting the muscle, it is activated until u_m decreases to the lower threshold denoted by $\gamma_j : \mathbb{R}_{\geq 0} \rightarrow \mathbb{R}_{\geq 0}$, which is initialized at $\gamma_1 \in \mathbb{R}_{>0}$, such that $\gamma_1 \leq \Gamma$. The threshold γ_j resets to γ_1 at the beginning of each biceps curl and updates every time it is reached, according to $\gamma_{j+1} = \rho\gamma_j$, where $j \in \mathbb{N}$ denotes the j^{th} time during the n^{th} biceps curl for which u_m decreases to γ_j after the FES control input u_m saturates at Γ . The selected constant $\rho \in (0, 1)$ denotes the amount that γ_j should decrease after each saturation. At the beginning of each biceps curl, the motor is not activated until u_m reaches Γ , and is again deactivated the next time that $u_m = \gamma_j$ or when a new biceps curl starts (i.e., when $\dot{q}_d > 0$). Let $T_{ext,n}, T_{flex,n} \in \mathbb{R}_{>0}$ denote the initial times during the n^{th} biceps curl for which $\dot{q}_d \leq 0$ and $\dot{q}_d > 0$.

The switched control input to the motor is designed as

$$u_e \triangleq \delta \left(k_{5,\Gamma} e_2 + (k_{6,\Gamma} + k_{7,\Gamma} \|z\| + k_{8,\Gamma} \|z\|^2) \text{sgn}(e_2) \right), \quad (4-7)$$

where $\{k_{i,\Gamma}\}_{i=5}^8 \in \mathbb{R}_{>0}$ are constant control gains and Γ , defined in (4-6), indicates which of two sets of control gains are implemented, correlating to forearm angle regions of FES and motor in combination and regions where only the motor is activated (i.e., extension). The switched signal, $\delta : \mathbb{R}_{\geq 0} \rightarrow [0, 1]$, is defined as

$$\delta = \begin{cases} 1, & u_M = \beta \\ 1, & \min(u_M) > \gamma_j, \forall t \in [T_{n,j}^u, T_{n,j}^l] \\ 0, & otherwise \end{cases}, \quad (4-8)$$

so that the motor controller is only used during extension and when the muscle stimulation reaches its saturation. Substituting (4-5) and (4-7) into (4-3) yields

$$\begin{aligned} M\dot{e}_2 = & \chi - V e_2 - e_1 - B_M \Gamma [\text{sat}_\beta (k_1 e_2 + (k_2 + k_3 \|z\| + k_4 \|z\|^2) \text{sgn}(e_2))] \\ & - B_e [\delta (k_{6,\Gamma} e_2 + (k_{7,\Gamma} + k_{8,\Gamma} \|z\| + k_{9,\Gamma} \|z\|^2) \text{sgn}(e_2))] . \end{aligned} \quad (4-9)$$

4.2 Stability Analysis

Let $V_L : \mathbb{R}^2 \rightarrow \mathbb{R}$ be a continuously differentiable, positive definite, common Lyapunov function candidate defined as

$$V_L(t) \triangleq \frac{1}{2} e_1^2 + \frac{1}{2} M e_2^2, \quad (4-10)$$

which satisfies the following inequalities:

$$\lambda_A \|z\|^2 \leq V_L \leq \lambda_B \|z\|^2, \quad (4-11)$$

where $\lambda_A, \lambda_B \in \mathbb{R}_{>0}$ are known positive constants defined as $\lambda_A \triangleq \min(\frac{1}{2}, \frac{c_M}{2})$, $\lambda_B \triangleq \max(\frac{1}{2}, \frac{c_M}{2})$.

Theorem 4.1. *When the motor is inactivated, $\delta = 0$ and $B_\sigma > 0$, the FES controller in (4-5) ensures exponential tracking such that*

$$\|z(t)\| \leq \sqrt{\frac{\lambda_B}{\lambda_A}} \|z(t_{n,1})\| \exp\left[-\frac{1}{2}\lambda_2(t - t_{n,1})\right], \quad (4-12)$$

$\forall t \in [t_{n,1}, t_{n,2})$, where $t_{n,1}, t_{n,2} \in \mathbb{R}_{>0}$ are defined as $t_{n,1} \triangleq \max(T_{flex,n}, T_{n,j}^l)$ and $t_{n,2} \triangleq \min(T_{ext,n}, T_{n,j+1}^u)$, respectively, and $\lambda_2 \in \mathbb{R}_{>0}$ is defined as

$$\lambda_2 \triangleq \frac{1}{\lambda_B} \min(\alpha, k_1), \quad (4-13)$$

provided the following gain conditions are satisfied:

$$k_2 \geq c_1, \quad k_3 \geq c_2, \quad k_4 \geq c_3. \quad (4-14)$$

where c_1, c_2, c_3 are introduced in (4-4).

Proof. The motor is inactivated when $\dot{q}_d > 0$ and the FES control input has not yet reached the selected comfort threshold Γ since either starting the current biceps curl or decreasing to the lower threshold. Because of the signum function in the closed-loop error system in (4-9), the time derivative of (4-10) exists almost everywhere (a.e.), and $\dot{V}_L \stackrel{a.e.}{\in} \dot{\tilde{V}}_L$ [75] such that

$$\begin{aligned} \dot{\tilde{V}}_L \stackrel{a.e.}{=} & e_1(e_2 - \alpha e_1) + \left(\frac{1}{2}Me_2^2 - V\right) e_2^2 + e_2\chi - e_2e_1 \\ & - K [B_\sigma c_\sigma^{-1} (k_1 e_2^2 + (k_2 + k_3 \|z\| + k_4 \|z\|^2) |e_2|)], \end{aligned} \quad (4-15)$$

where $K[\cdot]$ is defined in [76]. Upper bounding (4-15) using Property 7 and (4-4) results in

$$\dot{\tilde{V}}_L \stackrel{a.e.}{\leq} -\alpha e_1^2 - k_1 e_2^2 - (k_2 - c_1) |e_2| - (k_3 - c_2) |e_2| \|z\| - (k_4 - c_3) |e_2| \|z\|^2$$

where $K[\text{sgn}(\cdot)] = \text{SGN}(\cdot)$, such that $\text{SGN}(\cdot) = \{1\}$ if $(\cdot) > 0$, $[-1, 1]$ if $(\cdot) = 0$, and $\{-1\}$ if $(\cdot) < 0$. Since $\dot{V}_L \stackrel{a.e.}{\in} \dot{\tilde{V}}_L$, further upper bounding of the Lyapunov derivative, provided the gain conditions in (4-14) are satisfied, results in

$$\dot{V}_L \leq -\lambda_2 V_L(t), \quad (4-16)$$

where λ_2 is defined in (4-13). Using (4-11), the result in (4-12) can be obtained. \square

Theorem 4.2. *When the desired trajectory indicates flexion (i.e., $\dot{q}_d > 0$), but the FES control input in (6-4) is saturated, the motor controller in (4-7) ensures exponential tracking such that*

$$\|z(t)\| \leq \sqrt{\frac{\lambda_B}{\lambda_A}} \|z(T_{n,j}^u)\| \exp\left[-\frac{1}{2}\lambda_3(t - T_{n,j}^u)\right], \quad (4-17)$$

$\forall t \in [T_{n,j}^u, \min(T_{ext,n}, T_{n,j}^l)]$, where $T_{ext,n}$ and $T_{n,j}^l$ were previously defined, and $\lambda_3 \in \mathbb{R}_{>0}$ is defined as

$$\lambda_3 \triangleq \frac{1}{\lambda_B} \min(\alpha, k_{5,1}), \quad (4-18)$$

provided the following gain conditions are satisfied:

$$k_{6,1} \geq c_1 + c_\Sigma \Gamma, \quad k_{7,1} \geq c_2, \quad k_{8,1} \geq c_3. \quad (4-19)$$

where c_1, c_2, c_3 are introduced in (4-4), c_Σ in Prop. 1, and Γ in (6-4).

Proof. When the FES is activated, but has saturated at the upper threshold at least once since $T_{flex,n}$ or $T_{n,j-1}^l$, the motor is also activated so $\delta = 1$, $\beta = 1$, and $B_\sigma > 0$. Because of the signum function in the closed-loop error system in (4-9), the time derivative of (4-10) exists a.e., and $\dot{V}_L \stackrel{a.e.}{\in} \dot{V}_L$ [75] such that

$$\begin{aligned} \dot{V}_L \stackrel{a.e.}{=} & -\alpha e_1^2 + e_2 \chi - K \left[B_\sigma e_2 \left(\text{sat}_\Gamma \left(c_\sigma^{-1} (k_1 e_2 \right. \right. \right. \\ & \left. \left. \left. + (k_2 + k_3 \|z\| + k_4 \|z\|^2) \text{sgn}(e_2) \right) \right) \right] \\ & - K \left[k_{5,1} e_2^2 - (k_{6,1} \right. \\ & \left. \left. + k_{7,1} \|z\| + k_{8,1} \|z\|^2) |e_2| \right] \end{aligned} \quad (4-20)$$

Noting the definitions of $K[\cdot]$ and $\text{sat}_\Gamma(\cdot)$, (4-20) can be expressed as

$$\begin{aligned} \dot{\tilde{V}}_L \stackrel{a.e.}{=} & -\alpha e_1^2 + \chi e_2 - B_\sigma e_2 \Gamma - k_{5,1} e_2^2 \\ & - (k_{6,1} + k_{7,1} \|z\| + k_{8,1} \|z\|^2) |e_2|. \end{aligned} \quad (4-21)$$

After using (4-4) and Prop. 1, (4-21) can be upper bounded as

$$\dot{\tilde{V}}_L \stackrel{a.e.}{\leq} -\alpha e_1^2 - k_{5,1} e_2^2, \quad (4-22)$$

assuming the gain conditions in (4-19) are satisfied, the first of which is formed noting that $\gamma_j \leq \Gamma, \forall n$. Using (4-11) and (4-18), (4-17) can be obtained. \square

Theorem 4.3. *When the desired trajectory indicates extension (i.e., $\dot{q}_d \leq 0$), only the motor is activated (i.e., $\delta = 1, \beta = 0, B_\sigma = 0$), and the motor controller in (4-7) results in global exponential tracking in the sense that*

$$\|z(t)\| \leq \sqrt{\frac{\lambda_B}{\lambda_A}} \|z(T_{ext,n})\| \exp\left[-\frac{1}{2}\lambda_1(t - T_{ext,n})\right], \quad (4-23)$$

$\forall t \in [T_{ext,n}, T_{flex,n+1})$, and $\lambda_1 \in \mathbb{R}_{>0}$ is defined as

$$\lambda_1 \triangleq \frac{1}{\lambda_B} \min(\alpha, k_{5,0}), \quad (4-24)$$

provided the following gain conditions are satisfied:

$$k_{6,0} \geq c_1, \quad k_{7,0} \geq c_2, \quad k_{8,0} \geq c_3. \quad (4-25)$$

where c_1, c_2, c_3 are introduced in (4-4).

Proof. Because of the signum function in the closed-loop error system in (4-9), the time derivative of (4-10) exists a.e., and $\dot{\tilde{V}}_L \stackrel{a.e.}{\in} \tilde{V}_L$ [75] such that

$$\begin{aligned} \dot{V}_L \stackrel{a.e.}{=} & e_1 (e_2 - \alpha e_1) + \left(\frac{1}{2} \dot{M} - V \right) e_2^2 + e_2 \chi - e_2 e_1 \\ & - K [k_{5,0} e_2^2 + (k_{6,0} + k_{7,0} \|z\| + k_{8,0} \|z\|^2) |e_2|], \end{aligned} \quad (4-26)$$

Cancelling common terms and using Prop. 7 and (4-4) allows (4-26) to be upper bounded as

$$\begin{aligned} \dot{V}_L \stackrel{a.e.}{\leq} & -\alpha e_1^2 - k_{5,0} e_2^2 - (k_{6,0} - c_1) |e_2| \\ & - (k_{7,0} - c_2) |e_2| \|z\| - (k_{8,0} - c_3) |e_2| \|z\|^2. \end{aligned}$$

Further upper bounding of the Lyapunov derivative results in

$$\dot{V}_L \leq -\lambda_1 V_L(t), \quad (4-27)$$

where λ_1 is defined in (4-24). Using (4-11), the result in (4-23) can be obtained. \square

Remark 4.1. Using (4-16), (4-22), (4-27) and Theorems 4.1-4.3, a common bound is created for the Lyapunov derivative, \dot{V}_L , as $\dot{V}_L \stackrel{a.e.}{\leq} -\lambda_s V_L$, and hence, the controllers in (6-4) and (4-7) yield global exponential tracking $\forall t \in [t_0, \infty)$, such that

$$\|z(t)\| \leq \sqrt{\frac{\lambda_B}{\lambda_A}} \|z(t_0)\| \exp \left[-\frac{1}{2} \lambda_s (t - t_0) \right], \quad (4-28)$$

where $\lambda_s \in \mathbb{R}_{>0}$ is defined as $\lambda_s \triangleq \min(\lambda_1, \lambda_2, \lambda_3)$. From [22, Th. 2.1, Remark 2.1], since all subsystems share the radially unbounded common Lyapunov function in (4-10), global exponential convergence to the desired trajectory holds true in all cases, according to (4-28).

4.3 Experiments

The performance of the controllers in (4-5) and (4-7) was demonstrated on two participants with neurological conditions that impaired their right arm. The first

participant had post-polio syndrome and the second participant had both a spinal cord injury (SCI) and an elbow that had been surgically removed and autografted with shoulder tissue, preventing any supination. Average position and velocity errors for the impaired and unimpaired arms of each participant are compared in Table 4-1.

4.3.1 Arm Testbed

The testbed used for the experiments in this study was composed of two aluminum plates, one of which the upper arm rested on and the other of which was strapped to the forearm and rotated about a hinge aligned with the elbow. The designed motor controller was applied to a 27 Watt, brushed, parallel-shaft 12 VDC gearmotor and the FES controller regulated the pulsewidth sent to the biceps brachii via a Hasomed stimulator and six 0.6" x 2.75" PALS® electrodes. The controllers were implemented using real-time control software (QUARC, MATLAB 2015b/Simulink, Windows 8). For consistent biceps coverage and evenly spaced electrode placement, the first electrode was placed at 21% of the distance from the elbow crease to the acromion, the sixth electrode at 50% of this distance, and the other four biceps electrodes spaced evenly between the first and last. A seventh electrode (3" x 5") was placed on the shoulder as the reference electrode for all six biceps electrode channels. Based on comfort and necessary torque values, stimulation amplitude was fixed at a current of 30 mA with a frequency of 35 Hz for each channel, while the closed-loop FES controller modulated the pulse-width.

4.3.2 Protocol

After all seven electrodes were placed on the participant's upper arm, the participant was seated such that the upper arm and forearm could comfortably rest on their respective parts of the testbed. The desired angular position, q_d , of the forearm was

selected as $q_d(t) = \begin{cases} \frac{7\pi}{18} \left(1 - \cos\left(\frac{\pi}{2} \frac{t-5}{T}\right)\right) + \frac{\pi}{9}, & t \geq 5 \\ 4t, & t < 5 \end{cases}$, where the period, T , or amount

of time for the forearm to move from 20 to 90 degrees, was 5 seconds. The motor first

brought the arm to 20 degrees, which was found to be the beginning of the region where the muscle could always produce sufficient torque, and from there 10 biceps curls were completed.

The control gains, $\{k_i\}_{i=1,\dots,4}$, $\{k_{i,\beta}\}_{i=5,\dots,8}$, introduced in (4-5) and (4-7), were adjusted to yield acceptable tracking performance with values for both the right and left arms as follows: $k_1 = 25$, $k_2 = k_3 = k_4 = 1$, $k_{5,0} = 15$, $k_{5,1} = 35$, $k_{6,\beta} = k_{7,\beta} = k_{8,\beta} = 1$. A saturation limit for the muscle control input was established based on comfort. The decay constant for γ_j was selected as $\rho = 0.8$. When the muscle control input was below saturation, electrical stimulation was used to control the forearm from 20 to 90 degrees, whereas both muscle stimulation and the DC motor were used at any point that the muscle controller reached the saturation limit. Only the DC motor brought the forearm from the highest forearm angle (90 degrees) to the starting position (20 degrees). The set of channels used to stimulate within the muscle control region (i.e., during flexion) varies with angular position as in [55], where $\varepsilon = 0.22$ was selected as the normalized torque threshold for all but the impaired right arm of the Participant 1, which was set to 0.10 due to no electrode locations producing sufficient isometric torque.

4.3.3 Results

Results from all four experiments (right and left arms of two participants) are included in Table 4-1, which presents the position and velocity RMS errors, as well as the FES and motor control inputs, averaged over times of desired flexion. Figure 4-1 shows both the position error and FES control input (stimulation pulsewidth) for the right (impaired) arm of Participant 2.

4.4 Discussion

As seen in Table 4-1, the position and velocity errors of the impaired and unimpaired arms for both participants are similar, despite each having movement disorders that significantly limit their impaired arm in daily activities. Thus, the motor and FES

Table 4-1. Average position and velocity errors, FES control input, and motor control input for both arms (one impaired, one unimpaired) for both Participants. P1 and P2 denote Participants 1 and 2; R and L denote the right and left arms.

	RMS position error (deg)	RMS velocity error (deg/s)	Average FES control input (μ s)	Average motor control input (Amps)
P1, impaired/ R arm	4.26	3.70	286.7	2.08
P1, unimpaired/ L arm	3.75	4.33	317.6	1.61
P2, impaired/ R arm	4.83	5.56	354.0	1.79
P2, unimpaired/ L arm	4.96	5.04	346.0	1.67

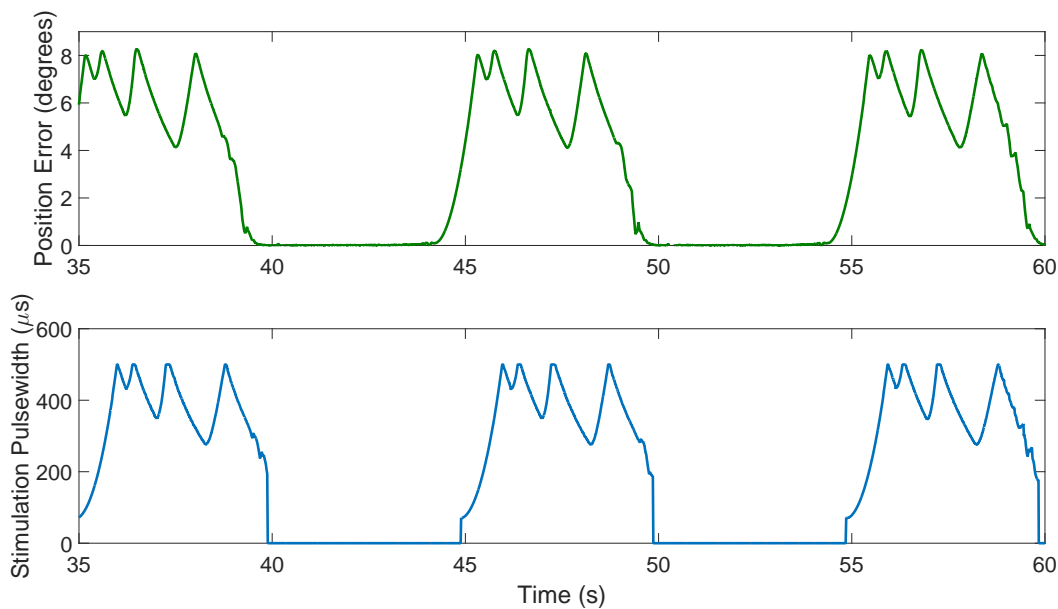


Figure 4-1. Position error and stimulation pulsewidth (i.e., FES input) for the right arm of Participant 2 during trials where the lower stimulation threshold iteratively decreased according to the constant $\rho = 0.8$. The zoomed view of biceps curls 4-6 is provided to easily compare the change in FES control input to the position error.

controllers developed in this chapter enable a participant with muscular asymmetries to perform similar tasks. Moreover, the motor only contributes as needed and the FES activates the biceps throughout flexion.

In [55], exponential tracking is achieved and the motor assists as needed when the stimulation comfort threshold Γ is reached; however, since it only assists for an instant before the error drops and the stimulation falls below the single threshold Γ , the motor is activated and deactivated frequently, to the point of chattering, in addition to the chattering due to sliding mode control. In the current development, the motor continues to assist the muscle until the lower threshold γ_j is reached by u_M , and motor assistance is deactivated. The constant ρ was used to decrease the lower threshold after every time the comfort threshold was reached in a single biceps curl. Lowering the lower threshold was motivated by the expectation that as the muscle fatigues, the FES control input would rise quicker to the comfort threshold after each successive bout of motor assistance. Thus, to prevent the motor from turning on and off more quickly towards the end of a biceps curl, the motor remains activated over a longer range of biceps curl angles. However, if desired, $\rho = 1$ would cause the lower threshold γ_j to remain constant throughout the protocol.

Figure 4-1 depicts an example of a typical portion of an experiment, where changes in the stimulation pulsewidth mirror changes in the position error. The relation is dependent on control gains; however, with a high dependence on the position error due to $\alpha = 40$ being selected (i.e., e_2 is 40 times more dependent on the position than the velocity error), the control input nearly mirrors the position error, which decreases during the bouts of continuous motor assistance.

The control technique in this chapter may depend on muscle delay even more so than other FES protocols [78, 79]. Because the motor instantaneously switches off after the γ_j condition is met, the muscle must react to the rapid increase in stimulation back to Γ that often occurred, as seen in Figure 4-1, which is likely due to a combination of

fatigue, an insufficiently high comfort threshold, and/or muscle delay. While a lower value of γ_j resulted in a smaller average error overall, this comes with more fluctuation of the error. Regardless, the error remains bounded at the error values that result in saturation of the FES controller.

4.5 Concluding Remarks

The muscle and motor track a desired forearm trajectory resembling a typical biceps curl. FES is the primary actuator for controlling the arm movement since it is desired to work the muscle as much as possible; however, the motor assists in tracking when the stimulation input reaches the participant's comfort threshold. To avoid chattering and to allow the error and stimulation to decay, even briefly, the motor continues to assist until the calculated stimulation input decreases to a lower threshold that discretely changes depending on controller performance. Switched sliding mode controllers are designed for both the FES and motor control input and exponential tracking is proved via Lyapunov methods. Experimental data is obtained from two participants with neuromuscular conditions that cause asymmetrical impairments, showing the result of varying bouts of motor assistance during a biceps curl. This chapter improves upon the previous chapter by implementing a second switching signal for activating an assistive electric motor. Implementation could be extended to a variety of FES exercises involving different muscle groups and the lower threshold could be adjusted and varied to accommodate a rehabilitation patient's specific goals.

CHAPTER 5
 CADENCE TRACKING FOR SWITCHED FES CYCLING COMBINED WITH
 VOLUNTARY PEDALING AND MOTOR RESISTANCE

This chapter focuses on the use of an FES cycle as a rehabilitation exercise for a wide variation in muscle strength and range of motion that exists in the movement disorder community. FES can be used to induce muscle contractions to assist a person who can contribute volitional coordinated torques and a motor can be used to both assist and resist a person's volitional and/or FES-induced pedaling. In this chapter and in [62], a multi-level switched system is applied to a two-sided control objective to maintain a desired range of cadence using FES, motor assistance, motor resistance, and volitional pedaling. A system with assistive, passive, and resistive modes are developed based on cadence, each with a different combination of actuators. Lyapunov-based methods for switched systems are used to prove global exponential tracking to the desired cadence range for the combined FES-motor control system. Experimental results show the feasibility and stability of the multi-level switched control system. Rather than switching stimulation amongst multiple electrodes on a single muscle group as in Chapters 3 and 4, subsystems in this chapter refer to separate muscle groups in the lower body, i.e., $m \in \mathcal{M} = \{RQ, RG, RH, LQ, LG, LH\}$ indicates the right (R) and left (L) quadriceps femoris (Q), gluteal (G), and hamstring (H) muscle groups, respectively. The rider's voluntary torque is denoted by $\tau_{vol} \in \mathbb{R}_{\geq 0}$. The function $T_m : \mathcal{Q} \rightarrow \mathbb{R}$ denotes the torque transfer ratio between each muscle group and the crank [47, 71]. Definitions for the subsequent stimulation regions and switching laws during the assistive mode are based on [47], where the portion of the crank cycle in which a particular muscle group is stimulated is denoted by $\mathcal{Q}_m \subset \mathcal{Q}$. In this manner, \mathcal{Q}_m is defined for each muscle group as

$$\mathcal{Q}_m \triangleq \{q \in \mathcal{Q} \mid T_m(q) > \varepsilon_m\}, \quad (5-1)$$

$\forall m \in \mathcal{M}$, where $\varepsilon_m \in (0, \max(T_m)]$ is the lower threshold for each torque transfer ratio, which limits the FES regions for each muscle so that each muscle group can only contribute to forward pedaling (i.e., positive crank motion). Based on the FES regions defined in (5-1), let $\sigma_m(q) \in \{0, 1\}$ be a piecewise left-continuous switching signal for each muscle group such that $\sigma_m(q) = 1$ when $q \in \mathcal{Q}_m$ and $\sigma_m(q) = 0$ when $q(t) \notin \mathcal{Q}_m$, $\forall m \in \mathcal{M}$. The region of the crank cycle where FES produces efficient torques, \mathcal{Q}_M , is defined as $\mathcal{Q}_M \triangleq \bigcup_{m \in \mathcal{M}} \{\mathcal{Q}_m\}$, $\forall m \in \mathcal{M}$.

Within the assistive mode, position-based switching is used to switch between subsets of muscle groups and the motor. When switching between assistive, passive, and resistive modes, the switching velocity values $\{\dot{q}_d, \dot{q}_\bar{d}\}$ are known but the position values are not, where $\dot{q}_d : \mathbb{R}_{>0} \rightarrow \mathbb{R}$ and $\dot{q}_\bar{d} : \mathbb{R}_{>0} \rightarrow \mathbb{R}$ are the minimum and maximum desired cadence values. To facilitate the analysis of a combination of position-based and velocity-based switching, switching times are denoted by $\{t_n^i\}$, $i \in \{s, e, p\}$, $n \in \{0, 1, 2, \dots\}$, representing the times when the system switches to use stimulation, the electric motor (either assistive or resistive), or neither (i.e., passive mode). For this chapter, the electrical stimulation intensity applied to each electrode channel, $u_m(q(t), t)$, is defined as

$$u_m(q(t), t) \triangleq \sigma_m(q(t)) k_m u_M(t), m \in \mathcal{M}, \quad (5-2)$$

where k_m , $\sigma_m(q(t))$, and $u_M(t)$ were all introduced in (3-2).

5.1 Control Development

The cadence tracking objective is quantified by the velocity error $e_1 : \mathbb{R}_{\geq 0} \rightarrow \mathbb{R}$ and auxiliary error $e_2 : \mathbb{R}_{\geq 0} \rightarrow \mathbb{R}$, defined as

$$e_1(t) \triangleq \dot{q}_d(t) - \dot{q}(t), \quad (5-3)$$

$$e_2(t) \triangleq e_1(t) + (1 - \sigma_a(t)) \Delta_d, \quad (5-4)$$

where \dot{q}_d was defined previously, along with $\dot{q}_{\bar{d}}$, which is now defined as $\dot{q}_{\bar{d}} \triangleq \dot{q}_d + \Delta_d$, where $\Delta_d \in \mathbb{R}_{>0}$ is the range of desired cadence values. The switching signal designating the assistive mode $\sigma_a : \mathbb{R}_{\geq 0} \rightarrow \{0, 1\}$ is designed as

$$\sigma_a = \begin{cases} 1 & \text{if } \dot{q} < \dot{q}_d \\ 0 & \text{if } \dot{q} \geq \dot{q}_d \end{cases}. \quad (5-5)$$

Note that $e_1 = e_2$ when $\sigma_a = 1$. Taking the time derivative of (5-3), multiplying by M , and using (2-8) yields

$$M\dot{e}_1 = -B_e u_e - B_M u_M - \tau_{vol} - V e_1 + \chi, \quad (5-6)$$

where $B_M : Q \times \mathbb{R} \rightarrow \mathbb{R}$ is the combined switched control effectiveness, defined for the cycle as

$$B_M(q(t), \dot{q}(t), t) = \sum_{m \in \mathcal{M}} B_m(q(t), \dot{q}(t), t) \sigma_m(q(t)) k_m \quad (5-7)$$

and where u_M was introduced in (3-2), the auxiliary term $\chi : Q \times \mathbb{R} \times \mathbb{R}_{\geq 0} \rightarrow 0$ is defined as

$$\chi = b_c \dot{q} + d_c + G + P + d_r + V \dot{q}_d + M \ddot{q}_d.$$

From Properties 1-6, χ can be bounded as

$$\chi \leq c_1 + c_2 |e_1|, \quad (5-8)$$

where $c_1, c_2 \in \mathbb{R}_{>0}$ are known constants and $|\cdot|$ denotes absolute value. Based on (5–6), (5–8), and the subsequent stability analysis, the FES control input to the muscle is designed as

$$u_M = \sigma_a (k_{1s} + k_{2s}e_1), \quad (5-9)$$

where $k_{1s}, k_{2s} \in \mathbb{R}_{>0}$ are constant control gains and σ_a is defined in (5–5). The switched control input to the motor is designed as

$$u_e = \sigma_e (k_{1e} \text{sgn}(e_1) + k_{2e}e_2), \quad (5-10)$$

where $k_{1e}, k_{2e} \in \mathbb{R}_{>0}$ are constant control gains and $\sigma_e : \mathbb{R} \rightarrow \mathbb{R}_{\geq 0}$ is the motor's switching signal, designed as

$$\sigma_e = \begin{cases} k_a & \text{if } \dot{q} < \dot{q}_d, q \notin Q_m \\ 0 & \text{if } \dot{q} < \dot{q}_d, q \in Q_m \\ 0 & \text{if } \dot{q}_d \leq \dot{q} \leq \dot{q}_d \\ k_r & \text{if } \dot{q} > \dot{q}_d \end{cases}, \quad (5-11)$$

where $k_a, k_r \in \mathbb{R}_{>0}$ are constant control gains. Substituting (5–9) and (5–10) into (5–6) yields

$$M\dot{e}_1 = -B_e \sigma_e (k_{1e} \text{sgn}(e_1) + k_{2e}e_2) - B_M \sigma_a (k_{1s} + k_{2s}e_1) - \tau_{vol} - V e_1 + \chi. \quad (5-12)$$

5.2 Stability Analysis

Let $V_L : \mathbb{R} \rightarrow \mathbb{R}$ be a continuously differentiable, positive definite, common Lyapunov function candidate defined as

$$V_L = \frac{1}{2} M e_1^2, \quad (5-13)$$

which satisfies the following inequalities:

$$\frac{c_{M1}}{2} e_1^2 \leq V_L \leq \frac{c_{M2}}{2} e_1^2, \quad (5-14)$$

where c_{M1} and c_{M2} are introduced in Property 1.

Theorem 5.1. *When $\dot{q} < \dot{q}_d$ and $q \in Q_m$, the closed-loop error system in (5-12) is exponentially stable in the sense that*

$$|e_1(t)| \leq \sqrt{\frac{c_{M2}}{c_{M1}}} |e_1(t_n^s)| \exp\left[-\frac{\lambda_s}{2}(t - t_n^s)\right], \quad (5-15)$$

for all $t \in (t_n^s, t_{n+1}^i) \forall i \in \{e, p\}, \forall n$, where $\lambda_s \in \mathbb{R}_{>0}$ is defined as

$$\lambda_s \triangleq \frac{2}{c_{M2}} (c_m k_{2s} - c_2), \quad (5-16)$$

provided the following sufficient gain conditions are satisfied:

$$k_{1s} > \frac{c_1}{c_m}, \quad k_{2s} > \frac{c_2}{c_m}, \quad (5-17)$$

where c_m is introduced in Property 11, c_1 and c_2 are introduced in (5-8), and k_{2s} and k_{1s} are introduced in (5-9).

Proof. When $\dot{q} < \dot{q}_d$ and $q \in Q_M$, $e_1 > 0$, $\sigma_a = 1$, and $\sigma_e = 0$ (i.e., the cycle-rider system is controlled by FES in the assistive mode). It can be demonstrated that, due to B_M discontinuously varying over time, the time derivative of (5-13) exists almost everywhere (a.e.), i.e., for almost all $t \in (t_n^s, t_{n+1}^i), \forall i \in \{e, p\}$, and after substituting (5-12), the derivative of (5-13) can be upper bounded using Properties 7 and 11, Assumption 1, and (5-8) as

$$\dot{V}_L \stackrel{\text{a.e.}}{\leq} -(c_m k_{1s} - c_1) e_1 - (c_m k_{2s} - c_2) e_1^2, \quad (5-18)$$

which is negative definite since $e_1 > 0$, provided the gain conditions in (5-17) are satisfied. Furthermore, (5-14) can be used to upper bound (5-18) as

$$\dot{V}_L \leq -\lambda_s V_L, \quad (5-19)$$

where λ_s was defined in (5-16). The inequality in (5-19) can be solved to yield

$$V_L(t) \leq V_L(t_n^s) \exp[-\lambda_s(t - t_n^s)], \quad (5-20)$$

for all $t \in (t_n^s, t_{n+1}^i)$, $\forall i \in \{e, p\}$, $\forall n$. Rewriting (5-20) using (5-14) and performing some algebraic manipulation yields (5-15). \square

Theorem 5.2. *When $\dot{q} < \dot{q}_d$ and $q \notin Q_M$, the closed-loop error system in (5-12) is exponentially stable in the sense that*

$$|e_1(t)| \leq \sqrt{\frac{c_{M2}}{c_{M1}}} |e_1(t_n^e)| \exp\left[-\frac{\lambda_{e1}}{2}(t - t_n^e)\right], \quad (5-21)$$

for all $t \in (t_n^e, t_{n+1}^i)$, $\forall i \in \{s, p\}$, $\forall n$, where $\lambda_{e1} \in \mathbb{R}_{>0}$ is defined as

$$\lambda_{e1} \triangleq \frac{2}{c_{M2}} (c_{be} k_a k_{2e} - c_2), \quad (5-22)$$

provided the following sufficient gain conditions are satisfied:

$$k_{1e} > \frac{c_1}{c_e k_a}, k_{2e} > \frac{c_2}{c_e k_a}, \quad (5-23)$$

where k_{1e} and k_{2e} are introduced in (5-10), c_1 and c_2 are introduced in (5-8), c_e is introduced in Property 12, and k_a is introduced in (5-11).

Proof. When $\dot{q} < \dot{q}_d$ and $q \notin Q_M$, $e_1 > 0$, $\sigma_a = 1$, and $\sigma_e = k_a$, but $B_M = 0$ by its definition in (5-7) and the definition of σ_m . It can be demonstrated that, due to the signum function in (5-12), the time derivative of (5-13) exists a.e., i.e., for almost all $t \in (t_n^e, t_{n+1}^i)$, $\forall i \in \{s, p\}$, and, after substituting (5-4) and (5-12), can be upper

bounded using Properties 7 and 12, Assumption 1, and (5–8) as

$$\dot{V}_L \stackrel{\text{a.e.}}{\leq} -(c_e k_a k_{1e} - c_1) e_1 - (c_e k_a k_{2e} - c_2) e_1^2, \quad (5-24)$$

which is negative definite since $e_1 > 0$, provided the control gain conditions in (5–23) are satisfied. Furthermore, (5–14) can be used to upper bound (5–24) as

$$\dot{V}_L \leq -\lambda_{e1} V_L, \quad (5-25)$$

where λ_{e1} was defined in (5–22). The inequality in (5–25) can be solved to yield

$$V_L(t) \leq V_L(t_n^e) \exp[-\lambda_{e1}(t - t_n^e)], \quad (5-26)$$

for all $t \in (t_n^e, t_{n+1}^i)$, $\forall i \in \{s, p\}$, $\forall n$. Rewriting (5–26) using (5–14), and performing some algebraic manipulation yields (5–21). \square

Remark. Exponential convergence to \dot{q}_d throughout the assistive mode (Theorems 5.1 and 5.2) is guaranteed in the sense that

$$|e_1(t)| \leq \sqrt{\frac{c_{M2}}{c_{M1}}} |e_1(t_n^i)| \exp\left[-\frac{\lambda_a}{2}(t - t_n^i)\right], \quad (5-27)$$

for all $t \in (t_n^i, t_{n+1}^p)$ $\forall i \in \{e, s\}$, $\forall n$, where $\lambda_a \in \mathbb{R}_{>0}$ is defined as

$$\lambda_a \triangleq \min\{\lambda_s, \lambda_{e1}\}.$$

Since (5–27) holds for all combinations of σ_e and σ_m while $\sigma_a = 1$, V_L is indeed a common Lyapunov function for switching during the assistive mode.

Theorem 5.3. *When $\dot{q} > \dot{q}_d$, the closed-loop error system in (5–12) is exponentially stable in the sense that*

$$|e_1(t)| \leq \sqrt{\frac{c_{M2}}{c_{M1}}} \Delta_d \exp\left[-\frac{\lambda_{e2}}{2}(t - t_n^e)\right], \quad (5-28)$$

for all $t \in (t_n^e, t_{n+1}^i)$, $i = p$, $\forall n$, where $\lambda_{e2} \in \mathbb{R}_{>0}$ is defined as

$$\lambda_{e2} \triangleq \frac{2}{c_{M2}} (c_e k_r k_{2e} - c_2), \quad (5-29)$$

provided the following gain conditions are satisfied:

$$k_{1e} > \frac{c_1 + c_{vol} + c_E k_{2e} k_r \Delta_d}{c_e k_r}, \quad k_{2e} > \frac{c_2}{c_e k_r}, \quad (5-30)$$

where c_e and c_E are introduced in Property 12, c_{vol} is introduced in Assumption 1, k_r is introduced in (5-11), c_1 and c_2 are introduced in (5-8), and Δ_d is introduced in (5-4).

Proof. When $\dot{q} > \dot{q}_d$, $\sigma_a = 0$, $e_2 < 0$, $e_1 < 0$, and $\sigma_e = k_r$ (i.e., the cycle-rider system is in the motor-resistance control mode). Due to the signum function in (5-12), the time derivative of (5-13) exists a.e., i.e., for almost all $t \in (t_n^e, t_{n+1}^p)$, and for all n , and, after substituting (5-4) and (5-12), can be upper bounded using Properties 7 and 12, Assumption 1, and (5-8) as

$$\dot{V}_L \stackrel{\text{a.e.}}{\leq} - (c_e k_r k_{1e} - c_E k_r k_{2e} \Delta_d - c_1 - c_{vol}) |e_1| - (c_e k_r k_{2e} - c_2) e_1^2, \quad (5-31)$$

which is negative definite provided the control gain conditions in (5-30) are satisfied.

Furthermore, (5-31) can be upper bounded as

$$\dot{V}_L \leq -\lambda_{e2} V_L,$$

where λ_{e2} was defined in (5-29), and solved to yield

$$V_L(t) \leq V_L(t_n^e) \exp[-\lambda_{e2}(t - t_n^e)], \quad (5-32)$$

for all $t \in (t_n^e, t_{n+1}^i)$, $i = p, \forall n$. Rewriting (5-32) using (5-14), noting that $|e_1(t_n^e)| = |e_2(t_n^e) - \Delta_d| = \Delta_d$ when $\sigma_a = 0$, and performing algebraic manipulation yields (5-28). \square

Remark. To ensure exponential tracking to the desired cadence range for both the resistive and assistive motor modes, the gain conditions from (5-23) and (5-30) are combined as $k_{1e} > \max \left\{ \frac{c_1}{c_e k_a}, \frac{c_1 + c_{vol} + c_E k_{2e} k_r \Delta_d}{c_e k_r} \right\}$, $k_{2e} > \max \left\{ \frac{c_2}{c_e k_a}, \frac{c_2}{c_e k_r} \right\}$.

Theorem 5.4. When $\dot{q}_d \leq \dot{q} \leq \dot{q}_d$, the closed-loop error system in (5–12) can be bounded as

$$|e_1(t)| \leq \text{sat}_{\Delta_d} \left\{ \left(\frac{c_{M2}}{c_{M1}} e_1^2(t_n^p) \exp[\lambda_p(t - t_n^p)] + \frac{1}{c_{M1}} \exp[\lambda_p(t - t_n^p)] - \frac{1}{c_{M1}} \right)^{\frac{1}{2}} \right\}, \quad (5-33)$$

for all $t \in [t_n^p, t_{n+1}^i]$, $\forall i \in \{s, e\}$, $\forall n$, where $\text{sat}_{\Delta_d}(\cdot)$ is defined as $\text{sat}_{\Delta_d}(\kappa) \triangleq \kappa$ for $|\kappa| \leq \Delta_d$ and $\text{sat}_{\Delta_d}(\kappa) \triangleq \text{sgn}(\kappa)\Delta_d$ for $|\kappa| > \Delta_d$, where Δ_d was defined previously, and where $\lambda_p \in \mathbb{R}_{>0}$ is defined as

$$\lambda_p \triangleq 2 \max \left\{ \frac{2c_2}{c_{M1}}, \frac{(c_1 + c_{vol}) \sqrt{2c_{M1}}}{c_{M1}} \right\}. \quad (5-34)$$

Proof. In the passive mode, $\sigma_a, \sigma_e = 0$ so the time derivative of (5–13) can be expressed using (5–12) and Property 7 as

$$\dot{V}_L = e_1(-\tau_{vol} + \chi), \quad (5-35)$$

which can be upper bounded using Assumption 1, (5–8), and (5–14) as

$$\dot{V}_L \leq (c_1 + c_{vol}) \sqrt{\frac{2}{c_{M1}}} \sqrt{V_L} + \frac{2c_2}{c_{M1}} V_L. \quad (5-36)$$

The right-hand side of (5–36) can be upper bounded in a piecewise manner as

$$\dot{V}_L \leq \begin{cases} \frac{\lambda_p}{2} (V_L + 1) & \text{if } V_L \leq 1 \\ \lambda_p V_L & \text{if } V_L > 1 \end{cases}, \quad (5-37)$$

where λ_p is defined in (5–34). Since both V_L and λ_p are positive, (5–37) can always be upper bounded as

$$\dot{V}_L \leq \lambda_p \left(V_L + \frac{1}{2} \right). \quad (5-38)$$

The solution to (5–38) over the interval $t \in [t_n^p, t_{n+1}^i]$, $\forall i \in \{s, e\}$, $\forall n$ yields the following upper bound on V_L in the passive mode:

$$V_L(t) \leq V_L(t_n^p) \exp[\lambda_p(t - t_n^p)] + \frac{1}{2} \{\exp[\lambda_p(t - t_n^p)] - 1\}, \quad (5-39)$$

for all $t \in [t_n^p, t_{n+1}^i]$, $\forall i \in \{s, e\}$, $\forall n$. Rewriting (5–39) using (5–14), performing some algebraic manipulation, and noting that $0 \leq e_1 \leq \Delta_d$ always holds true in the passive mode, yields (5–33). □

Remark. The inequality in (5–33) indicates that in the passive mode, the absolute error is bounded by an exponentially *increasing* envelope. This bound is due to the conservative Lyapunov analysis. In practice, the person may be able to pedal for long periods of time in the passive region, and may never reach the upper cadence target. Since the passive mode is defined by $0 \leq e_1 \leq \Delta_d$, the error is always bounded in the passive mode; however, the conservative analysis shows the bound on the growth of the error. As described in (5–15), (5–21), (5–28), and the remark in the proof of Theorem 3, $|e_1|$ decays at an exponential rate in both the assistive and resistive modes. By the definition of e_2 in (5–4), $|e_2|$ also decays exponentially in the assistive and resistive modes. Therefore, sufficient conditions for overall stability of the two-sided system can be developed based on the exponential time constants λ_s , λ_{e1} , λ_{e2} and λ_p . When the system enters the resistive mode, the cadence will instantly exponentially decay back into the passive mode and when entering the assistive mode, the FES and motor controllers will ensure the cadence exponentially increases back into the voluntary range of desired cadence. While short bouts of control authority at the boundary may result in chattering of the actuators, due to Property 13, a minimum dwell time greater than zero in all three modes can be assumed and Zeno behavior at the desired bounds on cadence range is avoided. For this particular application in FES cycling, where there is a desired cadence range, rather than a single desired trajectory, error convergence to a ball is desirable, rather than exponential error convergence to zero.

5.3 Experiments

To evaluate the performance of the FES and motor controllers in (5–9) and (5–10), respectively, experiments were performed on one able-bodied participant and nine participants post-stroke after they gave written informed consent approved by the University of Florida and Medical University of South Carolina Institutional Review Boards, respectively. The experiment on the able-bodied participant was conducted to provide proof-of-concept for the three modes of cycling. The participant was instructed to contribute to forward pedaling at various intensities to stay below, above, and within the desired region of cadence at during different portions of the 180s trial, showing the control system's three modes.

The nine stroke participants performed one uncontrolled and one controlled trial to demonstrate the advantage of the controller for people with neurological conditions. During the first 200 seconds of the trial they were asked to target a cadence within the desired range, which they could view, and during the last 50 seconds of each trial they were asked to pedal comfortably fast with the goal of reaching above the desired upper threshold. Self-selected and fastest comfortable walking speeds (SSWS and FCWS, respectively) were measured via an instrumented walkway (GAITRite Classic, CIR Systems) before conducting the FES-cycling experiments on the stroke participants, and are reported in Table 5-1 as an indicator of each individual's walking impairment following stroke.

5.3.1 Motorized FES-Cycling Testbed

Figure 5-1 depicts the motorized FES-cycling test bed. A commercially available recumbent tricycle (TerraTrike Rover X8) was placed on a stationary cycling trainer and riser rings (Kinetic by Kurt) to be used for the FES-cycling experiments. Orthotic boots were used to fix the rider's feet to the pedals, prevent dorsiflexion and plantarflexion of the ankles, and maintain sagittal alignment of the lower legs. An optical encoder (US Digital H1) was used to measure the crank position and velocity while coupled to the



Figure 5-1. The motorized FES-cycling test bed used for experiments, consisting of (A) an electric motor, (B) stimulator, and (C) orthotic pedals. Photo courtesy of Matthew Bellman. Gainesville, FL.

cycle's crank via spur gears. The data acquisition hardware (Quanser Q8-USB) was used to measure the encoder signal and deliver the motor current to a 250 Watt, 24 DC brushed motor (Unite Motor Co. Ltd.), which was enabled by an ADVANCED Motion Controls¹ (AMC) PS300W24 power supply, controlled by an AMC AB25A100 motor driver, and filtered with an AMC FC15030 to reduce electrical noise. Both the motor and FES controllers were implemented on a personal computer running real-time control software (QUARC, MATLAB/Simulink, Windows 10) at a sampling rate of 500 Hz.

Biphasic, symmetric, rectangular pulses were delivered to the participants' muscle groups with a current-controlled stimulator (Hasomed RehaStim) via self-adhesive, PALS[®] electrodes. The stimulation amplitudes were fixed at 90 mA for the quadriceps

¹ ADVANCED Motion Controls supported the development of this testbed by providing discounts on their branded items.

and 80 mA for the hamstrings and gluteus muscle groups. The stimulation pulse width for each muscle group was determined by u_m and u_e from (5–9) and (5–10), respectively, and commanded to the stimulator by the control software. Stimulation frequency was fixed at 60 Hz, as in [47] and [80]. For safety, an emergency stop switch was attached to the tricycle that enabled the subject to stop the experiment immediately if necessary, though the subject did not find it necessary.

5.3.2 Experimental Setup

Electrodes were placed over the participant’s quadriceps femoris, hamstrings, and gluteus muscle groups according to Axelgaard’s electrode placement manual. The participant was then seated on the tricycle with their feet secured in the orthotic boots attached to the pedals. The seat position was adjusted so that the participant was comfortable and to ensure that full knee extension would not occur at any crank position. Measurements of the lower limbs of the participant were taken to calculate the switching pattern for stimulation and motor in the assistance mode, as in [47].

In the experiments on participants with stroke, participants completed a warm-up protocol of volitional pedaling at approximately 50 RPM while the resistance of the magnetic trainer was progressively increased. Participant heart rate was measured by a fingertip pulse oximeter. The wheel resistance for subsequent experiments was determined either by the Karvonen formula [81] for desired min/max training heart rate (beginner exercise, 40-50% effort) or by each participant’s self report of significant effort that they did not wish to exceed, whichever occurred first. The remaining protocol consisted of two trials, each five minutes long if fully completed. The first consisted only of volitional pedaling, and the 3 mode controller was implemented on the second after the participant’s heart rate returned to baseline and the participant stated that they were physically ready to continue. During both trials, participants were asked to maintain a cadence within the desired range of 50-55 RPM to the best of their abilities for the first four minutes. For this task, participants were shown a real-time plot of their cadence in

comparison to the desired range. Four minutes into each trial, participants were asked to pedal as fast as comfortably possible. Participants were never asked to intentionally pedal below the minimum cadence, but some were incapable of volitionally maintaining a cadence above the minimum threshold. Although the goal was five minutes, ultimately, each 3 mode trial lasted between four and five minutes, depending on patient fatigue and willingness to continue.

In both sets of experiments, it was desired to start from 0 rpm and smoothly approach the minimum desired cadence of the desired cadence range (selected as 45-55 RPM for the able-bodied experiment and 50-55 RPM for the nine experiments on post-stroke participants). During the first 10 seconds, only the motor was used to bring the participant's legs to near the minimum desired cadence. After the first 10 seconds, the range of crank angles corresponding to the stimulation of each muscle group and activation of the motor within assistive mode were determined based on the lower thresholds for the torque transfer ratios, which were calculated as $\varepsilon_{*quad} = 0.42$, $\varepsilon_{*ham} = 0.42$, $\varepsilon_{*glute} = 0.38$ (see (??)) for both the left and right legs of the able-bodied participant. Only the quadriceps of the post-stroke participants were stimulated and the lower thresholds of the torque transfer ratios were calculated as $\varepsilon_{quad} \in (0.2476, 0.4022)$ for the right and left legs of all nine participants. The control gains from the FES and motor controllers in (5–9) and (5–10), respectively, are selected as follows: $k_{1s} \in (18.75, 43.75)$, $k_{2s} \in (56.25, 131.25)$, $k_{1e} \in (0.375, 1.375)$, $k_{2e} \in (3.75, 4.5)$, $k_a \in (0.6, 0.8)$, $k_r = 1$.

5.3.3 Results

Figure 5-2 depicts the trial from the able-bodied participant. The motor and FES switched activation as the cycle's cadence varies below, within, and above the set bounds during the experiment. Also depicted is the cadence and desired cadence range for the 180s trial, which was chosen as 45-55 RPM.

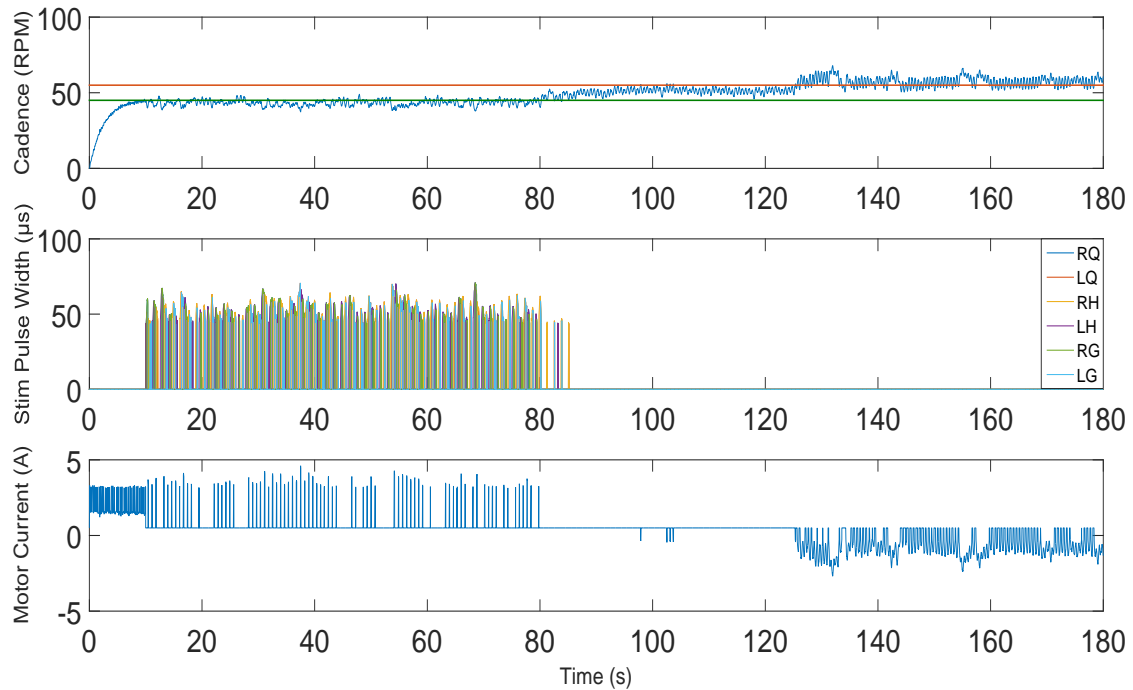


Figure 5-2. Cycle Cadence (top plot), stimulation pulse width (middle plot), and motor current (bottom plot) for 180 seconds of cycling. Motor current greater than 0.5A indicates assistance, motor current less than 0.5A indicates resistance, and an offset of 0.5 amps is used to combat friction within the motor. The solid green line at 45 RPM and red line at 55 RPM of the cadence plot indicate the chosen upper and lower bounds for the purely volitional pedaling mode. Seconds 10-80 depict the assistance mode (i.e., the subject does not maintain the minimum desired cadence on their own), the next 45 seconds depict the passive mode (i.e., the subject was able to maintain cadence within the desired range on their own), and the last 55 seconds depict the resistive mode (i.e., the participant fairly consistently voluntarily output a torque that resulted in a cadence above the maximum desired threshold).

Table 5-1. Participant description

Participant	1	2	3	4	5	6	7	8	9
Age	24	55	49	61	72	48	67	65	36
Sex	M	F	M	M	M	F	F	M	M
Affected side	R	L	R	R	R	R	L	L	L
Time since stroke (months)	87	36	25	35	72	42	76	38	172
Self selected walking speed (cm/s)	115.5	92.2	125.8	109.0	61.7	116.4	52.1	134.8	53.4
Fastest comfortable walking speed (cm/s)	154.5	117.5	141.1	155.5	90.4	178.9	77.4	200.0	90.4

The root mean square (RMS) cadence error and the standard deviation of the cadence was lower for the 3 mode trial than the volitional trial for all portions of the trial. Table 5-2 indicates average and standard deviation of the cadence, RMS cadence error, and percent time in each zone for both the volitional and 3 mode trials for all nine participants. Overall (OA) metrics are separated by the first four minutes (F240), and the final portion (FP) of pedaling to show the effects of the additional volitional effort at the end of each trial. Error is calculated as the difference between the actual cadence and the lower cadence threshold when below the desired range, and the difference between the actual cadence and the upper cadence threshold when above the desired range. Pedaling within the uncontrolled mode/desired cadence range is quantified by an error of zero. Since the participant was asked to pedal with more effort during final portion, it was expected that the percent time in each mode would be different between first 240s and final portion and the overall deviation in cadence was expected to be large. Thus, overall metrics for standard deviation of cadence and percent time in each mode are not included in Table 5-2. overall metrics for average cadence and RMS cadence error

Table 5-2. Cycling metrics from nine stroke participants.

Metric	Seg.	Cond.	Mean	p-value	Participant number								
					1	2	3	4	5	6	7	8	9
Avg. cad. (RPM)	OA	Vol	51.54	0.5553	50.96	48.65 [#]	55.51	53.60	49.80 [^]	53.67	47.35 [^]	59.26	45.08 [^]
		3M	51.01		51.86 [^]	48.22	54.67	51.81	49.16 [^]	53.48	49.40 [^]	52.88 [^]	47.60 [^]
	F240	Vol	49.91	0.1434	50.68	48.95	52.42	51.47	49.80 [^]	52.10	47.35 [^]	52.07	44.39
		3M	50.67		51.81	47.76	53.78	50.73	49.13	53.14	49.34	52.86	47.49
	FP	Vol	62.34	0.1201	52.08	47.23 [#]	67.87	61.13	-	59.93	-	88.03	60.16 [^]
		3M	53.99		55.39 [^]	50.05	58.23	56.13	50.25 [^]	54.82	49.81 [^]	59.84 [^]	51.37 [^]
Cad. SD (RPM)	F240	Vol	4.61	0.0223 [*]	2.68	4.38	2.07	2.02	5.79 [^]	2.35	7.70 [^]	2.96	7.04
		3M	2.28		2.62	2.73	1.64	2.01	1.93	1.65	2.97	2.24	2.35
	FP	Vol	8.98	0.5786	2.73	4.82 [#]	2.19	2.34	-	2.72	-	3.54	22.45 [^]
		3M	4.68		3.92 [^]	3.23	2.40	2.38	3.67 [^]	2.03	2.69 [^]	9.79 [^]	6.26 [^]
RMS cad. error (RPM)	OA	Vol	6.16	0.0109 [*]	1.60	5.36 [#]	5.90	3.43	5.49 [^]	2.68	7.53 [^]	14.95	9.66 [^]
		3M	1.90		1.20 [^]	3.25	1.88	1.39	1.92 [^]	0.68	2.36 [^]	1.08 [^]	3.35 [^]
	F240	Vol	3.56	0.0336 [*]	1.68	3.94	0.96	0.78	5.49 [^]	1.03	7.53 [^]	1.87	8.74
		3M	1.68		1.16	3.44	0.62	1.00	1.88	0.36	2.42	0.90	3.32
	FP	Vol	12.48	0.0407 [*]	1.25	5.24 [#]	13.06	7.50	-	5.63	-	33.22	21.45 [^]
		3M	3.64		3.09 [^]	2.36	4.01	2.38	2.81 [^]	1.34	1.95 [^]	10.32 [^]	4.52 [^]
% Time in assist. mode	F240	Vol	37.92	0.5469	36.68	54.53	10.56	23.24	32.65 [^]	17.39	65.32 [^]	19.83	81.07
		3M	41.74		22.04	80.47	0.28	38.10	68.13	3.35	63.28	11.73	88.30
	FP	Vol	16.17	0.8243	20.34	70.59 [#]	0.00	0.00	-	0.00	-	0.00	22.23 [^]
		3M	22.51		8.64 [^]	46.56	0.00	0.27	41.09 [^]	0.94	56.52 [^]	12.14 [^]	36.47 [^]
% Time in uncontr. mode	F240	Vol	55.60	0.3498	59.27	39.61	82.27	72.31	66.03 [^]	73.69	19.12 [^]	72.88	15.23
		3M	50.48		65.40	19.17	75.79	59.86	31.53	84.01	32.42	75.15	11.01
	FP	Vol	13.18	0.0817	65.83	24.01 [#]	0.00	0.00	-	0.98	-	0.00	1.42 [^]
		3M	35.77		36.05 [^]	48.88	11.34	32.44	51.34 [^]	52.36	39.76 [^]	20.93 [^]	28.82 [^]
% Time in resist. mode	F240	Vol	6.48	0.6542	4.05	5.86	7.17	4.45	1.32 [^]	8.92	15.55 [^]	7.29	3.70
		3M	7.78		12.57	0.36	23.94	2.04	0.34	12.64	4.29	13.11	0.69
	FP	Vol	70.66	0.1717	13.83	5.40 [#]	100	100	-	99.02	-	100	76.35 [^]
		3M	41.72		55.32 [^]	4.56	88.66	67.28	7.57 [^]	46.70	3.72 [^]	66.93 [^]	34.71 [^]

[^] = did not complete trial (or portion of the trial)

[#]The last 10 seconds of data was removed since they temporarily stopped pedaling due to instruction confusion.

^{*}Statistical significance for $p < 0.05$, but not significant when adjusted with the Holm-Bonferroni correction for $n = 14$ comparisons

OA = overall, F240 = first 240 seconds, FP = final portion, Vol = volitional-only trial, 3M = three mode controller trial

Table 5-3. R correlation coefficients for various data amongst all nine participants.

		SSWS		FCWS	
		Vol.	3M	Vol.	3M
Avg. cad. (RPM)	OA	0.888	0.850	0.870	0.774
	F240	0.865	0.837	0.785	0.783
	FP	0.493	0.886	0.603	0.858
Cad. SD (RPM)	F240	-0.941	-0.440	-0.861	-0.425
	FP	-0.894	0.140	-0.716	0.292
RMS cad. err. (RPM)	OA	-0.038	-0.681	0.072	-0.767
	F240	-0.934	0.384	-0.851	0.453
	FP	0.024	-0.755	0.185	-0.750
% Time in assist. mode*	F240	-0.819	-0.864	-0.746	-0.816
	FP	-0.482	-0.833	-0.583	-0.816
% Time in uncontr. mode*	F240	0.803	0.865	0.731	0.852
	FP	0.040	-0.408	-0.070	-0.267
% Time in resist. mode*	F240	-0.069	0.729	-0.059	0.574
	FP	0.271	0.790	0.396	0.714

*The 3 modes of control do not exist for the volitional-only trial; however, for comparison, the percentage time calculations are based on the same cadence thresholds as in 3 mode trials.

Participants that did not start the final portion of the volitional trial (indicated by a “-” in Table 5-2) are excluded from the calculation of the R correlation for the final portion of the volitional-only trial.

OA = overall, F240 = first 240 seconds, FP = final portion, Vol = volitional-only trial, 3M = three mode controller trial, SSWS = self-selected walking speed, FCWS = fastest comfortable walking speed

are included to demonstrate that, despite varying intensity of volitional contribution, on average the controllers enforced a cadence within the desired uncontrolled range.

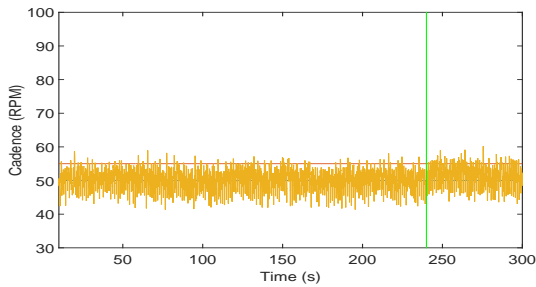
Unlike the volitional trials, all nine participants completed the first four minutes of pedaling during the 3 mode trials, showing the benefit of the 3 mode control system.

However, with more intense effort required after the fourth minute due to additional resistance from the electric motor, Participants 5, 7, and 9 stopped pedaling during the final portion of the trial, but before completion, due to fatigue. During the final portion of the 3 mode trial, Participant 8 produced sufficient volitional torque to cause the chain to slip off the motor sprocket. This could be avoided in the future by remounting the idler sprocket to increase the amount of chain wrap around the motor sprocket; however, it was not feasible to do so during the session. Figures 5-3a-5-3i depict the cadence from

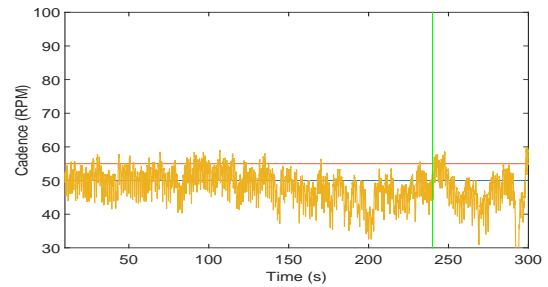
all nine participants during the purely volitional trials. Figures 5-4a-5-4i depict the activation of both the motor and FES as the cycle's cadence varies below, within, and above the set cadence thresholds during the 3 mode trials for all nine participants. Data from the final portion of the trial (i.e., when participants were asked to attempt to pedal faster) was not obtained for the volitional trials for Participants 5 or 7 since they were unable to continue cycling on their own past 100 and 120 seconds, respectively.

Participant 9 stopped at 250 seconds, shortly after the cue to pedal harder. Participant 2 stopped pedaling momentarily near the end of the volitional trial due to confusion regarding when the trial was supposed to end, so the final 10 seconds were not included in the statistics (but are depicted in Figure 5-4b).

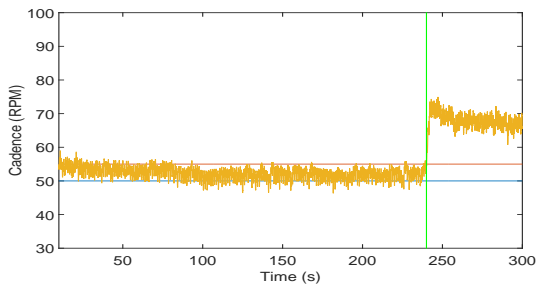
As seen in Figures 5-4a-5-4i, despite each participant's efforts to stay within the desired cadence range, participants experienced all 3 modes, due to a small cadence range relative to the participants' abilities. FES and positive motor current alternated when cadence was below the lower threshold, and the motor provided resistive torques when participants pedaled above target speeds. The average cadence across all nine participants during the 3 mode trials was within the desired range when calculated over



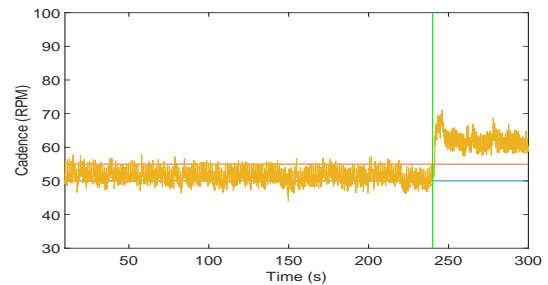
(a) Participant 1



(b) Participant 2

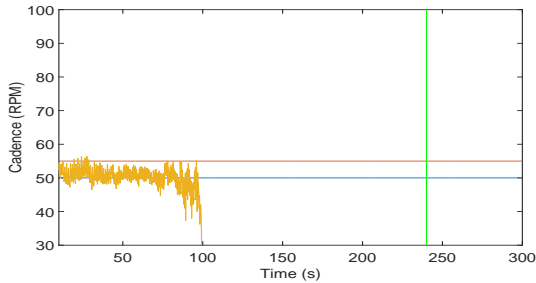


(c) Participant 3

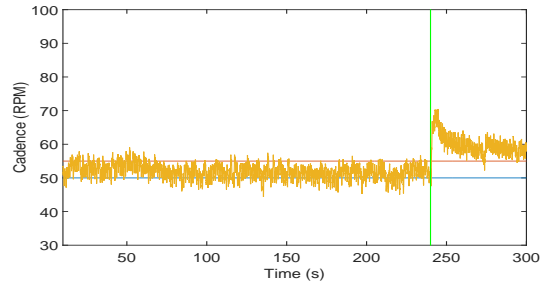


(d) Participant 4

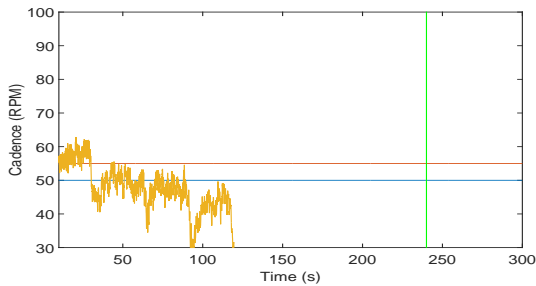
Figure 5-3. Cycling cadence in comparison to the desired cadence range during volitional pedaling of target 5 minutes. Upper and lower cadence thresholds are depicted in red and blue and the actual cadence in yellow, respectively, all of which were shown to the participants throughout the trial. Individual results during the volitional-only trials highlight differences in functional performance across participants, and can be compared to the 3 mode trials depicted in Figures 5-4a-5-4d. The vertical green line represents the four minute mark when the participants were asked to pedal at maximum effort.



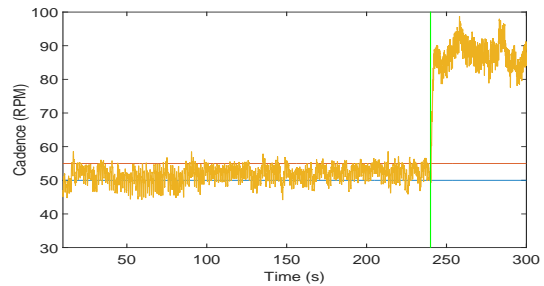
(e) Participant 5



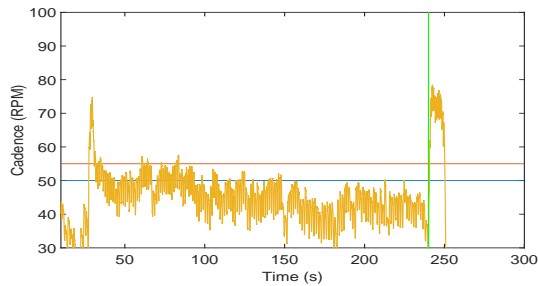
(f) Participant 6



(g) Participant 7



(h) Participant 8



(i) Participant 9

Figure 5-3. Cycling cadence in comparison to the desired cadence range during volitional pedaling of target 5 minutes. Upper and lower cadence thresholds are depicted in red and blue and the actual cadence in yellow, respectively, all of which were shown to the participants throughout the trial. Individual results during the volitional-only trials highlight differences in functional performance across participants, and can be compared to the 3 mode trials depicted in Figures 5-4e-5-4i. The vertical green line represents the four minute mark when the participants were asked to pedal at maximum effort.

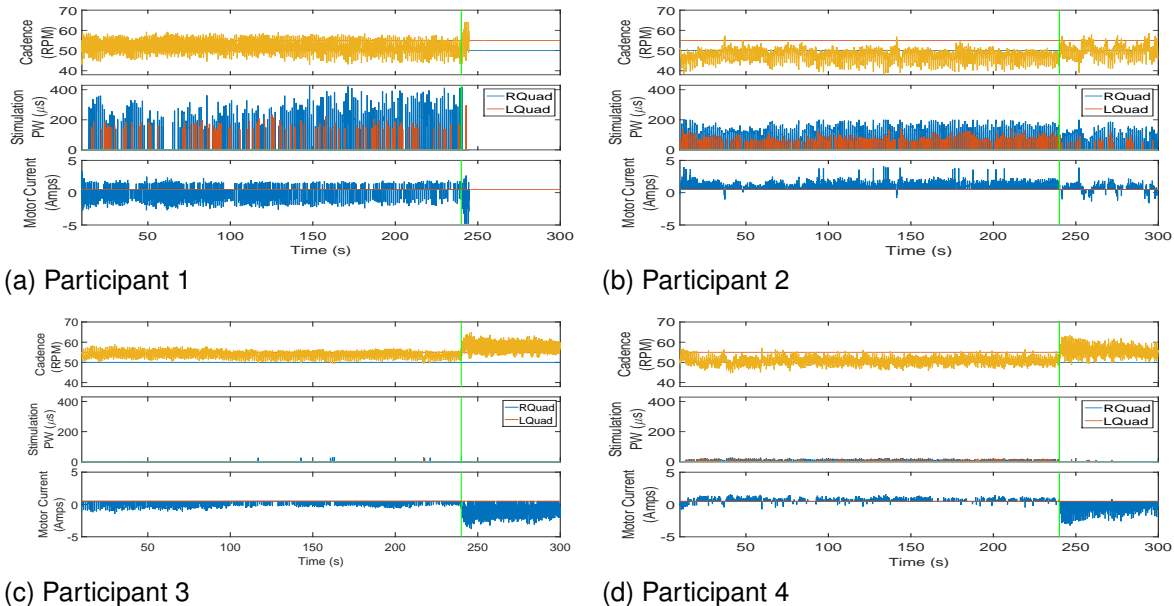
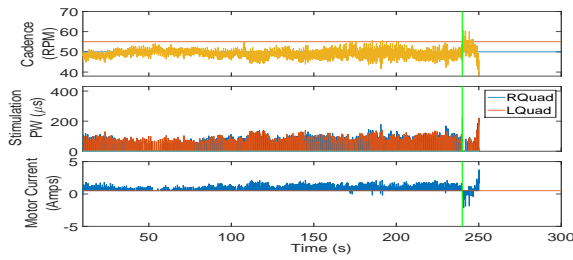
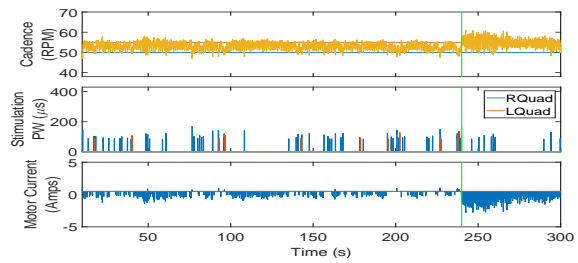


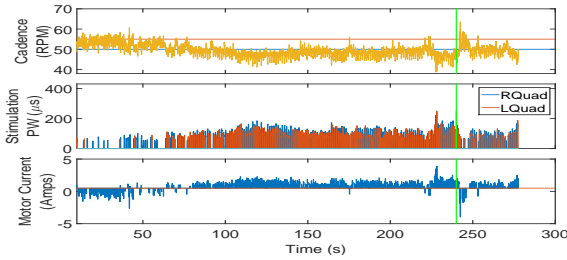
Figure 5-4. Cycling cadence (top), stimulation pulsewidth (middle) sent to the right (blue) and left (red) quadriceps, and motor current (bottom) across nine participants. Individual results during the 3 mode trials highlight how the developed algorithm accommodates for individual differences. The vertical green line represents the four minute mark when the participants were asked to pedal at maximum effort. A current of 0.5 amps (orange line) is used as a feed forward to the motor, so motor current greater than 0.5 amps corresponds to assistance and motor current less than 0.5 amps corresponds to resistance. At steady state, the blue line at 50 RPM and red line at 55 RPM of the cadence plot indicate the selected upper and lower bounds for the uncontrolled mode and the yellow line depicts actual cadence, all of which were shown to the participants throughout the trial. The plots depict the participant attempting to stay within the desired cadence range until minute 4, after which the participant attempts to pedal faster, often transitioning from the uncontrolled mode to the resistive mode. For all participants, when the cadence is below the lower threshold, positive motor input and FES input alternates to assist the participant. When the cadence is above the upper threshold, there is negative motor input.



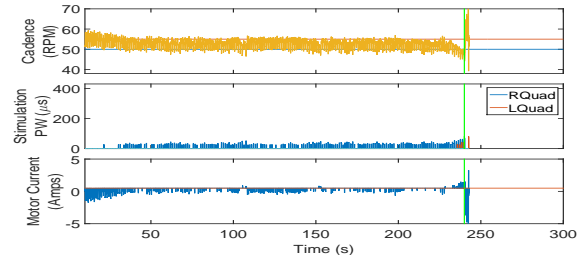
(e) Participant 5



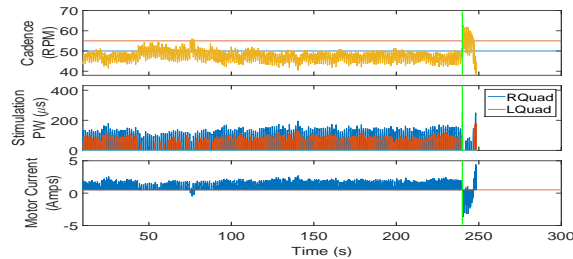
(f) Participant 6



(g) Participant 7



(h) Participant 8



(i) Participant 9

Figure 5-4. Cycling cadence (top), stimulation pulsewidth (middle) sent to the right (blue) and left (red) quadriceps, and motor current (bottom) across nine participants. Individual results during the 3 mode trials highlight how the developed algorithm accommodates for individual differences. The vertical green line represents the four minute mark when the participants were asked to pedal at maximum effort. A current of 0.5 amps (orange line) is used as a feed forward to the motor, so motor current greater than 0.5 amps corresponds to assistance and motor current less than 0.5 amps corresponds to resistance. At steady state, the blue line at 50 RPM and red line at 55 RPM of the cadence plot indicate the selected upper and lower bounds for the uncontrolled mode and the yellow line depicts actual cadence, all of which were shown to the participants throughout the trial. The plots depict the participant attempting to stay within the desired cadence range until minute 4, after which the participant attempts to pedal faster, often transitioning from the uncontrolled mode to the resistive mode. For all participants, when the cadence is below the lower threshold, positive motor input and FES input alternates to assist the participant. When the cadence is above the upper threshold, there is negative motor input.

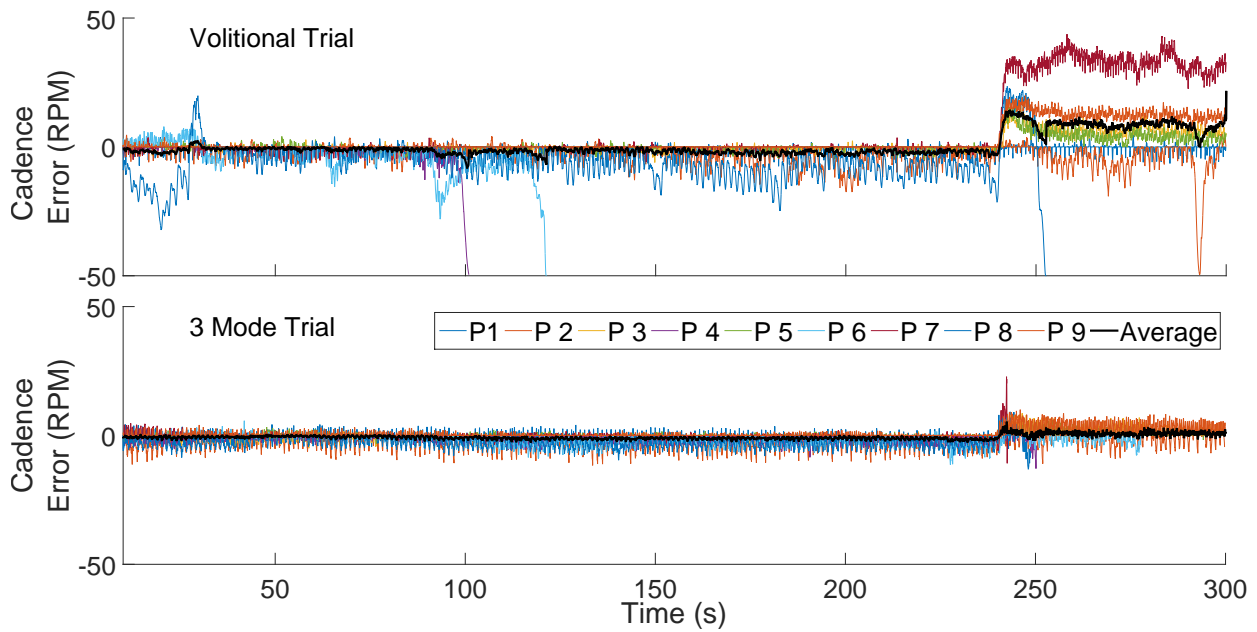


Figure 5-5. Cadence error from each participant and average cadence error, for both the volitional (top) and 3 mode (bottom) trials.

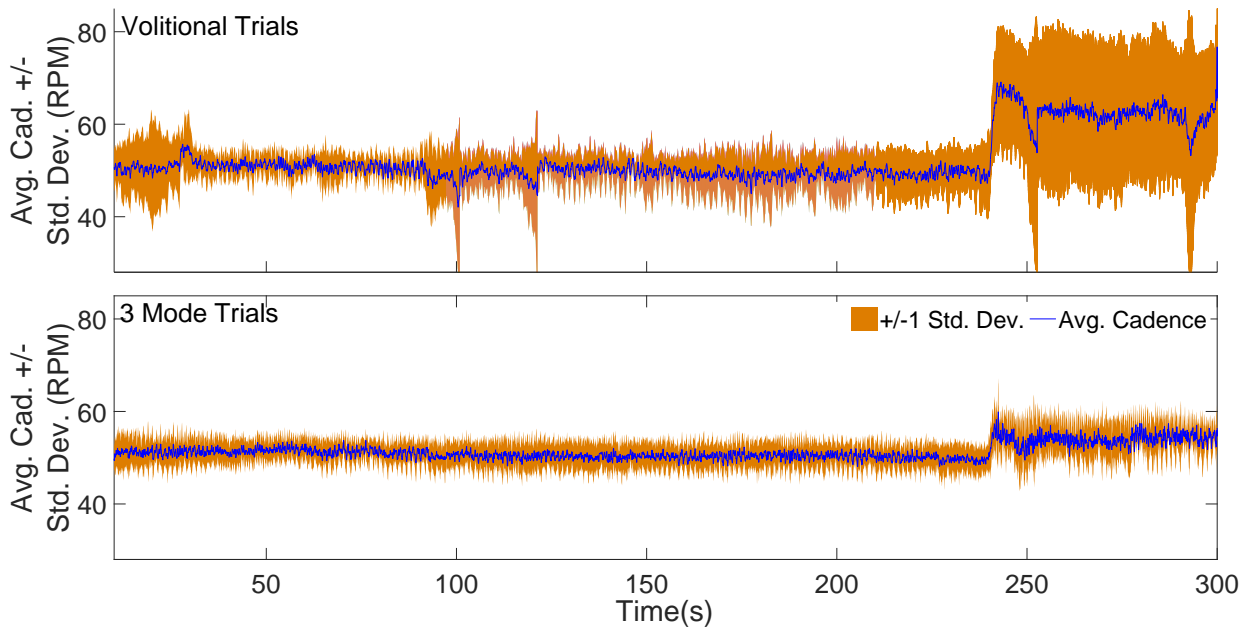


Figure 5-6. Cadence averaged over the nine subjects +/- the standard deviation over time for both the volitional (top) and 3 mode (bottom) trials.

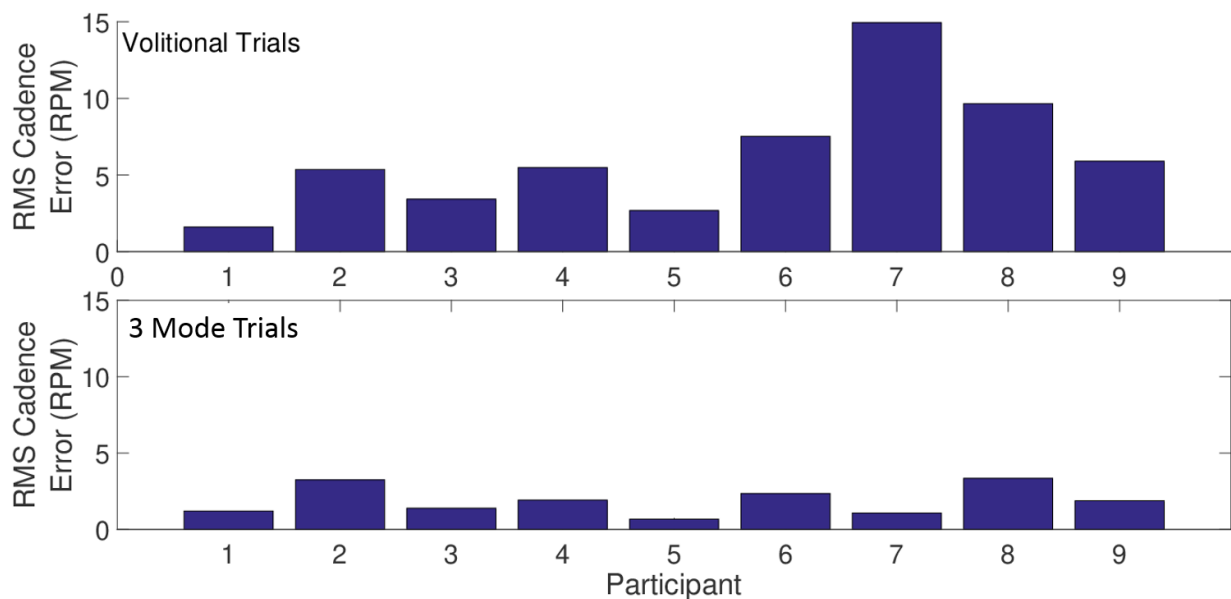


Figure 5-7. RMS cadence errors of each of the nine participants for the volitional (top) and 3 mode (bottom) trials.

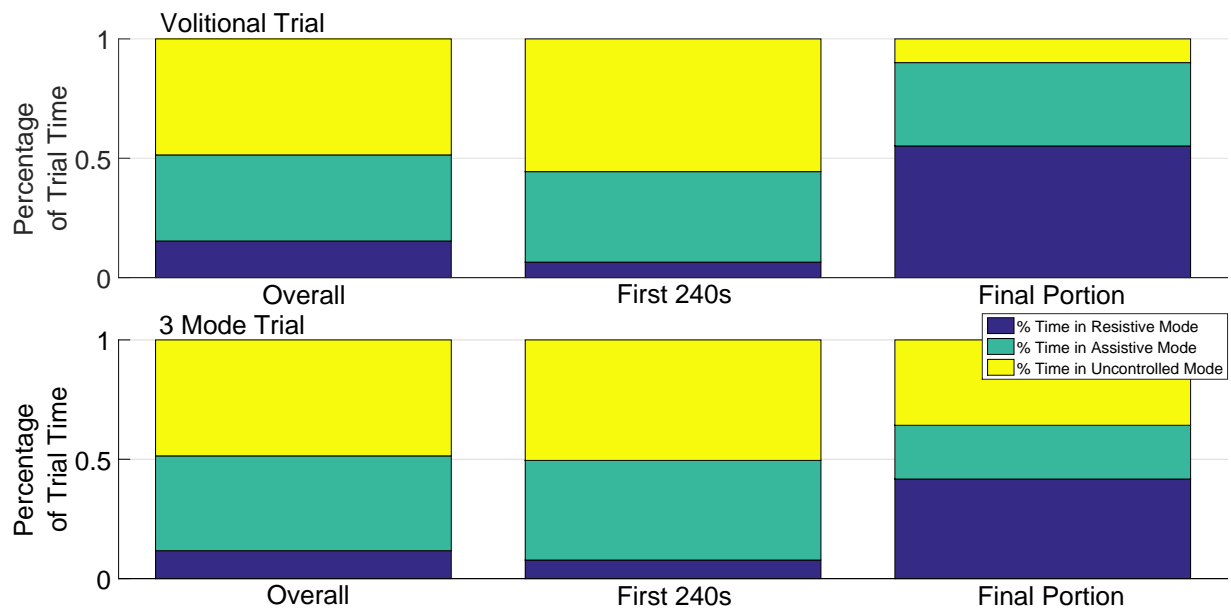


Figure 5-8. Average percentage of time in each of the three modes during the entire trial, first 240s, and final portion of both the volitional (top) and 3 mode (bottom) trials.

the entire experiment (51.0 RPM), during the first 4 minutes (50.7 RPM), and when the participants were asked to pedal faster at the end of the trial (54.0 RPM). Specifically, Figures 5-5 and 5-6 display the change in cadence error and average cadence during all parts of the volitional and 3 mode trials. Due to the ability of most participants to volitionally pedal around 50 RPM and since the average was still calculated for participants who fatigued before the trial completed, the overall average cadence did not change significantly from the volitional trials to the 3 mode trials; however the RMS error (displayed in Figure 5-7 for all nine subjects) was reduced from the volitional to the 3 mode trials for all portions of the trials, with p-values of 0.01, 0.03, and 0.04 (not statistically significant when the threshold is adjusted for multiple comparisons) for the entire trial, first 240s, and final portion of the trials, respectively.

With the data from nine subjects, there is some level of correlation between cycling and walking performance. Table 5-3 displays R correlation values for cadence metrics from Table 5-2 in comparison to SSWS and FCWS for both the volitional and 3 mode trials, where an R value equal to 1 would indicate perfect positive correlation, an R value of -1 would indicate perfect negative correlation, and an R value of 0 would indicate no correlation.

5.3.4 Discussion

The trial with the able-bodied participant was used to depict all three modes of the control system. After the first 10 seconds of the motor bringing the cadence up to 45 RPM, the participant was instructed to lightly pedal such that their voluntary efforts did not reach the minimum cadence threshold. As seen in Figure 5-2, control input was switched between FES and the motor during this time, often causing the cadence to cross above the lower threshold. From seconds 80-125, the participant was instructed to attempt to stay between the two cadence thresholds to demonstrate the passive mode. Figure 5-2 shows that there were few instances that input was sent to either FES or the motor, all of which corresponded to instances the cadence was above or below the

desired region. From seconds 125-180, the participant was instructed to pedal much harder than necessary to stay within the threshold lines to demonstrate the resistive mode. During this time, no FES input was sent and input below 0.5 Amps was sent to the motor, often sending the cadence back into the desired range. The goal of the trial with the able-bodied participant was to clearly depict the three modes of the control system separately in response to the cadence escaping the upper and lower bounds, which is expected to correspond to individuals at three different ability levels. However, it is possible that a person with a movement disorder or an able-bodied person pedaling at a higher cadence would switch modes more quickly and eventually fatigue such that assistance mode was utilized more, as in the first part of the current experiment.

The experimental trials for the post-stroke participants lasted 150 seconds instead of 180 seconds since they may be more susceptible to fatigue. Unlike with the able-bodied participant, the stroke patients were asked to volitionally contribute to maintain a cadence within the desired uncontrolled region to the best of their ability until the last 30 seconds when they were asked to pedal with as much force as they were comfortable. They were also asked to perform a completely uncontrolled trial where they were asked to try to pedal within (and then above for the last 30 seconds) the same cadence bounds using only their own volition.

Some participants had difficulty maintaining the minimum desired cadence (e.g., participants depicted in Figures [5-4b](#), [5-4e](#), [5-4g](#), [5-4i](#)), and thus frequently switched between the assistive and uncontrolled modes, utilizing both FES and the motor. Other participants were able to volitionally reach a desired cadence but had trouble maintaining a steady cadence that remained in the desired range (e.g., Participant 1, Figure [5-4a](#)), resulting in frequent switching between all 3 modes, but remaining close to the bounds due to the FES and motor controllers. Thus, the percentage of time spent in each of the 3 modes, of which the averages are shown in Figure [5-8](#), varied significantly amongst participants (i.e., standard deviations are often larger

than the average value), as seen in Table 5-2, indicating that the controller works to maintain a cadence range despite participant ability and various instances of actuators switching, making for an individualized approach. Although it was expected that the assistive and resistive modes would help individuals remain in the uncontrolled mode for a larger percentage of time than when voluntarily pedaling, this was not the case for many of the participants; however, note that this particular statistic is potentially misleading since it does not show how far into each mode the participant pedaled. Figures 5-4a-5-4i show that during the 3 mode trials when participants were pedaling in the assistive or resistive modes, their cadence was not far from the desired, whereas greater deviations occurred during the volitional trials. The range of cadence values within one standard deviation of the average is much larger for volitional trials than 3 mode trials, as shown in Figure 5-6, as well as larger RMS errors, as shown in Figure 5-7. Some participants with more strength and coordination were able to volitionally pedal in the desired range for the volitional trial; however, their cadence varied further outside the desired range during volitional trials than with the assistance and resistance of the FES and motor during the 3 mode trial. Moreover, since Participants 5, 7, and 9 did not complete the volitional trial due to fatigue, the percentage of time spent below the desired range would have likely been significantly more had they continued to try pedaling despite fatigue. Thus, the more noteworthy outcome from the results in Table 5-2 is the reduction in standard deviation of the cadence from the volitional pedaling trial to the 3 mode trial (and consequently, the reduction in RMS error), showing that a more consistent cadence could be maintained compared to volitional pedaling, which is a common goal in rehabilitative cycling [82]. Not all participants experienced a decrease in standard deviation from the final portion of the volitional trial to the final portion of the 3 mode trial; however, some participants opted to end trials before completion, rather than slow their cadence, which would've resulted in a larger standard deviation. Such is not reflected in the statistics for the final portion. In particular, Participants 4 and 6 would

likely had larger cadence error and standard deviation during the volitional trials if they had not opted to stop early. Moreover, participants may have exerted more effort than they could maintain for the entire final portion, resulting in a larger deviation in cadence than the first 240s. Standard deviation for the entire trials (i.e., OA) are not included in Table 5-2 since the participants were instructed to purposefully increase their cadence at the four minute mark.

In general, the slower the walker, the slower the cycling cadence in both the volitional and 3 mode trials, which is evident in the R correlation values between the SSWS and FCWS, both overall and in the first 240s, which ranged from 0.774-0.888, as listed in Table 5-3. Both walking speeds correlated more with cadence during the final portion of the 3 mode trials than volitional-only trials, with respective R correlation values of 0.886 (SSWS) and 0.858 (FCWS) versus 0.493 (SSWS) and 0.603 (FCWS). Thus, it may be concluded that a participant's ability to overcome the motor resistance better predicts their walking ability than pedaling at a more comfortable cadence does; however, with more than one participant stopping during the final portion of both trials, this statistic does not capture all of the data. Most notably, individuals with the slowest walking speeds (i.e., Participants 7 and 9) were the same participants that did not complete the volitional trial, and were not included in the statistics for the final portion of the volitional trials. There is strong evidence of negative correlation between walking speed and the standard deviation of cadence during volitional trials (between -0.941 and -0.716), but much less for 3 mode trials (between -0.440 and 0.140). Thus, functional ability is an indicator of a person's ability to maintain cycling cadence on their own, but the developed control scheme allowed patients to maintain consistent cadence, no matter their ability, resulting in a low correlation value. The assistance and resistance of the FES and the motor allowed all participants to remain close to the same desired cadence range, unlike volitional pedaling.

A sinusoidal-like cadence trajectory is natural when volitionally pedaling at a constant effort, as there are portions of the crank where pedaling is easier than others (i.e., kinematically efficient and inefficient regions), causing some of the variation in cadence. Healthy normals can pedal with a small variation in cadence (e.g., within 50-55 RPM) so any deviations show strengths and weaknesses in the participants. However, a higher, lower, wider, or narrower range selected in practice by a physical therapist could significantly alter the amount of time spent in each mode, and thus alter the error values. Regardless, since the motor and FES controllers are exponentially stable in both the assistive and resistive modes, the cadence is mathematically guaranteed to exponentially approach the desired cadence range (see appendix for proof). Even in the case of a patient with complete paralysis, stability can still be guaranteed (set $\tau_{vol} = 0$) and the controller will act as in previous FES studies performed by the authors (e.g., [47]).

5.4 Concluding Remarks

The novel combined motor and FES control system developed in this chapter is designed to enable a cycle rider to maintain a cadence within a desired range with volitional pedaling. With assistive, uncontrolled, and resistive modes, the control system has the potential to advance motorized FES-cycling as a rehabilitation exercise for people with movement disorders. Specifically, FES and a motor can assist those with minimal leg strength or at the onset of fatigue, and the motor can provide resistance to someone who can easily pedal faster than a desired range, for an additional challenge. A Lyapunov-like analysis proved stability of the controllers for the multi-level switched system, despite unknown disturbances, showing exponential convergence to the desired cadence range (i.e., $e_1 \in (0, \Delta_d)$). Preliminary experiments validated the use of the control system in all three modes for an able-bodied person. Nine post-stroke participants also participated in pedaling the custom tricycle. Despite a wide range of volitional abilities, the post-stroke participants were able to pedal a recumbent tricycle with average cadences ranging from 47.60 - 54.67 RPM, compared to the desired range

of 50-55 RPM. With assistive, passive, and resistive modes, the developed control system has the potential to advance motorized FES-cycling as a rehabilitation exercise for people with movement disorders.

CHAPTER 6 SPLIT-CRANK CYCLING

This chapter focuses on control of a cycle with a decoupled crank (i.e., a split-crank cycle). Without the gravitational force of one leg affecting the motion of the opposite leg (like with a coupled crank arm), a split-crank cycle is much more difficult to pedal than a single-crank cycle. To show the benefit of the controller, able-bodied participants were asked to perform two trials with volitional contribution, one with and one without activation of FES and the motors; however, only two of the three able-bodied participants were capable of sustaining a pedaling motion on the split-crank cycle. The results of participants with neurological conditions are compared to those of able-bodied participants since the ultimate goal of rehabilitation technology is to enable users to move normally despite any neurological condition. Experiments were performed on three people with neurological conditions and three able-bodied participants.

As in [62], [68], and Chapter 5, this chapter implements a controller that switches between three modes (i.e., assistive, uncontrolled, and resistive modes) as the continuous state-dynamics evolve. In this chapter, three levels of switching are used on each side of the cycle-rider system. High-level switching denotes switching amongst the three modes and is based on cadence and position for the non-dominant and dominant sides, respectively. Mid-level position-dependent switching within the assistive mode of each side will occur between the quadriceps, gluteal, and hamstring muscle groups, and the electric motor, similar to the protocol developed in [47]. Low-level switching denotes the arbitrary switching to distribute partial control authority to the motor within FES regions of the assistive mode whenever the FES control input saturates at the individually selected comfort threshold for each muscle group.

6.1 Split-Crank Model

Unlike the single crank considered in Chapter 5, the switched dynamics in (2–8) of the cycle-rider system are considered separately for both sides and are derived in [68] as^{1 2}

$$\sum_{m \in \mathcal{M}} B_m u_{m_l} + B_{e_l} u_{e_l} + \tau_{vol_l} = M_l \ddot{q}_l + b_{c_l} \dot{q}_l + d_{c_l} + V_l \dot{q}_l + G_l + P_l + d_{r_l}, \quad (6-1)$$

$\forall l \in S \triangleq \{1, 2\}$, which indicates the impaired/non-dominant ($l = 1$) and dominant ($l = 2$) sides, respectively, and $m \in \mathcal{M} = \{Q, G, H\}$ indicates the quadriceps femoris (Q), gluteal (G), and hamstring (H) muscle groups, respectively. High-level switching occurs on both sides of the cycle (i.e., $\forall l \in S$) between assistive, uncontrolled, and resistive modes according to the subsequently designed switching signals. On the non-dominant side, the velocity- (i.e., cadence-) based high-level switching laws are defined as

$$\sigma_{a_1} \triangleq \begin{cases} 1 & \text{if } \dot{q}_1 \leq \dot{q}_{d1} \\ 0 & \text{if } \dot{q}_1 > \dot{q}_{d1} \end{cases}, \quad \sigma_{r_1} \triangleq \begin{cases} 1 & \text{if } \dot{q}_1 \geq \dot{q}_{\bar{d}1} \\ 0 & \text{if } \dot{q}_1 < \dot{q}_{\bar{d}1} \end{cases}, \quad (6-2)$$

where the switching signals $\sigma_{a_1} : \mathbb{R} \rightarrow \{0, 1\}$ and $\sigma_{r_1} : \mathbb{R} \rightarrow \{0, 1\}$ define the assistive (i.e., $\sigma_{a_1} = 1, \sigma_{r_1} = 0$) and resistive (i.e., $\sigma_{a_1} = 0, \sigma_{r_1} = 1$) modes for the non-dominant side, respectively. The switching point between the assistive and uncontrolled (i.e., $\sigma_{a_1} = 0, \sigma_{r_1} = 0$) modes is denoted by $\dot{q}_{d1} : \mathbb{R}_{>0} \rightarrow \mathbb{R}$ and is the selectable minimum desired cadence value. The switching point between the uncontrolled and resistive modes is denoted by $\dot{q}_{\bar{d}1} : \mathbb{R}_{>0} \rightarrow \mathbb{R}$ and is the selectable maximum desired cadence value. Thus, the uncontrolled mode for the non-dominant side is active when

¹ For notational brevity, all functional dependencies are suppressed unless required for clarity of exposition.

² With the exception of the subscript denoting the side of the cycle, all terms hold the same meaning as when introduced in Chapter 2.

$\dot{q}_1 \in [\dot{q}_{d1}, \dot{q}_{\bar{d}1}]$. Similarly, high-level switching between the three modes (i.e., assistive, resistive, and uncontrolled) on the dominant side is based on position, such that

$$\sigma_{a_2} \triangleq \begin{cases} 1 & \text{if } q_2 \leq q_{d2} \\ 0 & \text{if } q_2 > q_{d2} \end{cases}, \quad \sigma_{r_2} \triangleq \begin{cases} 1 & \text{if } q_2 \geq q_{\bar{d}2} \\ 0 & \text{if } q_2 < q_{\bar{d}2} \end{cases}, \quad (6-3)$$

where the switching signals $\sigma_{a_2} : Q \rightarrow \{0, 1\}$ and $\sigma_{r_2} : Q \rightarrow \{0, 1\}$ define the assistive (i.e., $\sigma_{a_2} = 1, \sigma_{r_2} = 0$) and resistive (i.e., $\sigma_{a_2} = 0, \sigma_{r_2} = 1$) modes for the dominant side, respectively. The dominant side is designed to track the non-dominant side's position such that the switching points between the uncontrolled (i.e., $\sigma_{a_2} = 0, \sigma_{r_2} = 0$) mode and the assistive and resistive modes are denoted by $q_{d2} : \mathbb{R}_{>0} \rightarrow \mathbb{R}$ and $q_{\bar{d}2} : \mathbb{R}_{>0} \rightarrow \mathbb{R}$, respectively, and defined as $q_{d2} \triangleq q_1 - \pi - \Delta_{d2}$ and $q_{\bar{d}2} \triangleq q_1 - \pi + \Delta_{d2}$, where $\Delta_{d2} \in \mathbb{R}_{>0}$ is the range of allowable position values for the dominant leg to deviate from the non-dominant side. Thus, q_{d2} and $q_{\bar{d}2}$ are the selectable minimum and maximum desired position values that bound the dominant side's uncontrolled mode, and are centered around $q_1 - \pi$ to maintain a 180 degree offset³. Each subsystem is in its respective uncontrolled mode when $\sigma_{a_l} = \sigma_{r_l} = 0, \forall l \in S$. Within the assistive mode for both the non-dominant and dominant subsystems, low-level switching amongst the muscle groups and motor is based on definitions for the subsequent FES regions for each muscle group $\mathcal{Q}_m \subset \mathcal{Q}, \forall m \in \mathcal{M}$, as in [62] and Chapter 5. The stimulation intensity applied to each muscle group u_{m_l} is defined as

$$u_{m_l} \triangleq \sigma_{a_l} \sigma_{m_l} \text{sat}_{\beta_{m_l}} [k_{m_l} u_{M_l}], \quad (6-4)$$

$\forall l \in S, \forall m \in \mathcal{M}$, where σ_{a_l} was defined in (6-2) and (6-3), the subsequently designed FES control input is denoted by $u_{M_l} : \mathbb{R}_{>0} \rightarrow \mathbb{R}$, and $k_{m_l} \in \mathbb{R}_{>0}$ is a selectable constant

³ Definitions for q_{d2} and $q_{\bar{d}2}$ represent a shift of π radians; however, this offset could be arbitrarily selected or time-varying.

control gain. The saturation function $\text{sat}_{\beta_{m_l}}(\cdot)$ is defined as $\text{sat}_{\beta_{m_l}}(\kappa) \triangleq \kappa$ for $|\kappa| \leq \beta_{m_l}$ and $\text{sat}_{\beta_{m_l}}(\kappa) \triangleq \text{sgn}(\kappa)\beta_{m_l}$ for $|\kappa| > \beta_{m_l}$, where $\beta_{m_l} \in \mathbb{R}_{>0}$ is the user-defined comfort threshold for each muscle group on each side. The low-level switching signal $\sigma_{m_l} : Q \rightarrow \{0, 1\}$ is designed for each muscle group such that $\sigma_{m_l}(q_l) = 1$ when $q_l \in \mathcal{Q}_m$ and $\sigma_{m_l}(q_l) = 0$ when $q_l(t) \notin \mathcal{Q}_m, \forall l \in S, \forall m \in \mathcal{M}$. The overall FES region, \mathcal{Q}_M , is identical for each side and defined as the union of individual muscle regions, i.e., $\mathcal{Q}_M \triangleq \bigcup_{m \in \mathcal{M}} \{\mathcal{Q}_m\}, \forall m \in \mathcal{M}$.

The applied motor current u_{e_l} is defined as

$$u_{e_l} \triangleq (\sigma_{r_l} + \sigma_{a_l}\sigma_{e_l})u_{r_l}, \quad (6-5)$$

$\forall l \in S$, where $u_{r_l} : \mathbb{R}_{>0} \rightarrow \mathbb{R}$ denotes the subsequently designed motor control input, and $\sigma_{e_l} : Q \times \mathbb{R}_{>0} \rightarrow \mathbb{R}_{\geq 0}$ is an auxiliary low-level switching signal for activation of the electric motor within the assistive mode, defined as

$$\sigma_{e_l} \triangleq \begin{cases} 1 & \text{if } q_l \notin \mathcal{Q}_{FES} \\ \gamma_l & \text{if } q_l \in \mathcal{Q}_{FES}, u_{m_l} = \beta_{m_l} \\ 0 & \text{if } q_l \in \mathcal{Q}_{FES}, u_{m_l} \neq \beta_{m_l} \end{cases}, \quad (6-6)$$

$\forall l \in S, \forall m \in \mathcal{M}$. Hence, the motor can be activated in the assistive mode in FES and non-FES regions, where $\gamma_l : \mathbb{R}_{\geq 0} \rightarrow \mathbb{R}_{\geq 0}$ is the motor's ratio of control authority, defined as $\gamma_l \triangleq \sum_{m \in \mathcal{M}} \frac{k_{m_l} u_{M_l} - \beta_{m_l}}{\beta_{m_l}}, \forall l \in S$. When a subsystem is in an FES region, the corresponding motor only activates when the stimulation input for any muscle group within that subsystem/side reaches its respective comfort threshold β_{m_l} and γ_l proportionately distributes the remaining control effort to the motor. Thus, the switching laws autonomously activate subsets of muscle groups and the motor based on position, velocity, and stimulation level.

Substituting (6-2)-(6-6) into (6-1) yields

$$\sum_{m \in \mathcal{M}} B_m \sigma_{a_l} \sigma_{m_l} \text{sat}_{\beta_{m_l}} [k_{m_l} u_{M_l}] + B_{E_l} u_{r_l} + \tau_{vol_l} = M_l \ddot{q}_l + b_{c_l} \dot{q}_l + d_{c_l} \quad (6-7)$$

$$+ V_l \dot{q}_l + G_l + P_l + d_{r_l},$$

$\forall l \in S$, where $B_{E_1} : Q \times \mathbb{R} \times \mathbb{R}_{\geq 0} \rightarrow \mathbb{R}$ and $B_{E_2} : Q \times \mathbb{R}_{\geq 0} \rightarrow \mathbb{R}$ are the switched motor control effectiveness for each side, defined as

$$B_{E_l} \triangleq B_e (\sigma_{r_l} + \sigma_{a_l} \sigma_{e_l}). \quad (6-8)$$

6.2 Control Development

Without loss of generality, the control objective is for the non-dominant subsystem to track a desired cadence range and for the dominant subsystem to regulate the cadence to a desired range and for the dominant subsystem to regulate the position to a desired range such that a crank phase difference within a desired range centered at 180 degrees from the dominant leg is maintained. However, open questions remain on whether or not varying the phase difference while FES-cycling would improve rehabilitation outcomes.

6.2.1 Non-dominant Side

The cadence tracking objective for the non-dominant leg is quantified by the velocity error $e_1 : \mathbb{R}_{\geq 0} \rightarrow \mathbb{R}$ and auxiliary error $r_1 : \mathbb{R}_{\geq 0} \rightarrow \mathbb{R}$, defined as

$$e_1 \triangleq \dot{q}_{d1} - \dot{q}_1, \quad (6-9)$$

$$r_1 \triangleq e_1 + (1 - \sigma_{a_l}) \Delta_{d1}. \quad (6-10)$$

where \dot{q}_{d1} , $\dot{q}_{\bar{d}1}$, and Δ_{d1} were defined previously. Taking the time derivative of (6-9), multiplying by M_1 , and using (6-7) with $l = 1$ yields

$$\begin{aligned}
M_1 \dot{e}_1 &= -B_{E_1} u_{r_1} - \tau_{vol_1} - V_1 r_1 + \chi_1, \\
&\quad - \sum_{m \in \mathcal{M}} B_m \sigma_{a_1} \sigma_{m_1} \text{sat}_{\beta_{m_1}} [k_{m_1} u_{M_1}]
\end{aligned} \tag{6-11}$$

where the auxiliary term $\chi_1 : Q \times \mathbb{R} \times \mathbb{R}_{\geq 0} \rightarrow \mathbb{R}$ is defined as $\chi_1 \triangleq b_{c_1} \dot{q}_1 + d_{c_1} + G_1 + P_1 + d_{r_1} + V_1 \dot{q}_{d1} + V_1 (1 - \sigma_{a_1}) \Delta_{d1} + M_1 \ddot{q}_{d1}$. From Properties 1-6, χ_1 can be bounded as

$$\chi_1 \leq c_1 + c_2 |e_1|, \tag{6-12}$$

where $c_1, c_2 \in \mathbb{R}_{>0}$ are known constants, and $|\cdot|$ denotes the absolute value. Based on (6-11), (6-12), and the subsequent stability analysis, the FES control input to the muscle groups on the non-dominant side is designed as

$$u_{M_1} = k_{1s} + k_{2s} r_1, \tag{6-13}$$

where $k_{1s}, k_{2s} \in \mathbb{R}_{>0}$ are constant selectable control gains. The switched control input to the motor is designed as

$$u_{r_1} = k_{1e} \text{sgn}(r_1) + k_{2e} r_1, \tag{6-14}$$

where $k_{1e}, k_{2e} \in \mathbb{R}_{>0}$ are constant selectable control gains. Substituting (6-13) and (6-14) into (6-11) yields

$$\begin{aligned}
M_1 \dot{e}_1 &= - \sum_{m \in \mathcal{M}} B_m \sigma_{a_1} \sigma_{m_1} \text{sat}_{\beta_{m_1}} [k_{m_1} (k_{1s} + k_{2s} r_1)] \\
&\quad - B_{E_1} (k_{1e} \text{sgn}(r_1) + k_{2e} r_1) - \tau_{vol_1} - V_1 r_1 + \chi_1.
\end{aligned} \tag{6-15}$$

6.2.2 Dominant Side

The position tracking objective for the dominant leg is quantified by the error $e_2 : \mathbb{R}_{\geq 0} \rightarrow \mathbb{R}$ and auxiliary errors $r_2 : \mathbb{R}_{\geq 0} \rightarrow \mathbb{R}$ and $r_3 : \mathbb{R}_{\geq 0} \rightarrow \mathbb{R}$, defined as

$$e_2 \triangleq \dot{q}_{d2} - \dot{q}_2, \quad (6-16)$$

$$r_2 \triangleq e_2 + (1 - \sigma_{a2}) \Delta_{d2}, \quad (6-17)$$

$$r_3 \triangleq \dot{e}_2 + \alpha e_2, \quad (6-18)$$

where $\alpha \in \mathbb{R}_{>0}$ is a constant selectable control gain, and \dot{q}_{d2} , \ddot{q}_{d2} , and Δ_{d2} were defined previously. Taking the time derivative of (6-18), multiplying by M_2 , and using (6-7) with $l = 2$ and (6-16) yields

$$M_2 \dot{r}_3 = -B_{E2} u_{r2} - \tau_{vol2} - V_2 r_3 - r_2 + \chi_2 - \sum_{m \in \mathcal{M}} B_m \sigma_{a2} \sigma_{m2} \text{sat}_{\beta_{m2}} [k_{m2} u_{M2}], \quad (6-19)$$

where the auxiliary term $\chi_2 : Q \times \mathbb{R} \times \mathbb{R}_{\geq 0} \rightarrow \mathbb{R}$ is defined as $\chi_2 \triangleq b_{c2} \dot{q}_2 + d_{c2} + G_2 + P_2 + d_{r2} + V_2 \dot{q}_{d2} + V_2 \alpha e_2 + M_2 \ddot{q}_{d2} + M_2 \alpha r_3 - M_2 \alpha^2 e_2 + r_2$. From Properties 1-6, χ_2 can be bounded as

$$\chi_2 \leq c_3 + c_4 \|z\| + c_5 \|z\|^2, \quad (6-20)$$

where $z \triangleq [r_2 \ r_3]^T$, $\|\cdot\|$ is the Euclidean norm, and $c_3, c_4, c_5 \in \mathbb{R}_{>0}$ are known constants. Based on (6-19), (6-20), and the subsequent stability analysis, the FES control input to the muscle groups on the dominant side is designed as

$$u_{M2} = k_{3s} r_3 + (k_{4s} + k_{5s} \|z\| + k_{6s} \|z\|^2) \text{sgn}(r_3), \quad (6-21)$$

where $k_{3s}, k_{4s}, k_{5s}, k_{6s} \in \mathbb{R}_{>0}$ are constant selectable control gains. The switched control input to the motor on the dominant side is designed as

$$u_{e2} = k_{3e}r_3 + (k_{4e} + k_{5e} \|z\| + k_{6e} \|z\|^2) \operatorname{sgn}(r_3), \quad (6-22)$$

where $k_{3e}, k_{4e}, k_{5e}, k_{6e} \in \mathbb{R}_{>0}$ are constant selectable control gains. Substituting (6-21) and (6-22) into (6-19) yields

$$\begin{aligned} M_2 \dot{r}_3 = & - \sum_{m \in \mathcal{M}} B_m \sigma_{a2} \sigma_{m2} \operatorname{sat}_{\beta_{m2}} \left[k_{m2} k_{3s} r_3 + k_{m2} (k_{4s} + k_{5s} \|z\| + k_{6s} \|z\|^2) \operatorname{sgn}(r_3) \right] \\ & - B_{E2} \left[k_{3e} r_3 + (k_{4e} + k_{5e} \|z\| + k_{6e} \|z\|^2) \operatorname{sgn}(r_3) \right] - \tau_{vol2} - V_2 r_3 - r_2 + \chi_2. \end{aligned} \quad (6-23)$$

6.3 Stability Analysis

The stability analysis is divided into non-dominant (Section IV, A) and dominant (Section IV, B) subsystems. To facilitate the analysis of switching signals, switching times are denoted by $\{t_{n,l}^i\}$, $i \in \{a, r, u\}$, $n \in \{0, 1, 2, \dots\}$, $\forall l \in S$, representing the times when each side's subsystem switches into the assistive ($i = a$), resistive ($i = r$), or uncontrolled ($i = u$) modes (i.e., every time a switch occurs, $n^+ = n + 1$).

6.3.1 Stability of the Non-Dominant Subsystem

Let $V_{L1} : \mathbb{R} \rightarrow \mathbb{R}$ be a continuously differentiable, positive definite, common Lyapunov function candidate defined as

$$V_{L1} \triangleq \frac{1}{2} M_1 r_1^2, \quad (6-24)$$

which satisfies the following inequalities:

$$\frac{c_m}{2} r_1^2 \leq V_{L1} \leq \frac{c_M}{2} r_1^2, \quad (6-25)$$

where c_m and c_M are introduced in Property 1. To facilitate the subsequent stability analysis, let the following gain conditions apply:

$$k_{1s} > \frac{c_1 + c_{vol}}{k_{min1} c_{b_m}}, \quad k_{2s} > \frac{c_2}{k_{min1} c_{b_m}}, \quad (6-26)$$

$$k_{1e} > \frac{c_{vol} + c_1}{c_{b_e} \min(1, \gamma_1)}, \quad k_{2e} > \frac{c_2}{c_{b_e} \min(1, \gamma_1)}, \quad (6-27)$$

where $k_{min1} \in \mathbb{R}_{>0}$ is defined as $k_{min1} \triangleq \min(k_{m_l}), \forall l \in S, \forall m \in \mathcal{M}$, γ_1 is introduced in (6-6), c_{b_m} is introduced in Property 8, c_{b_e} in Property 9, c_{vol} in Assumption 1, c_1 and c_2 in (6-12), Δ_{d1} in (6-10), k_{1s} and k_{2s} in (6-13), and k_{1e} and k_{2e} in (6-14).

Theorem 6.1. *Throughout the assistive mode, when $\dot{q}_1 \leq \dot{q}_{d1}$, the closed-loop error system in (6-15) results in exponential convergence of the cadence on the non-dominant side to \dot{q}_{d1} , in the sense that*

$$|e_1(t)| \leq \sqrt{\frac{c_M}{c_m}} |e_1(t_{n,1}^a)| \exp\left[-\frac{\lambda_{a1}}{2}(t - t_{n,1}^a)\right], \quad (6-28)$$

$\forall t \in [t_{n,1}^a, t_{n+1,1}^u)$, $\forall n$, *where $\lambda_{a1} : \mathbb{R}_{\geq 0} \rightarrow \mathbb{R}_{>0}$ is defined as*

$$\lambda_{a1} \triangleq \frac{2}{c_M} [\min(c_{b_e} k_{2e}, c_{b_m} k_{min1} k_{2s}, c_{b_e} \gamma_1 k_{2e}) - c_2],$$

provided the sufficient gain conditions in (6-26) and (6-27) are satisfied.

Proof. When $\dot{q}_1 \leq \dot{q}_{d1}$, $e_1 = r_1 \geq 0$, $\sigma_{a1} = 1$, and $\sigma_{r1} = 0$ (i.e., the non-dominant side subsystem is in the assistive mode and controlled by either FES, the motor, or both). Since B_{m_1} and B_{E_1} are discontinuous, the time derivative of (6-24) exists almost everywhere (a.e.) within $t \in [t_{n,1}^a, t_{n+1,1}^u)$, $\forall n$, and $\dot{V}_{L1} \stackrel{a.e.}{\in} \dot{\tilde{V}}_{L1}$ [83]. After substituting (6-8) and (6-15), the derivative of (6-24) can be solved using Filippov's differential inclusion [76] to yield

$$\dot{V}_{L1} \stackrel{\text{a.e.}}{\leq} \begin{cases} -B_{e_1} (k_{1e} |r_1| + k_{2e} r_1^2) - \tau_{vol_1} r_1 + \chi_1 r_1 & \text{if } \sigma_{e_1} = 1 \\ -\sum_{m \in \mathcal{M}} B_m \sigma_{m_1} k_{m1} (k_{1s} r_1 + k_{2s} r_1^2) - \tau_{vol_1} r_1 + \chi_1 r_1 & \text{if } \sigma_{e_1} = 0 \\ -B_{e_1} \gamma_1 (k_{1e} |r_1| + k_{2e} r_1^2) \\ -\sum_{m \in \mathcal{M}} B_m \sigma_{m_1} \text{sat}_{\beta_{m_1}} [k_{m1} (k_{1s} + k_{2s} r_1)] r_1 - \tau_{vol_1} r_1 + \chi_1 r_1 & \text{if } \sigma_{e_1} = \gamma_1 \end{cases} \quad (6-29)$$

which can be upper bounded using Properties 7 and 8, Assumption 1, and (6-12) as

$$\dot{V}_{L1} \stackrel{\text{a.e.}}{\leq} -(A - c_{vol} - c_1) r_1 - (B - c_2) r_1^2, \quad (6-30)$$

which is negative definite in all cases since $r_1 \geq 0$, provided the gain conditions in (6-26) and (6-27) are satisfied. In (6-30), the values of $A : Q \times \mathbb{R}_{>0} \times \mathbb{R}_{\geq 0} \rightarrow \mathbb{R}_{>0}$ and $B : Q \times \mathbb{R}_{>0} \times \mathbb{R}_{\geq 0} \rightarrow \mathbb{R}_{>0}$ depend on the switching signals, and are defined as

$$A \triangleq \begin{cases} c_{b_e} k_{1e} & \text{if } \sigma_{e_1} = 1 \\ c_{b_m} k_{min1} k_{1s} & \text{if } \sigma_{e_1} = 0 \\ c_{b_e} \gamma_1 k_{1e} + c_{b_m} \beta_{m1} & \text{if } \sigma_{e_1} = \gamma_1 \end{cases},$$

$$B \triangleq \begin{cases} c_{b_e} k_{2e} & \text{if } \sigma_{e_1} = 1 \\ c_{b_m} k_{min1} k_{2s} & \text{if } \sigma_{e_1} = 0 \\ c_{b_e} \gamma_1 k_{2e} & \text{if } \sigma_{e_1} = \gamma_1 \end{cases}.$$

Furthermore, (6-25) can be used to upper bound (6-30) as

$$\dot{V}_{L1} \stackrel{\text{a.e.}}{\leq} -\lambda_{a1} V_{L1}, \quad (6-31)$$

$t \in [t_{n,1}^a, t_{n+1,1}^u), \forall n$, where λ_{a1} was defined previously. Solving the inequality in (6-31), using (6-25), and performing some algebraic manipulation yields exponential convergence of r_1 and e_1 to zero, as in (6-28). Since (6-28) holds for all combinations of

σ_{e_1} and σ_{m_1} while $\sigma_{a_1} = 1$, V_{L1} is a common Lyapunov function for switching during the assistive mode of the non-dominant side. \square

Theorem 6.2. *Throughout the resistive mode, when $\dot{q}_1 \geq \dot{q}_{d1}$, the closed-loop error system in (6–15) results in exponential convergence of the cadence on the non-dominant side to \dot{q}_{d1} , in the sense that*

$$|r_1(t)| \leq \sqrt{\frac{c_M}{c_m}} |r_1(t_{n,1}^r)| \exp\left[-\frac{\lambda_{r1}}{2}(t - t_{n,1}^r)\right], \quad (6-32)$$

$\forall t \in [t_{n,1}^r, t_{n+1,1}^u)$, $\forall n$, where $\lambda_{r1} \in \mathbb{R}_{>0}$ is defined as $\lambda_{r1} \triangleq \frac{2}{c_M}(c_{be}k_{2e} - c_2)$, provided the sufficient gain conditions in (6–27) are satisfied.

Proof. When $\dot{q}_1 \geq \dot{q}_{d1}$, $\sigma_{a_1} = 0$, $\sigma_{r_1} = 1$, and $e_1 + \Delta_{d1} = r_1 \leq 0$ (i.e., the non-dominant side subsystem is in the resistive mode and controlled by the motor). Due to the signum function in (6–15), the time derivative of (6–25) exists a.e. within $t \in [t_{n,1}^r, t_{n+1,1}^u)$, $\forall n$, and $\dot{V}_{L1} \stackrel{\text{a.e.}}{\in} \dot{\tilde{V}}_{L1}$. After substituting (6–10) and (6–15), the derivative of (6–25) can be upper bounded using Properties 7 and 9, Assumption 1, and (6–12) as

$$\dot{V}_{L1} \stackrel{\text{a.e.}}{\leq} -(c_{be}k_{1e} - c_{vol} - c_1 - c_2\Delta_{d1})|r_1| - (c_{be}k_{2e} - c_2)r_1^2, \quad (6-33)$$

$\forall t \in [t_{n,1}^r, t_{n+1,1}^u)$, $\forall n$, which is negative definite provided the sufficient gain conditions in (6–27) are satisfied. Furthermore, since $\dot{V}_{L1} \stackrel{\text{a.e.}}{\in} \dot{\tilde{V}}_{L1}$, (6–33) can be upper bounded as

$$\dot{V}_{L1} \stackrel{\text{a.e.}}{\leq} -\lambda_{r1}V_{L1}, \quad (6-34)$$

$\forall t \in [t_{n,1}^r, t_{n+1,1}^u)$, $\forall n$, where λ_{r1} was defined previously. Solving (6–34), rewriting using (6–25), and performing algebraic manipulation yields (6–32). \square

Remark 6.1. Since the non-dominant side is in the uncontrolled mode when $-\Delta_{d1} < e_1 < 0$, the error is always bounded in the uncontrolled mode. As described in Theorems 6.1 and 6.2, $|r_1|$ (which, by (6–10), is equivalent to e_1 in the assistive mode) decays at an exponential rate in both the assistive and resistive modes to zero. By extension,

$|e_1|$ also decays exponentially in the assistive and resistive modes, to values of 0 and Δ_{d1} , respectively. When the subsystem of the non-dominant side enters the resistive mode, the cadence will exponentially decay towards $\dot{q}_{\bar{d}1}$ (i.e., back into the uncontrolled mode), and when entering the assistive mode, the FES and motor controllers on the non-dominant side will ensure the cadence exponentially increases towards $\dot{q}_{\underline{d}1}$ (i.e., back into the uncontrolled mode). For this particular control objective, there was a desired cadence range, rather than a single value for the desired trajectory, so error convergence to a range (i.e., $[0, \Delta_{d1}]$) is desirable, rather than exponential error convergence to zero.

6.3.2 Stability of the Dominant Side

Let $V_{L2} : \mathbb{R}^2 \rightarrow \mathbb{R}$ be a continuously differentiable, positive definite, common Lyapunov function candidate defined as

$$V_{L2} \triangleq \frac{1}{2}r_2^2 + \frac{1}{2}M_2r_3^2, \quad (6-35)$$

which satisfies the following inequalities:

$$\frac{\min(c_m, 1)}{2} \|z\|^2 \leq V_{L2} \leq \frac{\max(c_M, 1)}{2} \|z\|^2, \quad (6-36)$$

where c_m and c_M are introduced in Property 1. To facilitate the subsequent stability analysis, let the following gain conditions apply:

$$k_{4s} > \frac{c_3 + c_{vol}}{c_{b_m} k_{min2}}, \quad k_{5s} > \frac{c_4}{c_{b_m} k_{min2}}, \quad k_{6s} > \frac{c_5}{c_{b_m} k_{min2}}, \quad (6-37)$$

$$k_{4e} > \frac{c_3 + c_{vol}}{c_{b_e} \max(1, \gamma_2)}, \quad k_{5e} > \frac{c_4}{c_{b_e} \max(1, \gamma_2)}, \quad k_{6e} > \frac{c_5}{c_{b_e} \max(1, \gamma_2)}, \quad (6-38)$$

where c_{b_m} and c_{b_M} are introduced in Property 8, c_{b_e} in Property 9, c_{vol} in Assumption 1, c_3 , c_4 , and c_5 in (6-20), Δ_{d2} in (6-17), k_{4s} , k_{5s} , and k_{6s} in (6-21), and k_{4e} , k_{5e} , and k_{6e} in (6-22).

Theorem 6.3. When $q_2 \leq q_{d2}$, the closed-loop error system in (6–23) results in exponential convergence of the position and cadence on the dominant side to q_{d2} and \dot{q}_1 , respectively, in the sense that

$$\|z(t)\| \leq \sqrt{\frac{\max(c_M, 1)}{\min(c_m, 1)}} \|z(t_{n,2}^a)\| \exp\left(-\frac{\lambda_{a2}}{2}(t - t_{n,2}^a)\right), \quad (6-39)$$

$\forall t \in [t_{n,2}^a, t_{n+1,2}^u)$, $\forall n$, where $\lambda_{a2} : \mathbb{R}_{>0} \rightarrow \mathbb{R}_{>0}$ is defined as

$$\lambda_{a2} \triangleq \frac{2 \cdot \min(c_{b_e} k_{3e}, c_{b_m} k_{min2} k_{3s}, c_{b_e} \gamma_2 k_{3e}, \alpha)}{\max(c_M, 1)} \quad (6-40)$$

, and provided the gain conditions in (6–37) and (6–38) are satisfied.

Proof. When $q_2 \leq q_{d2}$, $\sigma_{a2} = 1$, $\sigma_{r2} = 0$, and $r_2 = e_2 \geq 0$ (i.e., the dominant side subsystem is in the assistive mode and controlled by FES and/or the motor). Similar to the proof of Theorem 1, the time derivative of (6–35) exists a.e. within $t \in [t_{n,2}^a, t_{n+1,2}^u)$, $\forall n$, and $\dot{V}_{L2} \stackrel{\text{a.e.}}{\in} \dot{\tilde{V}}_{L2}$. After substituting (6–23) and the derivative of (6–35), the following inequality is obtained

$$\dot{V}_{L2} \stackrel{\text{a.e.}}{\leq} \left\{ \begin{array}{l} -B_{e2} [k_{3e} r_3^2 + (k_{4e} + k_{5e} \|z\| + k_{6e} \|z\|^2) |r_3|] \\ \quad -\tau_{vol2} r_3 + \chi_2 r_3 - \alpha r_2^2 \quad \text{if } \sigma_{e2} = 1 \\ -\sum_{m \in \mathcal{M}} B_m \sigma_{m2} [k_{m2} k_{3s} r_3^2 + k_{m2} (k_{4s} + k_{5s} \|z\| + k_{6s} \|z\|^2) |r_3|] \\ \quad -\tau_{vol2} r_3 + \chi_2 r_3 - \alpha r_2^2 \quad \text{if } \sigma_{e2} = 0 \\ -B_{e2} \gamma_2 [k_{3e} r_3^2 + (k_{4e} + k_{5e} \|z\| + k_{6e} \|z\|^2) |r_3|] \\ -\sum_{m \in \mathcal{M}} B_m \sigma_{m2} \text{sat}_{\beta_{m2}} [k_{m2} k_{3s} r_3 + k_{m2} (k_{4s} + k_{5s} \|z\| + k_{6s} \|z\|^2) \text{sgn}(r_3)] r_3 \\ \quad -\tau_{vol2} r_3 + \chi_2 r_3 - \alpha r_2^2 \quad \text{if } \sigma_{e2} = \gamma_2 \end{array} \right. , \quad (6-41)$$

which can be upper bounded using Properties 7 and 8, Assumption 1, and (6–20) as

$$\dot{V}_{L2} \stackrel{\text{a.e.}}{\leq} -\min(c_{b_e} k_{3e}, c_{b_m} k_{min2} k_{3s}, c_{b_e} \gamma_2 k_{3e}) r_3^2 - \alpha r_2^2, \quad (6-42)$$

$\forall t \in [t_{n,2}^a, t_{n+1,2}^u)$, $\forall n$, provided the gain conditions in (6–37) and (6–38) are satisfied. Furthermore, (6–36) can be used to upper bound (6–42) as

$$\dot{V}_{L2} \stackrel{\text{a.e.}}{\leq} -\lambda_{a2} V_{L2}, \quad (6-43)$$

$\forall t \in [t_{n,2}^a, t_{n+1,2}^u)$, $\forall n$, where λ_{a2} was defined previously. The inequality in (6–43) can be solved and rewritten using (6–36). Performing some algebraic manipulation yields (6–39). Since (6–39) holds for all combinations of σ_{e2} and σ_{m2} while $\sigma_{a2} = 1$, V_{L2} is a common Lyapunov function for switching during the assistive mode of the dominant side. \square

Theorem 6.4. *When $q_2 \geq q_{\bar{d}2}$, the closed-loop error system in (6–23) results in exponential convergence in the sense that*

$$\|z(t)\| \leq \sqrt{\frac{\max(c_M, 1)}{\min(c_m, 1)}} \|z(t_{n,2}^r)\| \exp[-\lambda_{r2}(t - t_{n,2}^r)], \quad (6-44)$$

$\forall t \in [t_{n,2}^r, t_{n+1,2}^u)$, $\forall n$, where $\lambda_{r2} \in \mathbb{R}_{>0}$ is defined as $\lambda_{r2} \triangleq 2 \frac{\min(c_{b_e} k_{3e}, \alpha)}{\max(c_M, 1)}$, and provided the gain conditions in (6–38) are satisfied.

Proof. When $q_2 \leq q_{\bar{d}2}$, $r_2 \leq 0$, $e_2 \leq 0$, and $\sigma_{r2} = 1$ (i.e., the cycle-rider system is in the motor-resistance mode). After substituting (6–17) and (6–23), the derivative of 6–35 can be upper bounded using Properties 7 and 9, Assumption 1, (6–20), and noting that $r_2 \leq 0$, as

$$\dot{V}_{L2} \stackrel{\text{a.e.}}{\leq} -c_{b_e} k_{3e} r_3^2 - \alpha r_2^2, \quad (6-45)$$

which is negative definite provided the gain conditions in (6–38) are satisfied. Furthermore, since $\dot{V}_{L2} \stackrel{\text{a.e.}}{\in} \dot{V}_{L2}$, (6–45) can be upper bounded as

$$\dot{V}_{L2} \leq -\lambda_{r2} V_{L2}, \quad (6-46)$$

where λ_{r2} is previously defined, and (6–46) can be solved and rewritten using (6–36), and algebraic manipulation yields (6–44). \square

Table 6-1. Participant Demographics

Participant	Age	Sex	Injury	Active in FES	Active in PT/OT*	TSI†
N1	25	M	Spina bifida (L5-S1), Arnold-Chiari malformation	Y	Y	25yr
N2	64	M	Parkinson's disease	N	Y	19yr
N3	52	M	Drug-induced secondary parkinson's disease	N	N	1yr
C4	25	F	--	--	--	--
C5	26	M	--	--	--	--
C6	24	M	--	--	--	--

*PT/OT: Physical therapy/occupational therapy

†TSI: Time since injury

Remark 6.2. Since r_2 exponentially decays to zero in both the assistive and resistive modes, (6-17) can be used to show that e_2 exponentially decays to 0 in the assistive mode and to Δ_{d2} in the resistive mode. As designed, the position of the dominant leg exponentially approaches a neighborhood of $[q_{d2}, q_{\bar{d}2}]$ centered around a 180 degree offset from the actual position of the non-dominant leg (i.e., q_1), and the cadence of the dominant leg exponentially approaches the cadence of the non-dominant leg.

6.4 Experiments

To evaluate the performance of the FES and motor controllers in (6-13), (6-14), (6-21), and (6-22), experiments were conducted on three able-bodied participants and three participants with neurological conditions, whose demographics are listed in Table 6-1. All participants gave written informed consent approved by the University of Florida Institutional Review Board.

6.4.1 Split-Crank Motorized FES-Cycling Testbed

Similar to the stationary recumbent tricycle (TerraTrike Rover) in [47], orthotic boots fixed the rider's feet to the pedals, preventing dorsiflexion and plantarflexion of the ankles, and maintained sagittal alignment of the lower legs. Each side of the split-crank cycle included an optical encoder (US Digital H1), a 250 Watt, 24 V DC brushed electric motor (Unite Motor Co. Ltd.), an ADVANCED Motion Controls⁴ (AMC) PS300W24 power supply and an AMC AB25A100 motor driver. Data acquisition hardware (Quanser Q-PIDe) was used to measure the encoder signals and deliver the motor current. A computer running real-time control software (QUARC, MATLAB/Simulink, Windows 10) at a sampling rate of 500 Hz was used to implement both the motor and FES controllers. Biphasic, symmetric, rectangular pulses were delivered to the subject's muscle groups with a current-controlled stimulator (Hasomed RehaStim) via self-adhesive, PALS[®] electrodes⁵. The stimulation amplitudes were fixed at 90 mA for the quadriceps and 80 mA for the hamstrings and gluteus muscle groups. The stimulation pulse width for each muscle group was determined by u_{m_i} from (6-4) and u_{M_i} from (6-13) and (6-21), and commanded to the stimulator by the control software. Stimulation frequency was fixed at 60 Hz, as in [47] and [80]. For safety, an emergency stop switch was attached to the tricycle that enabled participants to stop the stimulation immediately, but no participant found it necessary.

6.4.2 Protocol

Electrodes were placed over the participant's quadriceps femoris, hamstrings, and gluteus muscle groups according to Axelgaard's electrode placement manual⁶.

⁴ ADVANCED Motion Controls supported the development of this testbed by providing discounts on their branded items.

⁵ Surface electrodes were provided compliments of Axelgaard Manufacturing Co., Ltd.

⁶ <http://www.palsclinicalsupport.com/videoElements/videoPage.php>

The participant was then seated on the tricycle with their feet secured in the orthotic boots attached to the pedals. The seat position was adjusted so that the subject was comfortable and so that full knee extension would not occur at any crank position. Measurements of the participant's lower limbs and seat position were taken to calculate the torque transfer ratios, which establish the switching signals in the assistance mode for stimulation and the motor, as in [47]. To avoid large initial errors, the motor tracked a linear cadence increasing from zero to \dot{q}_{d1} before the developed control scheme was implemented for a remaining 120 seconds. Participants were asked to contribute volitionally while the FES and motor controllers for each side were implemented to maintain a cadence within the desired cadence region and a desired phase shift centered around 180 degrees. Compared to a standard single-crank cycle, a significant challenge with the split-crank cycle is to build momentum and sustain a pedaling motion. For comparison and to demonstrate the significance of the controllers on a split-crank cycle, able-bodied participants were asked to perform a separate trial (random order) where they attempted to remain in the desired bounds with only volitional input and no input from the controllers; however, one able-bodied participant was not able to initiate continuous pedaling on the split-crank cycle. For all participants, the right leg was treated as the non-dominant side and tracked the desired cadence range, while the left leg was treated as the dominant side and tracked the position offset from the right side. The participant was able to view the real-time cadence of the non-dominant side in relation to the upper and lower thresholds, as in the top left plot in Figures 6-1-6-6. Thus, the minimum desired crank velocity \dot{q}_{d1} was defined as $\dot{q}_{d1} \triangleq \frac{5\pi}{3}$ rad/s and the velocity range Δ_{d1} was defined as $\Delta_{d1} \triangleq \frac{\pi}{3}$ rad/s for participants with neurological conditions and $\Delta_{d1} \triangleq \frac{\pi}{6}$ rad/s for able-bodied participants to increase the difficulty level. The desired crank position and position range for the non-dominant leg were defined as $q_{d2} \triangleq q_1 - \pi - \Delta_{d2}/2$ rad and $\Delta_{d2} \triangleq \frac{\pi}{36}$ rad. The control gains were selected within the following ranges: $k_{1e} \in [1, 4]$, $k_{2e} \in [7.5, 20]$, $k_{3e} \in [2, 2.4]$, $k_{4e} \in [3, 3.6]$, $k_{5e} \in [2, 2.4]$,

$k_{6e} \in [8, 9.6]$, $k_{1s} \in [20, 26.4]$, $k_{2s} \in [18, 21.6]$, $k_{3s} \in [12, 15]$, $k_{4s} \in [15, 18]$, $k_{5s} \in [1, 2]$,
 $k_{6s} \in [1, 3]$, $\alpha = 1$.

6.4.3 Results

Figures 6-1-6-6 depict performance data from two minutes of split-crank cycling with intermittent FES and motor inputs to the volitionally pedaling participants. Data from the uncontrolled trials are overlaid for the two participants that completed the uncontrolled trial. Position and cadence errors from the left and right legs, respectively, are listed in Table 6-2 for the controlled and uncontrolled (i.e., only volition) trials, along with the cadence differential between the two legs. Errors are calculated and plotted as the difference between the lower bound and the actual position/cadence when below the desired range, the difference between the upper bound and the actual position/cadence when above the desired range, and equal to zero when pedaling anywhere between the lower and upper state bounds. Figures 6-7-6-12 display both the FES control inputs to the muscle groups as well as the motor control inputs to each side.

6.4.4 Discussion

The controller for each side switched between three modes which were based on velocity for the right side and position for the left side. When the right or left side was in the assistive mode, the corresponding control input switched between FES and the motor. When in the resistive mode, a negative control input was provided only to the motor on the corresponding side. In the uncontrolled mode, no control input was provided to FES or the motor for that side.

When pedaling on a split-crank cycle, the gravitational torques on the right and left legs do not balance each other like they do when pedaling a single-crank cycle. At points of the crank cycle where one leg is accelerated by gravity, the other decelerates, accounting for the larger position and cadence errors and standard deviations compared to other FES-cycling studies [47]. However, the performance of the three mode controller significantly improved upon the performance achieved when pedaling without FES

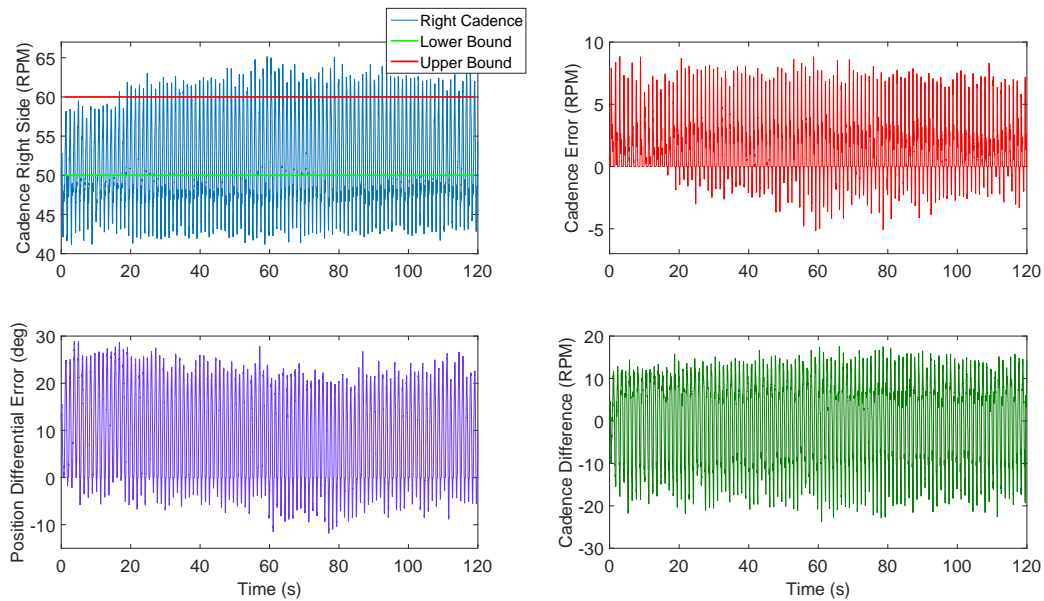


Figure 6-1. FES cycling data for Participant N1. (Top left) The right leg cycling cadence compared to the upper and lower bounds on the desired cadence region; (top right) right cadence error, calculated as the difference between the lower bound and the actual cadence when below the desired range, the difference between the upper bound and the actual cadence when above the desired range, and equal to zero when pedaling anywhere between the lower and upper state bounds; (bottom left) left position error, calculated similar to the right cadence error; and (bottom right) the cadence differential between the two sides.

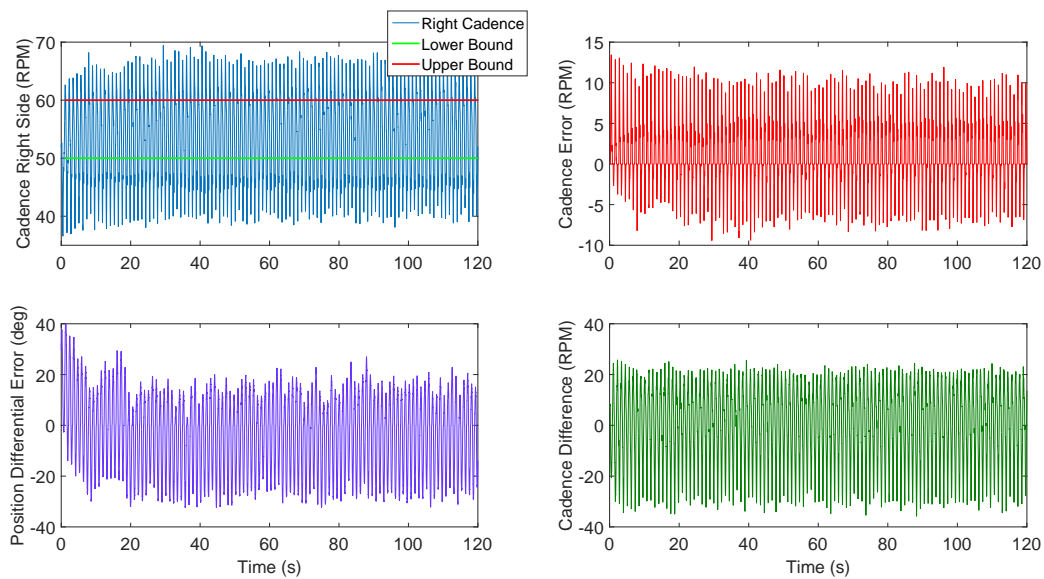


Figure 6-2. FES cycling data for Participant N2. (Top left) The right leg cycling cadence compared to the upper and lower bounds on the desired cadence region; (top right) right cadence error, calculated as the difference between the lower bound and the actual cadence when below the desired range, the difference between the upper bound and the actual cadence when above the desired range, and equal to zero when pedaling anywhere between the lower and upper state bounds; (bottom left) left position error, calculated similar to the right cadence error; and (bottom right) the cadence differential between the two sides.

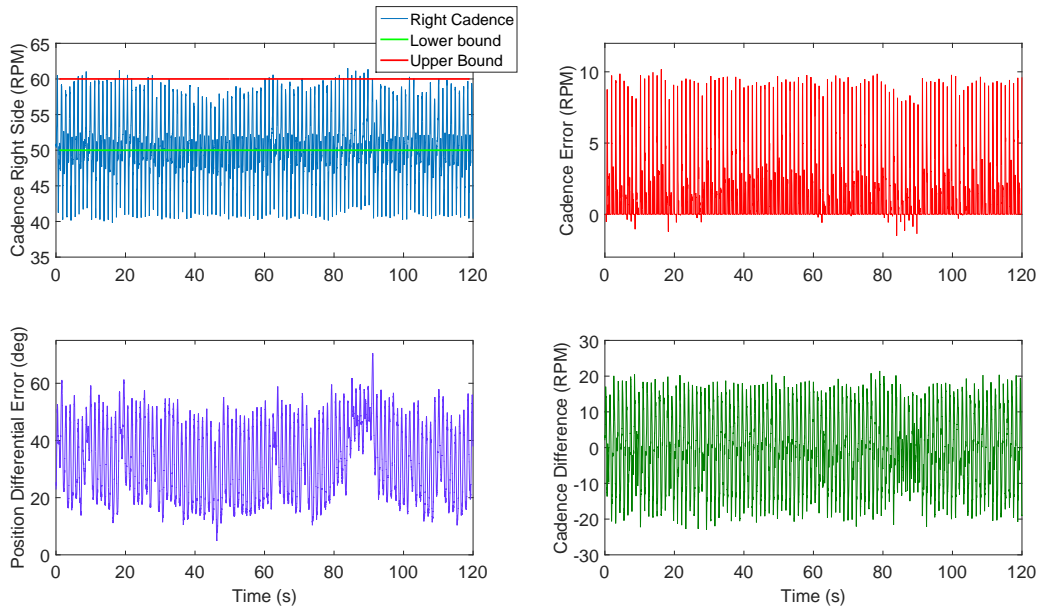


Figure 6-3. FES cycling data for Participant N3. (Top left) The right leg cycling cadence compared to the upper and lower bounds on the desired cadence region; (top right) right cadence error, calculated as the difference between the lower bound and the actual cadence when below the desired range, the difference between the upper bound and the actual cadence when above the desired range, and equal to zero when pedaling anywhere between the lower and upper state bounds; (bottom left) left position error, calculated similar to the right cadence error; and (bottom right) the cadence differential between the two sides.

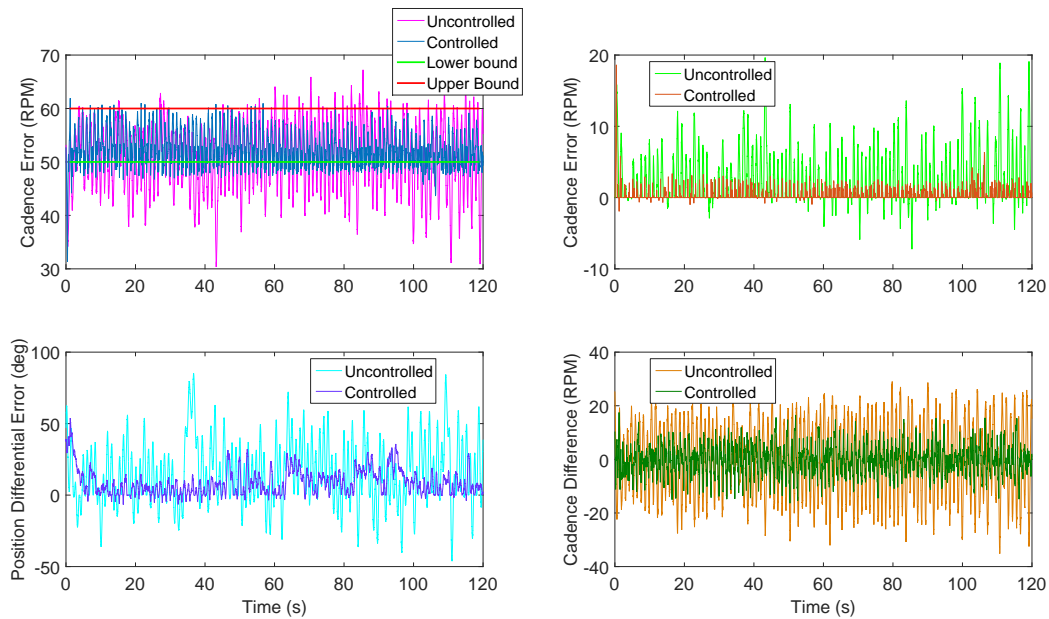


Figure 6-4. FES cycling data for Participant C4/V4 during both the controlled and uncontrolled trials. (Top left) The right leg cycling cadence compared to the upper and lower bounds on the desired cadence region; (top right) right cadence error, calculated as the difference between the lower bound and the actual cadence when below the desired range, the difference between the upper bound and the actual cadence when above the desired range, and equal to zero when pedaling anywhere between the lower and upper state bounds; (bottom left) left position error, calculated similar to the right cadence error; and (bottom right) the cadence differential between the two sides.

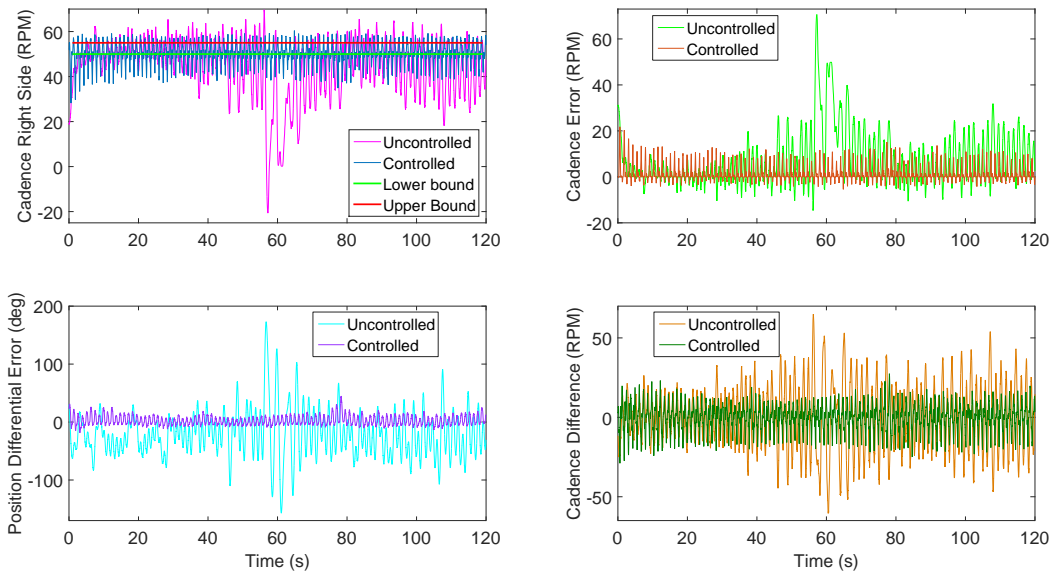


Figure 6-5. FES cycling data for Participant C5/V5 during both the controlled and uncontrolled trials. (Top left) The right leg cycling cadence compared to the upper and lower bounds on the desired cadence region; (top right) right cadence error, calculated as the difference between the lower bound and the actual cadence when below the desired range, the difference between the upper bound and the actual cadence when above the desired range, and equal to zero when pedaling anywhere between the lower and upper state bounds; (bottom left) left position error, calculated similar to the right cadence error; and (bottom right) the cadence differential between the two sides.

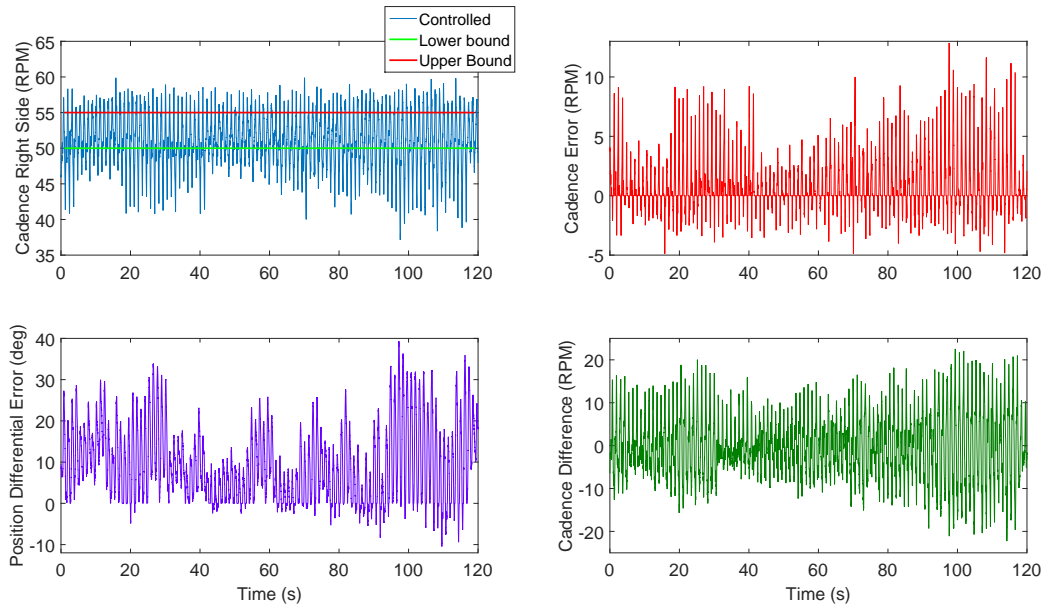


Figure 6-6. FES cycling data for Participant C6. (Top left) The right leg cycling cadence compared to the upper and lower bounds on the desired cadence region; (top right) right cadence error, calculated as the difference between the lower bound and the actual cadence when below the desired range, the difference between the upper bound and the actual cadence when above the desired range, and equal to zero when pedaling anywhere between the lower and upper state bounds; (bottom left) left position error, calculated similar to the right cadence error; and (bottom right) the cadence differential between the two sides.

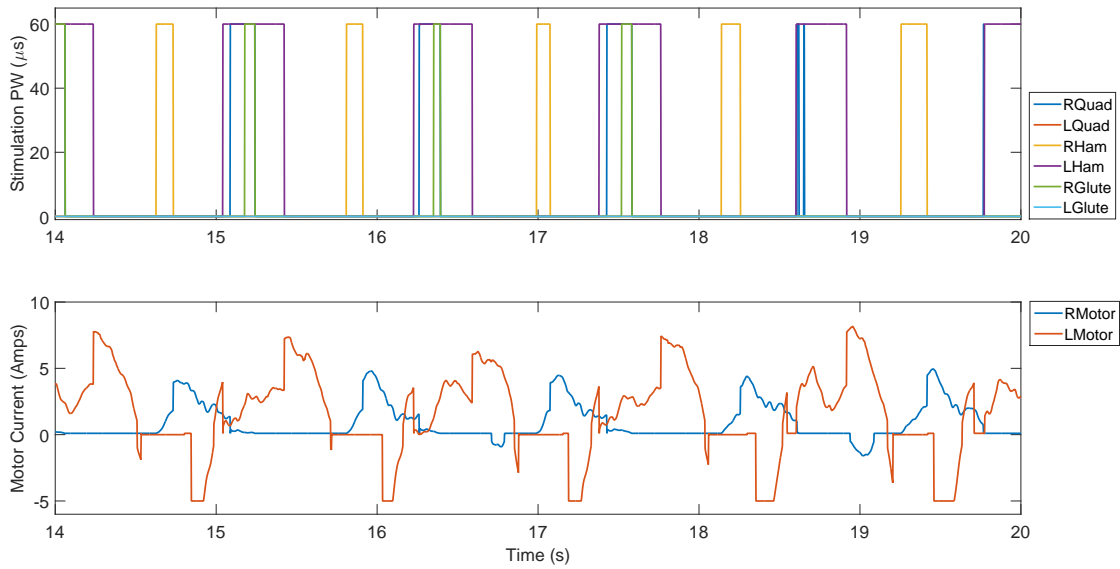


Figure 6-7. (Top) FES control input and (bottom) motor control inputs for Participant N1. For better resolution and understanding, the plots are magnified to show six seconds, or approximately five crank cycles that encompass the pattern seen throughout the trial.

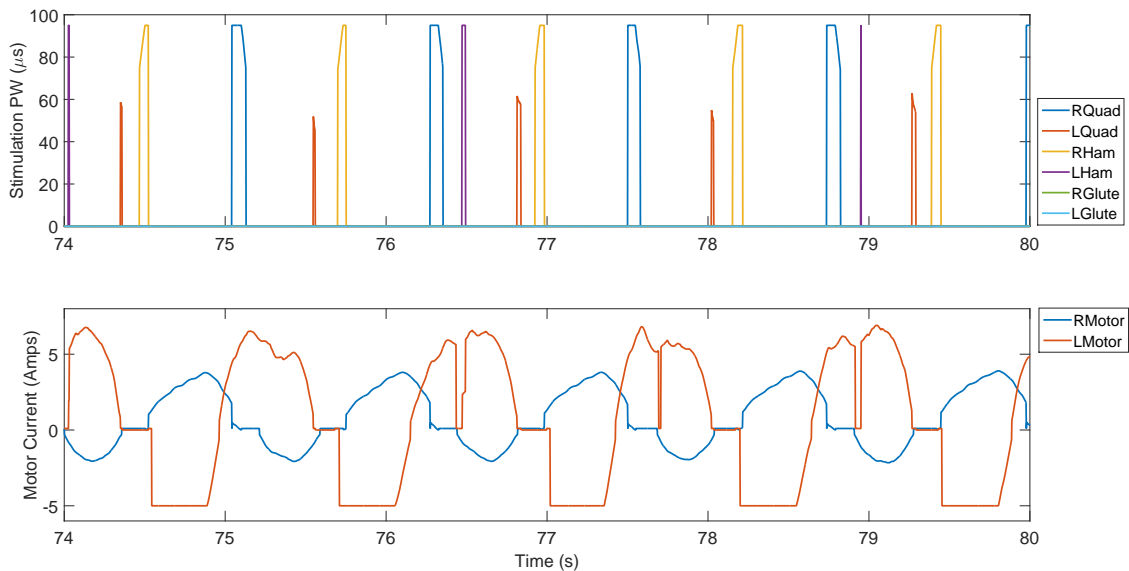


Figure 6-8. (Top) FES control input and (bottom) motor control inputs for seconds 74-80 of Experiment N2. For better resolution and understanding, the plots are magnified to show six seconds, or approximately five crank cycles that encompass the pattern seen throughout the trial.

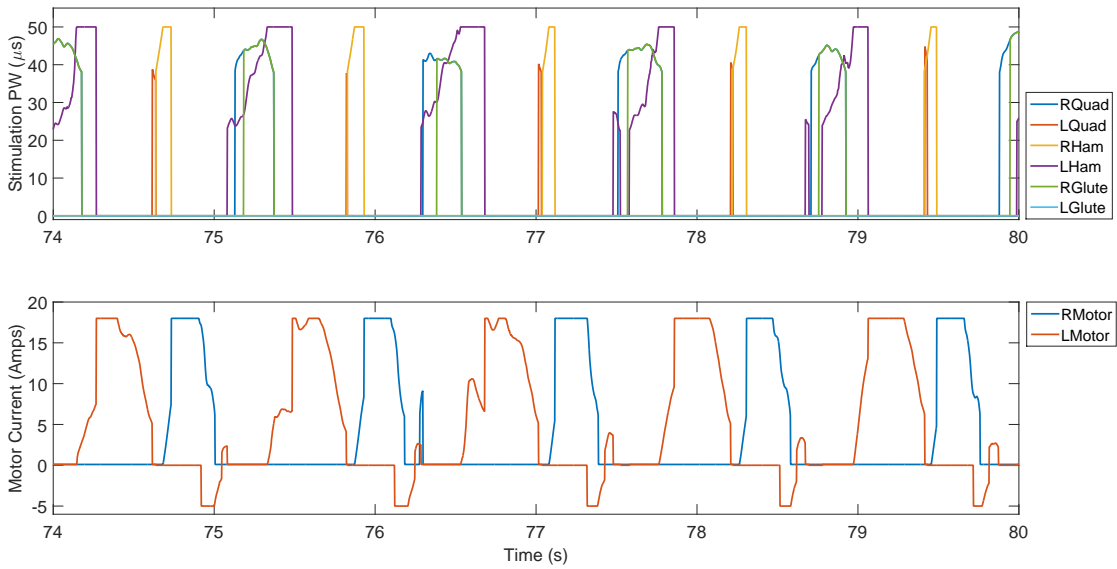


Figure 6-9. (Top) FES control input and (bottom) motor control inputs for seconds 74-80 of Experiment N3. For better resolution and understanding, the plots are magnified to show six seconds, or approximately five crank cycles that encompass the pattern seen throughout the trial.

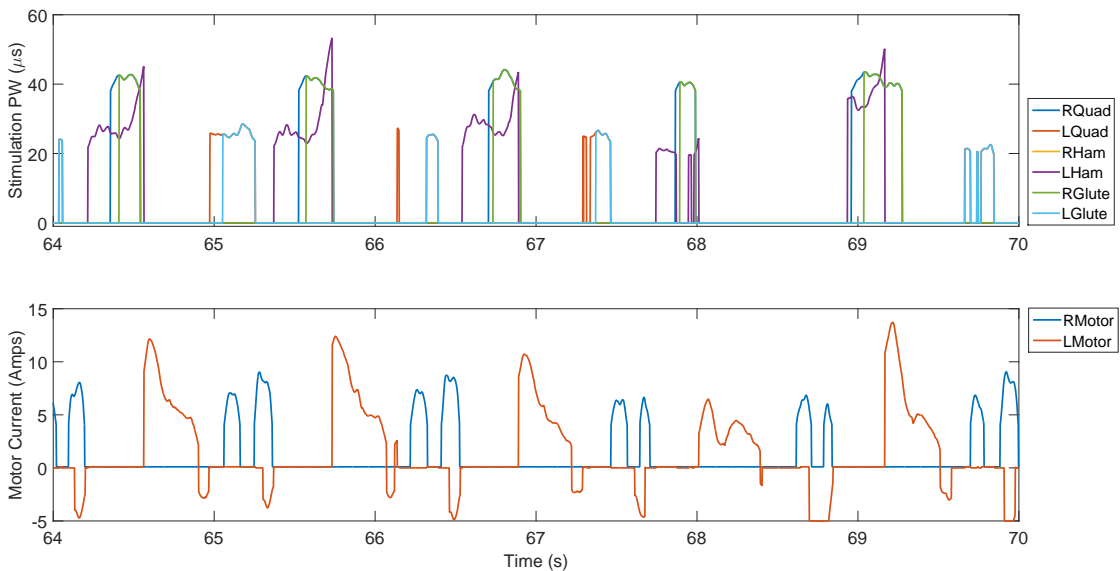


Figure 6-10. (Top) FES control input and (bottom) motor control inputs for seconds 64-70 of Experiment C4. For better resolution and understanding, the plots are magnified to show six seconds, or approximately five crank cycles that encompass the pattern seen throughout the trial.

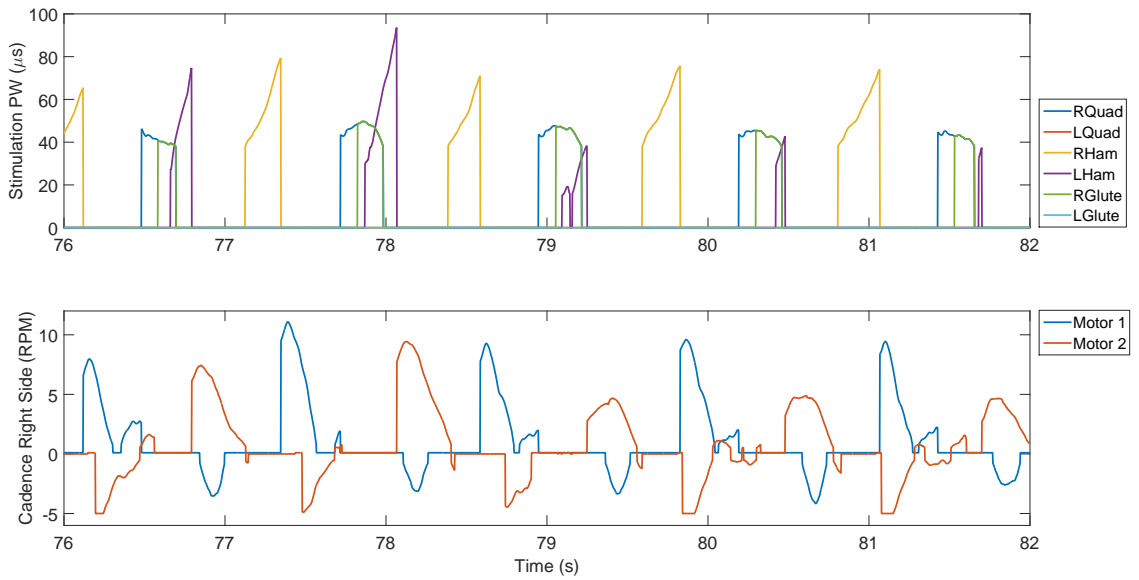


Figure 6-11. (Top) FES control input and (bottom) motor control inputs for seconds 76-82 of Experiment C5. For better resolution and understanding, the plots are magnified to show six seconds, or approximately five crank cycles that encompass the pattern seen throughout the trial.

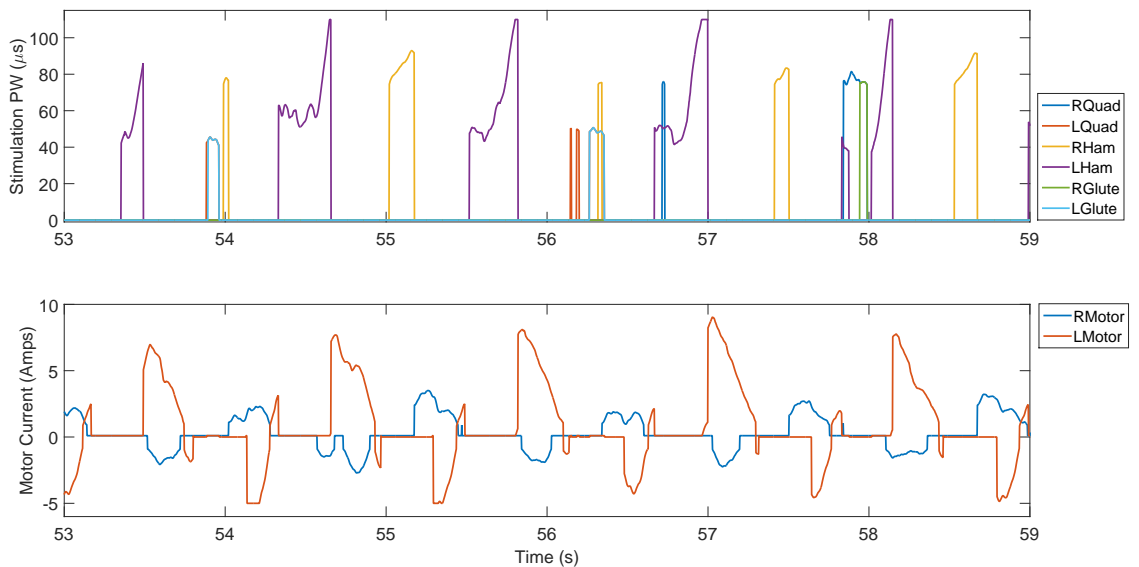


Figure 6-12. (Top) FES control input and (bottom) motor control inputs for seconds 53-59 of Experiment C6. For better resolution and understanding, the plots are magnified to show six seconds, or approximately five crank cycles that encompass the pattern seen throughout the trial.

Table 6-2. Performance metrics from the volitional and controlled trials

Participant/trial*	Cadence error, right leg (RMS (avg. \pm std. dev.), RPM)	Position error, left leg (RMS (avg. \pm std. dev.), deg)	Cadence differential (RMS (avg. \pm std. dev.), RPM)
N1	2.84 (1.35 \pm 2.50)	13.50 (8.96 \pm 10.10)	10.43 (-0.04 \pm 10.43)
N2	4.32 (-1.20 \pm 4.15)	16.44 (3.23 \pm 16.12)	16.25 (-0.16 \pm 16.25)
N3	3.16 (-1.73 \pm 2.65)	36.04 (-33.55 \pm 13.16)	2.56 (-1.78 \pm 1.84)
Mean of N trials	3.44 (0.27 \pm 3.19)	21.99 (-9.27 \pm 13.35)	11.22 (-0.67 \pm 11.20)
C4	1.00 (-0.30 \pm 0.95)	12.63 (-8.89 \pm 8.97)	5.29 (-0.13 \pm 5.29)
C5	3.65 (-1.49 \pm 3.34)	8.56 (-2.63 \pm 8.15)	8.76 (-0.27 \pm 8.76)
C6 [#]	2.43 (-0.83 \pm 2.28)	13.06 (-9.28 \pm 9.19)	7.65 (-0.06 \pm 7.65)
Mean of C trials	2.36 (-0.87 \pm 2.40)	11.42 (-6.93 \pm 8.78)	7.38 (-0.15 \pm 7.38)
V4	4.21 (-2.11 \pm 3.64)	26.71 (-15.12 \pm 22.02)	13.92 (-0.17 \pm 13.92)
V5	13.86 (-7.20 \pm 11.84)	45.42 (21.24 \pm 40.15)	20.64 (-0.29 \pm 20.64)
Mean of V trials	9.92 (-4.66 \pm 8.76)	32.95 (6.12 \pm 32.38)	17.60 (-0.23 \pm 17.60)

*N refers to participants with neurological conditions. C refers to controlled trials with able-bodied participants. V refers to completely volitional (uncontrolled) trials with able-bodied participants.

[#]Participant C6 was unable to pedal the split-crank cycle volitionally.

and motor contribution, as seen in the volitional trial results in Table 6-2. Moreover, one able-bodied participant could not achieve a cycling motion by pedaling volitionally without contribution from the developed controllers. The loss of momentum due to gravity caused each pedal to completely stop every crank cycle, despite volitional contribution, so the attempt at an uncontrolled trial was stopped.

As seen in Table 6-2, standard deviations on the left side were greater than those of the right side. The greater variance is because the right side was tracking a constant cadence range, whereas the left was tracking a range centered around the actual position and cadence of the right side. Moreover, it was difficult for participants to monitor their performance with respect to the bounds on both the right and left sides. Instead, the participant was asked to watch their cadence performance on the right side and attempt to maintain a proper phase shift of 180 degrees by feel.

With the nature of the split-crank cycle and the three modes of control, all six controlled results display a similar pattern. Since larger forces are required to rotate the crank through the portion of the crank cycle corresponding to hamstring activation (i.e., the “upward” motion), the control inputs (shown in Figures 6-7-6-12) and errors (Figures 6-1-6-6) are greater in those regions than in other regions of the crank cycle. For all participants, the cadence would slow and lag the opposing leg when in the hamstring region. On the contrary, gravitational forces caused each leg to accelerate during the “downward” portion of the crank cycle where the quadriceps are used to extend the legs. During this portion of the crank cycle, the leg typically entered the uncontrolled or resistive mode, whether or not the volitional contribution was large. If the right leg’s cadence is larger than the upper cadence bound or the left leg passes the upper position bound, then the respective motor applies a negative (i.e., resistive) control input, pushing the leg back into the desired uncontrolled mode. While the stability analysis ensures immediate transition back into the desired uncontrolled mode after crossing a cadence bound, the cadence and position errors deviate outside the desired

region for all participants, particularly during regions of opposing gravitational force. Gain tuning in favor of a higher control input at the bounds could limit these deviations; however, a strong immediate force may feel unnatural to the rider and unmodeled dynamics from human reaction may introduce further problems. Moreover, in Participant N3, the maximum motor control output was reached so increasing the gains would not have better constrained pedaling to the desired regions. The size of the desired uncontrolled regions for each side affect the error values since time spent in the desired region is characterized by an error of zero. Future works could base the error system for the assistive mode on the upper bound and the error system for the resistive mode on the lower bound, which effectively adds a feedforward term the size of the desired region, Δ_{dl} . However, modeling the rider's impulse reactions to stronger forces upon crossing the boundaries is an open problem.

While the results for the participants display many similarities, there were notable differences as well. For example, the FES input saturated more often for the participants with neurological impairments that necessitate higher stimulation and/or have hypersensitivity (and thus, a lower comfort threshold). Because Participant N1 had a comfort threshold of $60\mu\text{s}$, the FES controller saturated most often for Participant N1, as seen in the top plot of Figure 6-7. After saturation of the FES input, additional input was distributed to the motor, which is evident by the consistent motor input displayed in the bottom plot of Figure 6-7.

Participant N2 had a comfort threshold of $95\mu\text{s}$. As seen in the top plot of Figure 6-8, the FES controller saturated in the right and left hamstring regions, which aligns with the greater force required to lift the leg through that portion of the crank cycle. The control input to the right quadriceps also saturated during the portion of the trial displayed, but was not as consistently saturated as the hamstrings throughout the entire trial. To maintain full control authority when the FES saturates, the motor is also activated according to (6-5), yielding a cyclic pattern in the motor control input.

Participant N3 chose the lowest comfort threshold of $50\mu s$, yet muscle contractions were visible. Due to Participant N3's mobility and sitting position, both of his legs required more force than the others to rotate the crank through the portion of the crank corresponding to hamstring activation. Even with some volitional contribution, the FES controller saturated in both hamstring regions nearly every cycle, as seen in the top plot of Figure 6-9. Theoretically, the system can handle an unlimited control input by distributing the remainder to the corresponding motor, such as the scenario with Participants N1 and N2. However, the motor control input was saturated for safety and physical limitation. For Participant N3, both the FES and the motor control inputs saturated.

Participant C4 completed a volitional-only experiment (V4 in Table 6-2) and an experiment with motor and FES control implementation. Using only volition, the participant attempted to keep errors within the respective desired regions for both legs. Figure 6-4 displays the cadence over time and cadence and position errors for both the controlled and uncontrolled trials. Compared to volitional pedaling, Table 6-2 indicates that all average errors were significantly improved when the controller was implemented. Root mean square (RMS) errors improved by 76.3% from 4.20 RPM to 1.00 RPM, 52.7% from 26.71 degrees to 12.63 degrees, and 62.0% from 13.92 RPM to 5.29 RPM for the right cadence error, left position error, and cadence differential between the right and left.

Participant C5 also completed a volitional-only trial (V5 in Table 6-2). Figure 6-5 plots the cadence over time and cadence and position errors for both the controlled and uncontrolled trials. The cadence and position errors and cadence differential improved with the three mode controller by 73.6% from 13.86 RPM to 3.66 RPM, 81.1% from 45.42 degrees to 8.56 degrees, and 57.5% from 20.64 RPM to 8.76 RPM, respectively.

Participant C6 was unable to consistently pedal the split-crank cycle using only volitional input, hence only data from a controlled trial is shown in Figure 6-6. While

there is no volitional data to compare to the controlled data, the inability of the abled-bodied participant to pedal volitionally on the split-crank cycle undermines the benefit of the controller, particularly when the leg's motion is opposing gravitational forces.

In a previous study by the authors, nine stroke patients pedaled according to a similar three mode protocol, aiming only for a desired cadence range on a single-crank tricycle. The average percentage of time spent in the desired cadence region was 50.48%. Here, the average percentage of time spent in the desired cadence region on the right side was 40.8% for participants with a neurological condition and a comparable 49.4% for able-bodied participants.

As seen in Table 6-2, the right cadence errors, left position errors, and cadence differentials averaged across all participants with neurological conditions were higher than those of healthy participants with the three mode controller implemented, but lower than those of healthy participants pedaling with only volitional input.

6.5 Concluding Remarks

The development in this chapter provides a control strategy for a combination of FES and motor inputs to enable a volitionally contributing rider of a split-crank cycle to maintain a cadence within a desired range, as well as a phase shift between the two legs within a desired region centered around 180 degrees. Despite unknown disturbances and arbitrary switching, a Lyapunov-like analysis proved exponential convergence to the desired cadence range (i.e., $e_1 \in [0, \Delta_{d1}]$) on the non-dominant side and position range (i.e., $e_2 \in [0, \Delta_{d2}]$) on the dominant side. Experiments on healthy participants and participants with neurological conditions validated the use of the control system in all three modes for people with a broad range of abilities to pedal a tricycle decoupled at the crank within a desired range.

With assistive, uncontrolled, and resistive modes, the developed control system has the potential to advance established FES-cycling protocols for movement disorder rehabilitation exercises. The strategy in this chapter presents a way of addressing the

asymmetries associated with numerous movement disorders. Using the FES and motor controllers, a wide range of volitional abilities could be accommodated, such that any rider could pedal within desired cadence and position offset ranges.

CHAPTER 7 CONCLUSION

Human-machine interaction was investigated for the application of FES rehabilitation exercises. Switched systems theory provided tools to discontinuously switch between multiple actuators to control a system with continuous dynamics and ensure stability. While previous works switched between motor and muscle to promote limb coordination during rehabilitation exercises, this dissertation built upon that by implementing additional levels of switching. Not only were muscle groups and motors switched on and off as a function of position, but also as a function of velocity and the control input of other actuators. Moreover, switching within a single muscle group was explored. Thus, state-based and arbitrary switching were simultaneously used on the same human-machine system. In Chapter 2, a generic model of the human-machine system was presented. Chapter 3 explored switching stimulation input within a single muscle group, namely the biceps brachii, based on elbow angle. A multi-level switched system was first introduced in Chapter 4, where muscle and motor regions were defined based on direction of movement for high level switching; mid-level switching occurred within the biceps as in Chapter 3; and low-level switching activated the motor in the muscle regions whenever the FES control input hit the saturation limit, selected as the person's comfort threshold. The work in Chapter 5 came from the perspective that the person should be encouraged to volitionally contribute to a rehabilitation exercise as much as they can. The motor and FES assisted when pedaling below a minimum cadence bound and the motor resisted when pedaling above a maximum cadence bound, which created an uncontrolled cadence region where human volition was the only actuation to the system. Chapter 6 explored the use of a single crank cycle to implement a similar controller as in Chapter 5. Motivated by people with hemiparesis, the split-crank

cycle promoted equal contribution from both sides of the body. The low-level switching from Chapter 4 was also implemented to ensure patient comfort and full control authority.

The developed switched control systems have the potential to advance motorized FES rehabilitation exercises for people with movement disorders. Subjects with a wide range of volitional abilities can perform the same exercise with FES and a motor assisting those with minimal arm or leg strength or at the onset of fatigue, and with the motor providing resistance to someone who can easily perform above a desired outcome. Stability was proved for state-based and arbitrary switching within a single muscle group and between muscle and motor, on top of volitional contribution. Thus, the work in this dissertation extends to multiple scenarios within human-machine interaction, motivated by rehabilitation outcomes.

REFERENCES

- [1] M. Bélanger, R. B. Stein, G. D. Wheeler, T. Gordon, and B. Leduc, "Electrical stimulation: can it increase muscle strength and reverse osteopenia in spinal cord injured individuals?" *Arch. Phys. Med. Rehabil.*, vol. 81, no. 8, pp. 1090–1098, 2000.
- [2] M. Gomis, L. Gonzalez, F. Querol, J. Gallach, and J. Toca-Herrera, "Effects of electrical stimulation on muscle trophism in patients with hemophilic arthropathy," *Arch Phys Med Rehabil*, vol. 90, no. 11, pp. 1924–30, Nov. 2009.
- [3] M. M. Rodgers, R. M. Glaser, S. F. Figoni, S. P. Hooker, B. N. Ezenwa, S. R. Collins, T. Mathews, A. G. Suryaprasad, and S. C. Gupta, "Musculoskeletal responses of spinal cord injured individuals to functional neuromuscular stimulation-induced knee extension exercise training," *J. Rehabil. Res. Dev.*, vol. 28, no. 4, pp. 19–26, 1991.
- [4] T. Mohr, J. Pødenphant, F. Biering-Sørensen, H. Galbo, G. Thamsborg, and M. Kjær, "Increased bone mineral density after prolonged electrically induced cycle training of paralyzed limbs in spinal cord injured man," *Calcif. Tissue Int.*, vol. 61, no. 1, pp. 22–25, 1997.
- [5] B. Langhammer and J. Stanghelle, "Bobath or motor relearning program? a comparison of two different approaches of physiotherapy in stroke rehabilitation: a randomised controlled study," *Clin. Rehabil.*, vol. 14, pp. 361–9, 2000.
- [6] R. Riener, T. Nef, and G. Colombo, "Robot-aided neurorehabilitation of the upper extremities," *Med. Biol. Eng. Comput.*, vol. 43, no. 1, pp. 2–10, Jan. 2005.
- [7] N. A. Maffiuletti, "Physiological and methodological considerations for the use of neuromuscular electrical stimulation," *Eur J Appl Physiol*, vol. 110, no. 2, pp. 223–234, Dec. 2010.
- [8] J. Raymond, G. Davis, M. Climstein, and J. Sutton, "Cardiorespiratory responses to arm cranking and electrical stimulation leg cycling in people with paraplegia," *Med. Sci. Sports Exerc.*, vol. 31, no. 6, pp. 822–28, Jun. 1999.
- [9] J. Raymond, G. Davis, A. Fahey, M. Climstein, and J. R. Sutton, "Oxygen uptake and heart rate responses during arm vs combined arm/electrically stimulated leg exercise in people with paraplegia," *Spinal Cord*, vol. 35, no. 10, pp. 680–85, Oct. 1997.
- [10] S. P. Hooker, S. F. Figoni, M. M. Rodgers, R. M. Glaser, T. Mathews, A. G. Suryaprasad, and S. Gupta, "Metabolic and hemodynamic responses to concurrent voluntary arm crank and electrical stimulation leg cycle exercise in quadriplegics," *J Rehabil Res Dev*, vol. 29, no. 3, pp. 1–11, 1992.

- [11] C. S. Bickel, C. M. Gregory, and J. C. Dean, "Motor unit recruitment during neuromuscular electrical stimulation: a critical appraisal," *Eur. J. Appl. Physiol.*, vol. 111, no. 10, pp. 2399–2407, 2011.
- [12] C. M. Gregory and C. S. Bickel, "Recruitment patterns in human skeletal muscle during electrical stimulation," *Phys. Ther.*, vol. 85, no. 4, pp. 358–364, 2005.
- [13] M. Gobbo, P. Gaffurini, L. Bissolotti, F. Esposito, and C. Orizio, "Transcutaneous neuromuscular electrical stimulation: Influence of electrode positioning and stimulus amplitude setting on muscle response," *Eur. J. Appl. Physiol.*, vol. 111, no. 10, pp. 2451–2459, 2011.
- [14] M. Gobbo, N. A. Maffioletti, C. Orizio, and M. A. Minetto, "Muscle motor point identification is essential for optimizing neuromuscular electrical stimulation use," *J. Neuroeng. Rehabil.*, vol. 11, no. 1, p. 17, 2014.
- [15] R. Garnett and J. Stephens, "Changes in the recruitment threshold of motor units produced by cutaneous stimulation in man," *J Physiol (Lond)*, vol. 311, pp. 463–473, Feb. 1981.
- [16] M. J. Bellman, T. H. Cheng, R. J. Downey, C. J. Hass, and W. E. Dixon, "Switched control of cadence during stationary cycling induced by functional electrical stimulation," *IEEE Trans. Neural Syst. Rehabil. Eng.*, vol. 24, no. 12, pp. 1373–1383, 2016.
- [17] H. Chen, S. Chen, J. Chen, L. Fu, and Y. Wang, "Kinesiological and kinematical analysis for stroke subjects with asymmetric cycling movement patterns," *J. Electromyogr. Kinesiol.*, vol. 15, no. 6, pp. 587–595, Dec 2005.
- [18] L. Ting, S. Kautz, D. Brown, H. Van der Loos, and F. E. Zajac, "Bilateral integration of sensorimotor signals during pedaling," *Ann. N. Y. Acad. Sci.*, vol. 860, no. 1, pp. 513–516, 1998.
- [19] L. Ting, S. Kautz, D. Brown, and F. Zajac, "Contralateral movement and extensor force generation alter flexion phase muscle coordination in pedaling," *J. Neurophysiol.*, vol. 83, no. 6, pp. 3351–65, Jun 2000.
- [20] L. Ting, C. C. Raasch, D. Brown, S. Kautz, and F. E. Zajac, "Sensorimotor state of the contralateral leg affects ipsilateral muscle coordination of pedaling," *J. Neurophysiol.*, vol. 80, no. 3, pp. 1341–51, Sep 1998.
- [21] M. Van der Loos, L. Worthen-Chaudhari, and D. Schwandt, "A split-crank bicycle ergometer uses servomotors to provide programmable pedal forces for studies in human biomechanics," *IEEE Trans. Neural Syst. Rehabil. Eng.*, vol. 18, no. 4, pp. 445–52, April 2010.
- [22] D. Liberzon, *Switching in Systems and Control*. Birkhauser, 2003.

- [23] R. J. Downey, M. J. Bellman, H. Kawai, C. M. Gregory, and W. E. Dixon, "Comparing the induced muscle fatigue between asynchronous and synchronous electrical stimulation in able-bodied and spinal cord injured populations," *IEEE Trans. Neural Syst. Rehabil. Eng.*, vol. 23, no. 6, pp. 964–972, 2015.
- [24] R. Nguyen, K. Masani, S. Micera, M. Morari, and M. R. Popovic, "Spatially distributed sequential stimulation reduces fatigue in paralyzed triceps surae muscles: A case study," *Artif. Organs*, vol. 35, no. 12, pp. 1174–1180, 2011.
- [25] R. J. Downey, T.-H. Cheng, M. J. Bellman, and W. E. Dixon, "Closed-loop asynchronous electrical stimulation prolongs functional movements in the lower body," *IEEE Trans. Neural Syst. Rehabil. Eng.*, vol. 23, no. 6, pp. 1117–1127, 2015.
- [26] N. Malešević, L. Z. P. Maneski, V. Ilić, N. Jorgovanović, G. Bijelić, T. Keller, and D. B. Popović, "A multi-pad electrode based functional electrical stimulation system for restoration of grasp," *J. Neuroeng. Rehabil.*, vol. 9, no. 1, p. 66, 2012.
- [27] G. Muller-Putz and G. Pfurtscheller, "Control of an electrical prosthesis with an ssvep-based bci," *IEEE Trans Biomed Eng*, vol. 55, no. 1, pp. 361–364, December 2007.
- [28] R. J. Downey, T.-H. Cheng, M. Bellman, and W. E. Dixon, "Switched tracking control of a human limb during asynchronous neuromuscular electrical stimulation," in *Proc. Am. Control Conf.*, 2015, pp. 4504–4508.
- [29] M. Goffredo, M. Schmid, S. Conforto, F. Bilotti, C. Palma, L. Vegni, and T. D'Alessio, "A two-step model to optimise transcutaneous electrical stimulation of the human upper arm," *Int. J. comput. math. electr. electron. eng.*, vol. 33, no. 4, pp. 1329–1345, 2014.
- [30] N. Malešević, L. Z. Popović, G. Bijelić, and G. Kvaščev, "Muscle twitch responses for shaping the multi-pad electrode for functional electrical stimulation," *J. Autom. Control*, vol. 20, no. 1, pp. 53–58, 2010.
- [31] D. B. Popović and M. B. Popović, "Automatic determination of the optimal shape of a surface electrode: selective stimulation," *J. Neurosci. Methods*, vol. 178, no. 1, pp. 174–181, Mar. 2009.
- [32] A. Popović-Bijelić, G. Bijelić, N. Jorgovanović, D. Bojanić, M. B. Popović, and D. B. Popović, "Multi-field surface electrode for selective electrical stimulation," *Artif. Organs*, vol. 29, no. 6, pp. 448–452, 2005.
- [33] C. T. Freeman, "Electrode array-based electrical stimulation using ilc with restricted input substance," *Control Eng. Pract.*, vol. 23, no. 1, pp. 32–43, Feb. 2014.
- [34] C. Salchow, M. Valtin, and T. S. S. Schauer, "A new semi-automatic approach to find suitable virtual electrodes in aarray using an interpolation strategy," *Eur J Transl Myol*, vol. 26, no. 2, p. 6029, Jun. 2016.

- [35] P. Gad, J. Choe, M. Nandra, H. Zhong, R. Roy, Y.-C. Tai, and V. Edgerton, "Development of a multi-electrode array for spinal cord epidural stimulation to facilitate stepping and standing after a complete spinal cord injury in adult rats," *J Neuroeng Rehabil*, vol. 10, no. 2, pp. 1–17, 2013.
- [36] A. Elsaify, "A self-optimising portable fes system using an electrode array and movement sensors," Ph.D. dissertation, University of Leicester, May 2005.
- [37] T. A. Excell, C. T. Freeman, K. L. Meadmore, A.-M. Hughes, E. Hallewell, and J. Burridge, "Optimisation of hand posture stimulation using an electrode array and iterative learning control," *J. Autom. Control*, vol. 21, pp. 1–4, 2013.
- [38] C. Rouse, V. H. Duenas, C. Cousin, A. Parikh, and W. E. Dixon, "A switched systems approach based on changing muscle geometry of the biceps brachii during functional electrical stimulation," *IEEE Control Syst. Lett.*, vol. 2, no. 1, pp. 73–78, 2018.
- [39] C. Rouse, A. Parikh, V. Duenas, C. Cousin, and W. E. Dixon, "Compensating for changing muscle geometry of the biceps brachii during neuromuscular electrical stimulation: A switched systems approach," in *Proc. IEEE Conf. Decis. Control*, 2016, pp. 1328–1333.
- [40] D. J. Pons, C. L. Vaughan, and G. G. Jaros, "Cycling device powered by the electrically stimulated muscles of paraplegics," *Med. Biol. Eng. Comput.*, vol. 27, no. 1, pp. 1–7, 1989.
- [41] L. M. Schutte, M. M. Rodgers, F. E. Zajac, and R. M. Glaser, "Improving the efficacy of electrical stimulation-induced leg cycle ergometry: An analysis based on a dynamic musculoskeletal model," *IEEE Trans. Rehabil. Eng.*, vol. 1, no. 2, pp. 109–125, Jun. 1993.
- [42] M. Gföhler, T. Angeli, T. Eberharter, P. Lugner, W. Mayr, and C. Hofer, "Test bed with force-measuring crank for static and dynamic investigation on cycling by means of functional electrical stimulation," *IEEE Trans. Neural Syst. Rehabil. Eng.*, vol. 9, no. 2, pp. 169–180, Jun. 2001.
- [43] J. S. Petrofsky, "New algorithm to control a cycle ergometer using electrical stimulation," *Med. Biol. Eng. Comput.*, vol. 41, no. 1, pp. 18–27, Jan. 2003.
- [44] K. J. Hunt, B. Stone, N.-O. Negård, T. Schauer, M. H. Fraser, A. J. Cathcart, C. Ferrario, S. A. Ward, and S. Grant, "Control strategies for integration of electric motor assist and functional electrical stimulation in paraplegic cycling: Utility for exercise testing and mobile cycling," *IEEE Trans. Neural Syst. Rehabil. Eng.*, vol. 12, no. 1, pp. 89–101, Mar. 2004.
- [45] M. J. Bellman, T.-H. Cheng, R. J. Downey, and W. E. Dixon, "Stationary cycling induced by switched functional electrical stimulation control," in *Proc. Am. Control Conf.*, 2014, pp. 4802–4809.

- [46] H. Kawai, M. J. Bellman, R. J. Downey, and W. E. Dixon, "Tracking control for FES-cycling based on force direction efficiency with antagonistic bi-articular muscles," in *Proc. Am. Control Conf.*, 2014, pp. 5484–5489.
- [47] M. J. Bellman, R. J. Downey, A. Parikh, and W. E. Dixon, "Automatic control of cycling induced by functional electrical stimulation with electric motor assistance," *IEEE Trans. Autom. Science Eng.*, vol. 14, no. 2, pp. 1225–1234, April 2017.
- [48] K. Meadmore, A. Hughes, C. Freeman, Z. Cai, D. Tong, J. Burridge, and E. Rogers, "Functional electrical stimulation mediated by iterative learning control and 3d robotics reduces motor impairment in chronic stroke," *J. NeuroEng. Rehab.*, vol. 9, no. 32, June 2012.
- [49] A. Hughes, C. Freeman, J. Burridge, P. Chappell, P. Lewin, and E. Rogers, "Feasibility of iterative learning control mediated by functional electrical stimulation for reaching after stroke," *Neurorehabil. Neural Repair*, vol. 23, no. 6, pp. 559–568, 2009.
- [50] M. Dohring and J. Daly, "Automatic synchronization of functional electrical stimulation and robotic assist treadmill training," *IEEE Trans Neural Syst. Rehabil. Eng.*, vol. 16, no. 3, pp. 310–313, June 2008.
- [51] H. J. Asl, T. Narikiyo, and M. Kawanishi, "An assist-as-needed control scheme for robot-assisted rehabilitation," in *2017 American Control Conference*, 2017, pp. 198–203.
- [52] L. Marchal-Crespo and D. J. Reinkensmeyer, "Review of control strategies for robotic movement training after neurologic injury," *J. Neuroeng. Rehabil.*, vol. 6, no. 1, 2009.
- [53] G. Kraft, S. Fitts, and M. Hammond, "Techniques to improve function of the arm and hand in chronic hemiplegia," *Arch. Phys. Med. Rehab.*, vol. 73, no. 3, pp. 220–227, March 1992.
- [54] C. Rouse, C. Cousin, V. H. Duenas, and W. E. Dixon, "Varying motor assistance during biceps curls induced via functional electrical stimulation," in *Proc. ASME Dyn. Syst. Control Conf.*, 2018.
- [55] ———, "Switched motorized assistance during switched functional electrical stimulation of the biceps brachii to compensate for fatigue," in *IEEE Conf. Dec. Control*, 2017, pp. 5912–5918.
- [56] N. Hogan, H. I. Krebs, B. Rohrer, J. Palazzolo, L. Dipietro, S. Faoli, J. Stein, R. Hughes, W. Frontera, D. Lynch, and B. Volpe, "Motions or muscles? some behavioral factors underlying robotic assistance or motor recovery," *J. Rehabil. Res. Dev.*, vol. 43, no. 5, pp. 605–618, 2006.

- [57] A. U. Pehlivan, D. P. Losey, and M. K. O'Malley, "Minimal assist-as-needed controller for upper limb robotic rehabilitation," *IEEE Trans. Robot.*, vol. 32, no. 1, pp. 113–124, 2016.
- [58] S. Banala, S. Kim, S. Agrawal, and J. Scholz, "Robot assisted gait training with active leg exoskeleton (alex)." *IEEE T Neural Syst Rehabil Eng*, vol. 17, no. 1, pp. 2–8, Feb 2009.
- [59] S. Srivastava, P. Kao, D. Reisman, J. Scholz, S. Agrawal, and J. Higginson, "Robotic assist-as-needed as an alternative to therapist-assisted gait rehabilitation," *Int. J. Phys. Med. Rehabil.*, vol. 4, no. 5, p. 370, Oct 2016.
- [60] S. Srivastava, P. Kao, S. Kim, P. Stegall, D. Zanotto, J. Higginson, S. Agrawal, and J. Scholz, "Assist-as-needed robot-aided gait training improve walking function in individuals following stroke," *IEEE Trans. Neural Syst. Rehabil. Eng.*, vol. 23, no. 6, pp. 956–963, Nov 2015.
- [61] A. Duschau-Wicke, J. Von Zitzewitz, A. Caprez, L. Lunenburger, and R. Riener, "Path control: a method for patient-cooperative robot-aided gait rehabilitation," *IEEE Trans. Neur. Sys. Rehab. Eng.*, vol. 18, no. 1, pp. 38–48, 2010.
- [62] C. Rouse, C. Cousin, V. H. Duenas, and W. E. Dixon, "Cadence tracking for switched FES cycling combined with voluntary pedaling and motor resistance," in *Proc. Am. Control Conf.*, 2018, pp. 4558–4563.
- [63] G. Pfurtscheller, G. R. Muller, J. Pfurtscheller, H. J. Gerner, and R. Rupp, "'thought'-control of functional electrical stimulation to restore hand grasp in a patient with tetraplegia," *Neurosci Lett*, vol. 351, no. 1, pp. 33–36, November 2003.
- [64] E. Ambrosini, S. Ferrante, G. Ferrigno, F. Molteni, and A. Pedrocchi, "Cycling induced by electrical stimulation improves muscle activation and symmetry during pedaling in hemiparetic patients," *IEEE Trans. Neural Syst. Rehabil. Eng.*, vol. 20, no. 3, pp. 320–330, May 2012.
- [65] E. Ambrosini, S. Ferrante, A. Pedrocchi, G. Ferrigno, and F. Molteni, "Cycling induced by electrical stimulation improves motor recovery in postacute hemiparetic patients: A randomized controlled trial," *Stroke*, vol. 42, no. 4, pp. 1068–1073, 2011.
- [66] E. Ambrosini, S. Ferrante, T. Schauer, G. Ferrigno, F. Molteni, and A. Pedrocchi, "An automatic identification procedure to promote the use of fes-cycling training for hemiparetic patients," *J. Healthc. Eng.*, vol. 5, no. 3, pp. 275–292, 2014.
- [67] F. I. E. Estay, C. Rouse, M. Cohen, C. Cousin, and W. E. Dixon, "Cadence and position tracking for decoupled legs during switched split-crank motorized fes-cycling," in *Proc. Am. Control Conf.*, 2019.

- [68] C. Rouse, C. Cousin, B. C. Allen, and W. E. Dixon, "Split-crank cadence tracking for switched motorized fcs-cycling with volitional pedaling," in *Proc. Am. Control Conf.*, 2019.
- [69] M. Bellman, "Control of cycling induced by functional electrical stimulation: A switched systems theory approach," Ph.D. dissertation, University of Florida, 2015.
- [70] N. Sharma, K. Stegath, C. M. Gregory, and W. E. Dixon, "Nonlinear neuromuscular electrical stimulation tracking control of a human limb," *IEEE Trans. Neural Syst. Rehabil. Eng.*, vol. 17, no. 6, pp. 576–584, Jun. 2009.
- [71] E. S. Idsø, T. Johansen, and K. J. Hunt, "Finding the metabolically optimal stimulation pattern for FES-cycling," in *Proc. Conf. of the Int. Funct. Electrical Stimulation Soc.*, Bournemouth, UK, Sep. 2004.
- [72] J. L. Krevolin, M. G. Pandy, and J. C. Pearce, "Moment arm of the patellar tendon in the human knee," *J. Biomech.*, vol. 37, no. 5, pp. 785–788, 2004.
- [73] D. A. Winter, *Biomechanics and Motor Control of Human Movement*. New York: Wiley, 1990.
- [74] R. L. Lieber and J. Friden, "Functional and clinical significance of skeletal muscle architecture," *Muscle Nerve*, vol. 23, no. 11, pp. 1647–1666, Nov. 2000.
- [75] N. Fischer, R. Kamalapurkar, and W. E. Dixon, "LaSalle-Yoshizawa corollaries for nonsmooth systems," *IEEE Trans. Autom. Control*, vol. 58, no. 9, pp. 2333–2338, Sep. 2013.
- [76] B. E. Paden and S. S. Sastry, "A calculus for computing Filippov's differential inclusion with application to the variable structure control of robot manipulators," *IEEE Trans. Circuits Syst.*, vol. 34, no. 1, pp. 73–82, Jan. 1987.
- [77] N. Sharma, C. Gregory, and W. E. Dixon, "Predictor-based compensation for electromechanical delay during neuromuscular electrical stimulation," *IEEE Trans. Neural Syst. Rehabil. Eng.*, vol. 19, no. 6, pp. 601–611, 2011.
- [78] S. Obuz, R. J. Downey, A. Parikh, and W. E. Dixon, "Compensating for uncertain time-varying delayed muscle response in isometric neuromuscular electrical stimulation control," in *Proc. Am. Control Conf.*, 2016, pp. 4368–4372.
- [79] R. Downey, M. Merad, E. Gonzalez, and W. E. Dixon, "The time-varying nature of electromechanical delay and muscle control effectiveness in response to stimulation-induced fatigue," *IEEE Trans. Neural Syst. Rehabil. Eng.*, vol. 25, no. 9, pp. 1397–1408, September 2017.
- [80] P. C. Eser, N. Donaldson, H. Knecht, and E. Stussi, "Influence of different stimulation frequencies on power output and fatigue during FES-cycling in recently injured SCI people," *IEEE Trans. Neural Syst. Rehabil. Eng.*, vol. 11, no. 3, pp. 236–240, Sep. 2003.

- [81] M. Karvonen, E. Kentale, and O. Mustala, "The effects of training on heart rate; a longitudinal study," *Ann. Med. Exp. Biol. Fenn.*, vol. 35, no. 3, pp. 307–15, 1957.
- [82] A. Ridgel, H. Abdar, J. Alberts, F. Discenzo, and K. A. Loparo, "Variability in cadence during force cycling predict motor improvement in individuals with parkinson's disease," *IEEE Trans. Neural Syst. Rehabil. Eng.*, vol. 21, no. 13, pp. 481–89, May 2013.
- [83] R. Kamalapurkar, J. A. Rosenfeld, A. Parikh, A. R. Teel, and W. E. Dixon, "Invariance-like results for nonautonomous switched systems," *IEEE Trans. Autom. Control*, vol. 64, no. 2, pp. 614–627, Feb. 2019.

BIOGRAPHICAL SKETCH

Courtney Rouse received her bachelor's degree in mechanical engineering from Illinois Institute of Technology in 2015, after which she joined the Nonlinear Controls and Robotics lab at the University of Florida as a graduate student under the guidance of Dr. Warren E. Dixon. Courtney completed her master's degree in mechanical engineering with a biomedical engineering minor in 2018 and completed her doctoral degree in mechanical engineering in 2019. Courtney's doctoral research focused on human-robot interaction, specifically the theoretical development of switched robust control systems for applications involving rehabilitation exercises for movement disorders.